NOTE TO USERS

This reproduction is the best copy available.

UMI

University of Alberta

Sedimentology, Diagenesis, and Dolomitization of the Pedro Castle Formation on Cayman Brac, British West Indies

by

Alexander James MacNeil

©

A thesis submitted to the Faculty of Graduate Studies and Research in partial fulfillment of the requirements for the degree of Master of Science.

Department of Earth and Atmospheric Sciences

Edmonton, Alberta
Spring, 2001

National Library of Canada
Acquisitions and Bibliographic Services
395 Wellington Street
Ottawa ON K1A 0N4
Canada

Bibliothèque nationale du Canada
Acquisitions et services bibliographiques
395, rue Wellington
Ottawa ON K1A 0N4
Canada

Your file Votre référence

Our file Notre référence

The author has granted a non-exclusive licence allowing the National Library of Canada to reproduce, loan, distribute or sell copies of this thesis in microform, paper or electronic formats.

L'auteur a accordé une licence non exclusive permettant à la Bibliothèque nationale du Canada de reproduire, prêter, distribuer ou vendre des copies de cette thèse sous la forme de microfiche/film, de reproduction sur papier ou sur format électronique.

The author retains ownership of the copyright in this thesis. Neither the thesis nor substantial extracts from it may be printed or otherwise reproduced without the author's permission.

L'auteur conserve la propriété du droit d'auteur qui protège cette thèse. Ni la thèse ni des extraits substantiels de celle-ci ne doivent être imprimés ou autrement reproduits sans son autorisation.

0-612-60462-4

Canada

University of Alberta

Library Release Form

Name of Author: **Alexander James MacNeil**

Title of Thesis: **Sedimentology, Diagenesis, and Dolomitization of the Pedro Castle Formation on Cayman Brac, British West Indies**

Degree: **Master of Science**

Year this Degree Granted: **2001**

Permission is hereby granted to the University of Alberta Library to reproduce single copies of this thesis and to lend or sell such copies for private, scholarly, or scientific purposes only.

The author reserves all other publication and other rights in association with the copyright in the thesis, and except as herein before provided, neither the thesis nor any substantial portion thereof maybe printed or otherwise reproduced in any material form whatever without the author's prior written permission.

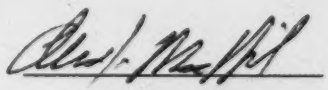

155 Dore Crescent
Saskatoon, Saskatchewan
S7K 4X6

January 30, 2001

University of Alberta

Faculty of Graduate Studies and Research

The undersigned certify that they have read, and recommend to the Faculty of Graduate Studies and Research for acceptance, a thesis entitled **Sedimentology, Diagenesis, and Dolomitization of the Pedro Castle Formation on Cayman Brac, British West Indies** submitted by **Alexander James MacNeil** in partial fulfillment of the requirements for the degree of **Master of Science**.

Dr. B. Jones (Supervisor)

Dr. B.D.E. Chatterton

Dr. D. Schmitt

Abstract

The Pedro Castle Formation on Cayman Brac is an unconformity bounded Pliocene sequence of shallow marine deposits. Deposition of the formation was controlled by an intricate interplay of sea level change and tectonic movement of the island.

The formation has experienced a complex history of diagenetic events, from the seafloor realm to recent meteoric diagenesis in the vadose environment. Partial dolomitization of the formation is texture preserving but non-mimetic. After dolomitization, diagenesis in the meteoric phreatic zone included cementation by coarse, drusy calcite, and stabilization of all remaining calcite to low-magnesium calcite.

The geochemistry of dolomite in the formation is similar to the geochemistry of island dolomites that have been interpreted to have formed in the meteoric – seawater mixing-zone. Close examination of this data, however, and consideration of the petrographic style of replacement, indicate that slightly modified seawater was responsible for partial dolomitization of the formation.

Acknowledgements

Well, I think that's it. There are so many people that helped over the past two years to make this thesis possible. Of course great thanks go to Dr. Brian Jones for his editorial skills, suggestions, and insightful discussions. Although he's perpetually busy, he was always available for at least a minute. Thanks also go to the friendly people of the Cayman Islands and Mike Wojcik for his help in the field.

Funding for the research and laboratory analyses was provided through an NSERC grant to Dr. Brian Jones. Husky Oil is thanked for funding provided to Dr. Brian Jones that helped in the completion of this thesis. The American Association of Petroleum Geologists are thanked for a Grant-in-Aid to myself.

There are so many people in the Department of Earth and Atmospheric Sciences at the University of Alberta that also need mentioning. Dr. Karlis Muehlenbachs is thanked for all of his help with the many(!) and repeated stable isotopic analyses, and many insightful discussions. Dr. Robert Creaser is thanked for his help with the strontium analyses and for use of his clean lab. Dr. Robert Luth is thanked for his help and insight with the XRD analyses. Olga Levner and Pat Cavell are thanked for help in the lab- they are incredibly meticulous and skilled in the laboratory – I think I picked up some of this. Don Resultay and Mark Labbe are thanked for all of the thin section work. Diane Card is thanked for all of her help in the XRD lab – I realize I'm one of those people who wanted the results yesterday. Lang Shi is thanked for all of

his help on the microprobe, and George Braybrook is thanked for his help on the SEM.

It was lots of fun working with and getting to know all of the other students and people. Jenny and Lisa are thanked for all the fun in the lab – and putting up with my music. All of the carbonate group- Rong-Yu, Morag, Sam, Bonny, Liz- were fun to work with. I also have to thank all my other friends in the department for all the fun we managed to have – I'm sure there'll be more – note the 2nd annual blender party is coming up! I'd also like to thank my "off-campus" friends – taekwon-do, Saskatoon people, friends from the U. of S. – for all the good times over the past couple of years. And then there's those of us that had a spiffalicious good time – you know who you are.

Lastly, but so ever importantly, I'd like to acknowledge
the love and support of my family.

Thanks.

Table of Contents

Chapter One - Introduction	
1.0 Introduction	1
1.1 Location and Physiography	1
1.2 Previous Research	3
1.3 Regional Geology	5
1.4 Geology of the Cayman Islands	9
1.4.1. The Brac Formation	9
1.4.2. The Cayman Formation	11
1.4.3. The Pedro Castle Formation	12
1.4.4. The Ironshore Formation	13
1.4.5. Regional Unconformities	13
1.5 Methodology	14
Chapter Two – Stratigraphy and Facies	
2.0 Stratigraphy	20
2.1 Cayman Formation – Pedro Castle Formation Unconformity	20
2.2 Facies	23
2.3 Facies in the Upper Part of the Cayman Formation	24
2.4 Facies in the Pedro Castle Formation	26
2.5 Facies Associations in the Pedro Castle Formation	40
2.6 Discussion	45
2.7 Summary	47
Chapter Three – Diagenesis and Dolomite Petrography	
3.0 Introduction	49
3.1 Diagenesis Stage I; Seafloor Diagenesis	49
3.2 Diagenesis Stage II; Pre-Dolomitization Diagenesis	54
3.3 Diagenesis Stage III; Dolomitization (Dolomite Petrography)	54
3.4 Diagenesis Stage IV; Meteoric Diagenesis	64
3.5 Summary	67
Chapter Four – Isotopic Geochemistry of Calcite	
4.0 Introduction	68
4.1 Results of Calcite Isotopic Analyses	68
4.2 Discussion	72
4.3 Analogy	79
Chapter Five – Dolomite Geochemistry	
5.0 Introduction	80
5.1 Analysis of Dolomite Population	81
5.2 Carbon, Oxygen, and Strontium Results	81
5.3 Discussion – Stoichiometry and Parent Fluid to Dolomitization	87
5.4 Summary	97
Chapter Six – Discussion and Summary	
6.0 Introduction	99
6.1 Tectonic Setting of Cayman Brac in the Pliocene	99
6.2 Pliocene Sea Level	101

6.3 Bank Morphology and Depositional History of the Pedro Castle Formation	103
6.3 Dolomite Genesis	108
6.4 Post-Dolomitization Diagenesis	110
6.5 The Age of Events	111
6.6 Summary	111
References	114
Appendix 1: Section Locations	122
Appendix 2: Sample Data	123
Appendix 3: Calcite – Dolomite Separation Method for Strontium Analysis	125

List of Tables

Table 2.1 Facies in the Cayman and Pedro Castle Formations on Cayman Brac	27
Table 2.2 Identified Foraminifera	28
Table 4.1 Calcite stable isotope data	71
Table 4.2 Water chemistry and temperatures from the Cayman Islands (I)	77
Table 5.1 Dolomite stable isotope data	84
Table 5.2 Water chemistry and temperatures from the Cayman Islands (II)	90

List of Figures

Fig.1.1. Map of Caribbean	2
Fig. 1.2. Regional structural geology	6
Fig. 1.3. Regional stratigraphy	8
Fig. 1.4. Cayman Brac geology	10
Fig. 1.5. Section Locations	15
Fig. 2.1. Cayman Unconformity	21
Fig. 2.2. Facies 1,2,3, and 5, Pedro Castle Formation, Cayman Brac	31
Fig. 2.3. Facies 6 and 7, Pedro Castle Formation, Cayman Brac	38
Fig. 2.4. North Coast Sections	41
Fig. 2.5. South Coast Sections	43
Fig. 2.6. Active Scott Quarry Sections	44
Fig. 2.7. Facies Associations distribution map	46
Fig. 3.1. Early marine diagenesis photomicrographs	50
Fig. 3.2. Marine cement photomicrographs	52
Fig. 3.3.Type I Dolomite photomicrographs	56
Fig. 3.4. Type II Dolomite photomicrographs	57
Fig. 3.5. Cloudy-centered clear-rimmed dolomite cement	58
Fig. 3.6. Limpid dolomite cement	60
Fig. 3.7. Allochem replacement	61
Fig. 3.8. Dolomite distribution map	63
Fig. 3.9. Meteoric diagenesis photos and photomicrographs	65
Fig. 4.1. Calcite stable isotope cross-plot	69
Fig. 4.2. Isotopic trend of calcite from individual sections	70
Fig. 4.3. Oxygen isotopes in calcite plotted against depth	74
Fig. 5.1. Dolomite stoichiometry	82
Fig. 5.2. Microprobe images of dolomite Ca/Mg compositions	83
Fig. 5.3. Dolomite stable isotope cross-plot	85
Fig. 5.4. Isotopic trend of dolomite from individual sections	86
Fig. 5.5 Strontium content vs. calcium content in dolomite	88
Fig. 5.6. %Ca and oxygen isotopic trends in individual sections	89
Fig. 6.1. Pliocene sea level curves	102
Fig. 6.2. Geological evolution of Cayman Brac in Pliocene	105
Fig. 6.3. Paragenetic sequence of deposition, diagenesis, and dolomitization of Pedro Castle Formation on Cayman Brac.	113

Chapter One - Introduction

1.0 Introduction

Cayman Brac, located in the northern Caribbean Sea, is a small carbonate island (~53 km^2) comprised of Oligocene to Pleistocene carbonate bank deposits. The Brac Formation (Late Oligocene), Cayman Formation (Middle Miocene), and Pedro Castle Formation (Pliocene) constitute three unconformity-bounded sequences. Collectively, these form the Bluff Group and the core of the island (Jones et al. 1994a). The Ironshore Formation (Pleistocene) forms an apron around the uplifted island core.

The Pedro Castle Formation was deposited in a dynamic, shallow marine environment, and has undergone extensive diagenesis and variable dolomitization. Water depth and energy across the bank, controlled by eustatic sea level changes and tectonic movement of the island, controlled deposition on the bank in the Pliocene. A complex diagenetic history that includes post-depositional dolomitization has altered the sequence following exposure of the formation. A geological investigation has been undertaken for the purpose of describing the depositional facies, the facies architecture, and the stages and types of diagenesis that impacted the Pedro Castle Formation on Cayman Brac. Characterization of the petrography, geochemistry, and geometry of dolomitization within the Pedro Castle Formation is a key focus of this study.

1.1 Location and Physiography

Located in the west Caribbean Sea, the Cayman Islands (Fig. 1.1) are situated approximately 220 kilometers west of Jamaica and 240 kilometers southwest of Cuba.

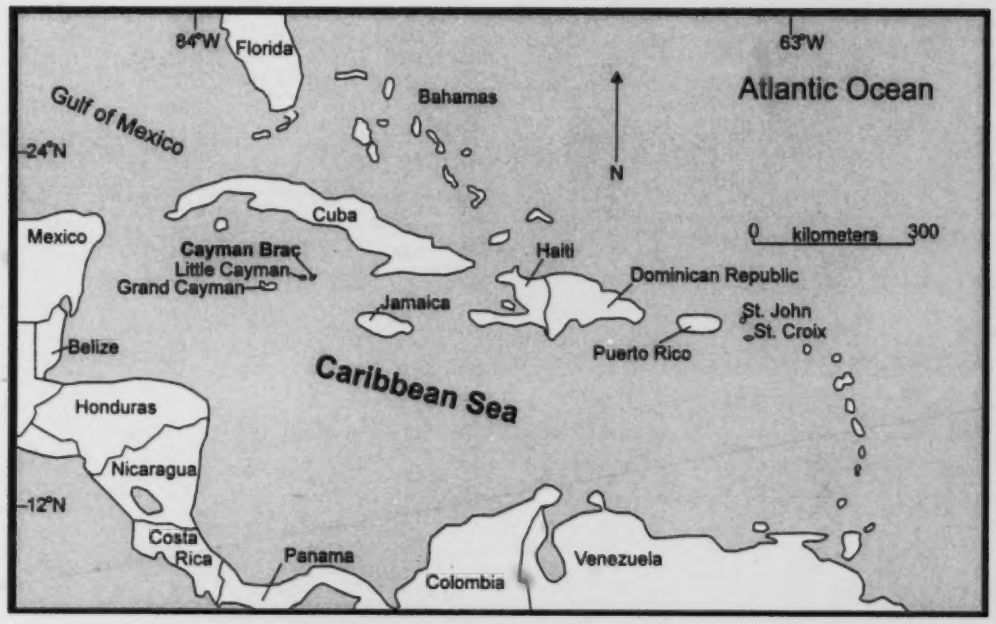

Fig. 1.1. Map of the Cayman Islands in the Caribbean.

Little Cayman and Cayman Brac are situated approximately 95 kilometers northeast of Grand Cayman. A tropical oceanic climate exists with predominant winds from the east and seasonal temperatures averaging between 25.8°C and 30°C (Darbyshire et al. 1976).

Cayman Brac (79°54'W, 19°41'N - 79°43'W, 19°46'N), which trends southwest – northeast, is ~53 km^2. Unlike Grand Cayman and Little Cayman which are low-lying islands not exceeding ~15 m above sea level (a norm of ~6 m), Cayman Brac attains an elevation of ~45 m along the northeast coast. The island is characterized by dense tropical flora and well-developed, rugged phytokarst. Outcrop can be difficult to access and rock faces are usually extensively weathered.

1.2 Previous Research

Numerous geological investigations have been conducted in the Cayman Islands. Matley (1924a, 1924b, 1925, 1926) conducted the first geological reconnaissance of the Cayman Islands and named the massive, bluff-forming rocks in the core of each island the Bluff Limestone. On Cayman Brac the Bluff Limestone was assigned an age of Middle Oligocene based on the observation of preserved *Lepidocyclina*. The Bluff Limestone on Grand Cayman and Little Cayman was assigned an age of Middle Miocene. Matley (1924a, 1924b, 1925, 1926) also identified the younger Ironshore Formation and described it as a coastal platform around the core of each of the Cayman Islands.

Investigations by Jones (1988, 1989, 1991, 1992a, 1992b), Jones and Hunter (1994a, 1994b) and Jones et al. (1989, 1994a, 1994b) have characterized various

geological aspects of the islands. Jones and Hunter (1989) divided the Bluff Formation (Matley 1926) into the Cayman Member and the Pedro Castle Member. Jones et al. (1994a) studied the stratigraphy of Cayman Brac and defined the Oligocene Brac Formation below the Bluff Formation.

Jones et al. (1994b) revised the stratigraphic nomenclature for the Cayman Islands. The Cayman Member and Pedro Castle Member were elevated to formation status and included with the previously defined Brac Formation to form the new Bluff Group. In addition to the type section for the Pedro Castle Member identified by Jones and Hunter (1989), a new reference section 21.7 m thick from well SH#3 on Grand Cayman (UTM 2138710N 461370E) was defined.

Pleydell (1987) studied the diagenesis and ichnology of the Bluff Formation on Grand Cayman and Pleydell et al. (1990) examined the dolomitization of the Bluff Formation on Grand Cayman. Arts (2000) studied the sedimentology and stratigraphy of the Pedro Castle Formation on southwest Grand Cayman, and determined that sea level in the Pliocene around the Cayman Islands rose ~30-35 m above the present level. These studies provide valuable information for comparison to the Pedro Castle Formation on Cayman Brac. Squair (1988) published a study of the surface karst on Grand Cayman that offers important information for comparison to the surface karst on Cayman Brac. Hunter (1994) published a study on the coral associations of the Cayman Islands that includes data from the Pedro Castle Formation on Cayman Brac.

Limited research has been specific to Cayman Brac. In addition to Jones et al. (1994a), Jones and Hunter (1994a) discussed the development of Cayman Brac as an isolated carbonate bank with a focus on the depositional facies and relationships

between the Brac Formation, Cayman Formation, and Pedro Castle Formation. No research specific to the Pedro Castle Formation on Cayman Brac has been published.

1.3 Regional Geology

The Cayman Islands are the tops of pinnacles situated on the Cayman Ridge; a structure comprised predominantly of metamorphic, plutonic and volcanic lithologies, that extends east-northeast across the Caribbean between Belize and Oriente Province, Cuba (Perfit and Heezen 1978; Holcombe et al. 1990). The depth of the ridge top varies from 0 to 3000 meters below sea level and the ridge width varies from 50 to 80 km (Holcombe et al. 1990). The Cayman Ridge is located along the southern edge of the North American Plate. The northern flank of the Cayman Ridge slopes gently beneath the Yucatan Abyssal Plain; the southern flank drops steeply to form the northern wall of the Cayman Trough (MacDonald and Holcombe 1978; Holcombe et al. 1990; Case et al. 1990).

The Cayman Trough, which lies to the south of the Cayman Ridge, is an east-west trending asymmetric depression (depths in excess of 7000 m) in the Caribbean crust. The trough extends 1600 km from the Windward Passage between Cuba and Hispaniola to the Gulf of Honduras, and is 120 to 180 km wide (Bowin 1968; Perfit and Heezen 1978; Holcombe et al. 1990). The deep axis lies along the northern wall in the eastern region of the Cayman Trough and the deep axis in the western region lies along the southern wall. These two regions of displacement are respectively defined as the Oriente Transform Fault and the Swan Island Transform Fault (MacDonald and Holcombe 1978; Perfit and Heezen 1978; Emery and Milliman

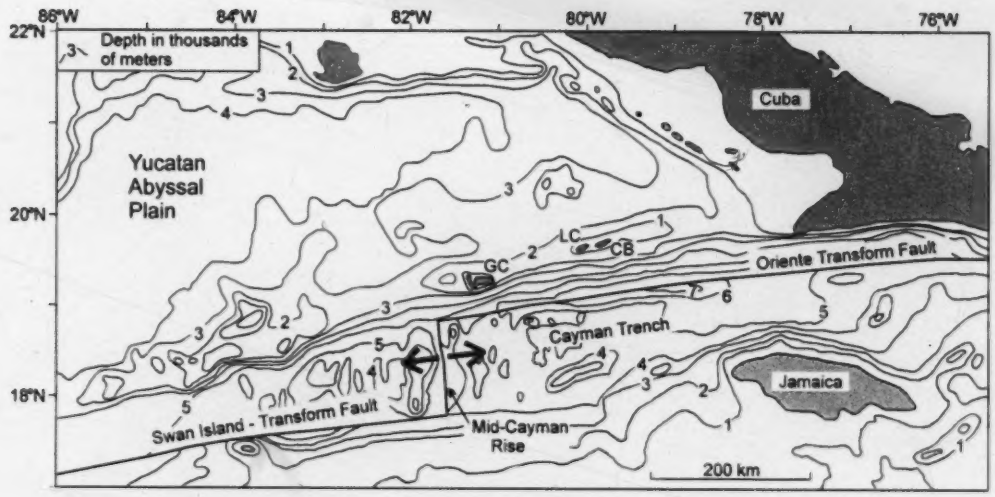

Fig. 1.2. Regional structural geology of the Caribbean Sea (modified from Holcombe et al. 1973). GC = Grand Cayman, LC = Little Cayman, and CB = Cayman Brac. Note the Cayman Ridge, Cayman Trench, and that the Cayman Islands are surrounded by deep water.

1980; Holcombe et al. 1990). The longitudinal deeps are connected in the central part of the structure (80° - 84° W) by a deep (5000-6000 m), V-shaped north-south valley defined as the Mid-Cayman Rise (Fig. 1.2) (Holcombe et al. 1973).

Comprised of oceanic basement of mafic and ultramafic affinity, several investigations have demonstrated that the Mid-Cayman Rise is an active spreading center (Holcombe et al. 1973; MacDonald and Holcombe 1978; Perfit and Heezen 1978; Pindell and Barrett 1990). The Nicaraguan Plateau along the northern edge of the Caribbean Plate forms the southern wall of the Cayman Trough (Perfit and Heezen 1978; Holcombe et al. 1990; Case et al. 1990).

Regionally the Cayman Trough is significant because it facilitates the left-lateral strike-slip movement of the North American Plate relative to the Caribbean Plate (MacDonald and Holcombe 1978; Perfit and Heezen 1978; Holcombe et al. 1990). Calculations indicate that initial opening of the Cayman Trough was in the Early Eocene, and that a cumulative offset of 1050-1100 km between the North American and Caribbean Plates has taken place since then (Pindell and Barrett 1990). Associated with this movement is the axial accretion of new oceanic crust at the Mid-Cayman Rise.

Each of the Cayman Islands are comprised of carbonate deposits of uncertain thickness on a basement lithology of granodiorite (Emery and Milliman 1980; Jones and Hunter 1994a). Drilling on Grand Cayman (Emery and Milliman 1980) to depths of 401 m and 159 m has recovered only carbonates and failed to reach the basement. Each of the Cayman Islands has also experienced independent tectonic movement,

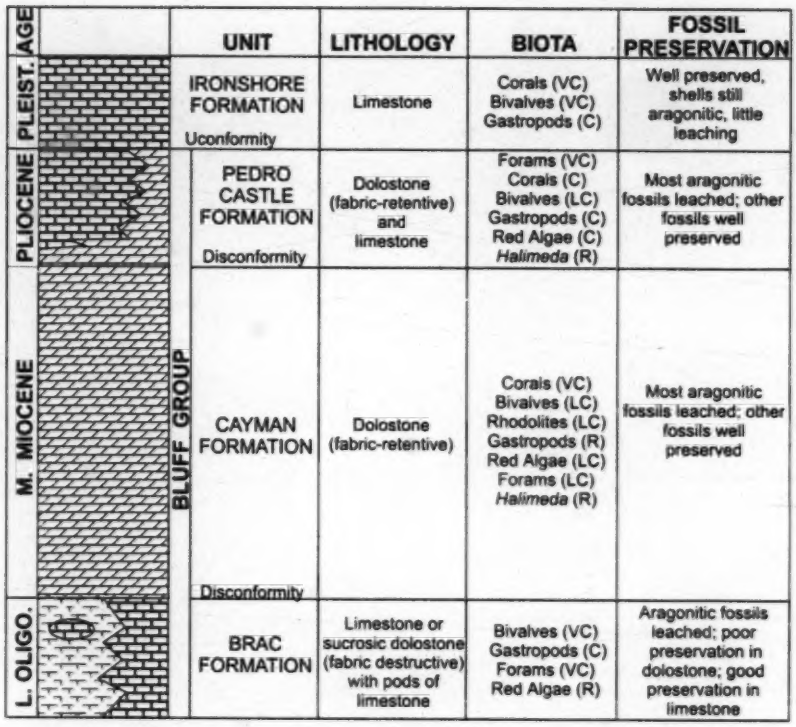

Fig. 1.3. Regional stratigraphy of the Cayman Islands (after Jones et al. 1994a).

and it is interpreted that each island is situated on a separate fault block extending from the Cayman Ridge (Perfit and Heezen 1978; Emery and Milliman 1980).

1.4 Geology of the Cayman Islands

The carbonate succession on the Cayman Islands can be divided into four formations divided by regional unconformities. The Bluff Group (Jones et al. 1994b) comprises the Late Oligocene Brac Formation, the Middle Miocene Cayman Formation, and the Pliocene Pedro Castle Formation (Fig. 1.3). On Cayman Brac (Fig. 1.4) the Bluff Group has a regional dip of 0.5° to the west (Jones and Hunter 1994a). Forming a coastal platform around the Bluff Group is the Pleistocene Ironshore Formation. Exposure and stratigraphic thickness of each formation varies between Grand Cayman, Cayman Brac, and Little Cayman.

1.4.1. The Brac Formation

The Brac Formation is only exposed on the eastern end of Cayman Brac. Along the southeastern coast the formation is comprised of sucrosic dolostone and dolomitic limestone. The formation is limestone along the northeastern coast. Exposed thickness of the formation is ~33 m; total thickness has not been determined because its lower boundary is not exposed. Bioclastic wackestone and packstone characterized by *Lepidocyclina* is the dominant facies. Foraminifera (rotalids, miliolids, small encrusting foraminifera, and *Carpentaria*), red algae, and echinoids, are also found in the Brac Formation. Corals are absent with the exception of scattered *Porites* branches near the top of the formation. Jones and Hunter (1994a) interpreted the

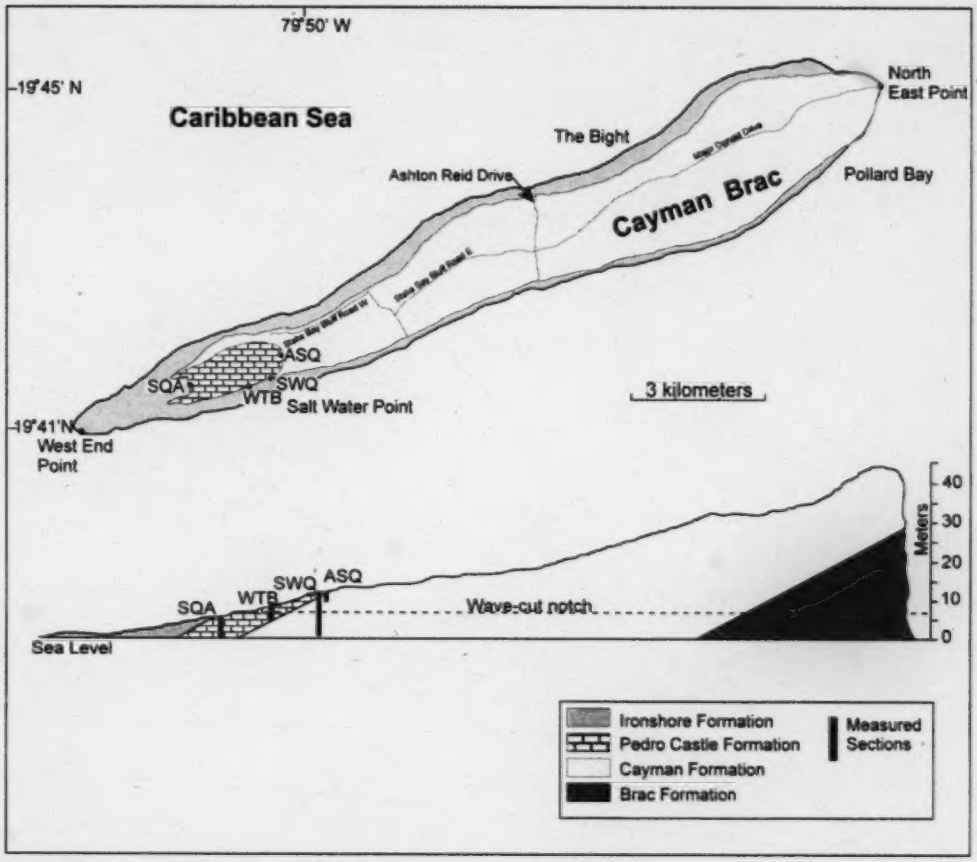

Fig. 1.4. Sketch map and island profile of Cayman Brac modified after Jones and Hunter (1994a). Sections ASQ, SWQ, WTB, and SQA are included for reference to Fig. 1.5.

facies as indicative of restricted environmental conditions on the basis of the lack of corals but the presence of opportunistic fauna including red algae and *Lepidocyclina*. Evidence that the formation originated as seagrass bed deposits in a low-energy environment includes the presence of micrite, coarse calcite spar filling shelter cavities, and the excellent preservation of skeletal allochems (Jones and Hunter 1994a).

1.4.2. The Cayman Formation

The Cayman Formation is well exposed on each of the Cayman Islands. On Grand Cayman the base of the formation has never been reached although drilling with core recovery has reached depths of ~155 m. The thickness is therefore assumed to exceed 155 meters. On Cayman Brac the Cayman Formation is estimated to be 100 m thick (Jones and Hunter 1994a). Fabric-retentive microcrystalline dolomitization is pervasive throughout the entire formation replacing the dominant mudstones, wackestones, and the minor beds and lenses of rudstone, packstone, and grainstone (Jones and Hunter 1994a). The biota in the Cayman Formation is more diverse than the Brac Formation. In addition to bivalves, gastropods, foraminifera, and red algae, different species of hemispherical colonial (*Diploria*, *Montastrea limbata*, *M. tampaensis*, *Siderastrea*, *Leptoseris*, *Porites*, *Favia*) and branching (*Stylophora*, *Porites*) coral are common (Jones et al. 1994a). Rhodolites are locally common.

The Cayman Formation is interpreted to represent deposition in a shallow marine open environment (Jones and Hunter 1994a). Jones and Hunter (1994a) established a correlation between different facies and the coral types and concluded that substrate

conditions rather than water depth or geographic position controlled the distribution of corals in the formation. Branching corals (ie. *Stylophora*, *Porites*) are associated with mudstone and wackestone facies. Massive colonial corals are associated with packstone and grainstone facies. There is no evidence of reefal development.

1.4.3. The Pedro Castle Formation

Most information about the Pedro Castle Formation is from Grand Cayman (Pleydell 1987; Jones and Hunter 1989; Pleydell et al. 1990; Ng 1990; Jones et al. 1990; Jones et al. 1994a; Jones et al. 1994b; Jones and Hunter 1994b; Hunter 1994; Wignall 1995; Arts 2000). On Cayman Brac exposure of the formation is limited and stratigraphic thickness is estimated to vary from 6 to 20 m. Correlation between previously studied sections has been incomplete due to the limited stratigraphic thickness of each section (ie. Jones et al. 1994b; Jones and Hunter 1994a).

Comprised of dolostone, dolomitic limestone, and limestone, the Pedro Castle Formation is characterized by skeletal wackestone and lesser amounts of mudstone and packstone (Jones and Hunter 1994a). The biota includes bivalves, gastropods, red algae, foraminifera (predominantly *Archaias angulata*, *Amphistegina sp.*, and *Globorotalia sp.*) and scattered corals (*Stylophora*, *Porites*, and fewer *Montastrea*). Jones and Hunter (1994a) concluded that the Pedro Castle Formation was deposited in a quieter marine environment than the underlying Cayman Formation and noted that the coral biota is less diverse and abundant. There is no evidence of reefal development and rhodolites are not common.

1.4.4. The Ironshore Formation

The Pleistocene Ironshore Formation forms a coastal platform around the Bluff Group on Grand Cayman (Rehman 1992; Shourie 1993), Cayman Brac, and Little Cayman. It is 0 to 13.7 m thick. The Ironshore Formation has not been dolomitized. On Cayman Brac the formation is stratigraphically horizontal, indicating that uplift and tilting of the island core took place prior to deposition of the Ironshore Formation (Shourie 1993).

The Ironshore Formation on the western half of Grand Cayman is formed by an upper subtidal shallowing upward sequence that was deposited in a quiet lagoon (Shourie 1993). The Ironshore Formation along the northeast coast of Grand Cayman is comprised of four unconformity-bounded sequences that record four sea-level highstands between 129 Ka to >400 Ka BP (Vezina 1997).

In addition to a well preserved, abundant and diverse shelly biota, the Ironshore Formation also includes reefal development. Ovate patch reefs up to 300 m long with a diverse coral biota developed and were separated by skeletal sands that were extensively bioturbated (Shourie 1993; Hunter 1994; Vezina 1997).

1.4.5. Regional Unconformities

The Brac Formation, Cayman Formation, and Pedro Castle Formation are stratigraphic sequences that represent the depositional segments of three transgressive – regressive cycles that controlled bank development from the Oligocene to Pliocene (Jones and Hunter 1994a). The regressive phase of these cycles is not preserved in

any of these formations (Jones and Hunter 1994a), implying that these were either rapid regressive events or that erosion has removed these deposits.

The unconformity between each formation represents a considerable period of time during which karst development and meteoric diagenesis was prevalent (Jones and Hunter 1994a). The Cayman – Pedro Castle Formation disconformity on Grand Cayman had a topographic variation up to 50 m across the island (Jones and Hunter 1994b). The same disconformity on Cayman Brac has not been studied in detail due to the difficulty of determining the actual contact between the Cayman Formation and Pedro Castle Formation (Jones and Hunter 1994a). A better understanding of this disconformity, which represents approximately 6 million years (Jones and Hunter 1994a), is required because topographic variations would have directly affected the depositional framework of the Pedro Castle Formation.

1.5 Methodology

Field work conducted on Cayman Brac involved the measurement and description of nine sections (Fig. 1.5, Appendix 1) and the collection of ~85 hand-sized samples for laboratory analyses at the University of Alberta. All sections were accessed by foot or vehicle and in certain cases permission had to be obtained from the local land owner.

A JENAPOL polarizing microscope was used for the transmitted light examination of ~48 thin sections. Alizarin Red S was used as a stain to discriminate calcite from dolomite. A blue stain was added to the epoxy to highlight porosity. A JENAMED fluorescence microscope was used for the examination of thin sections

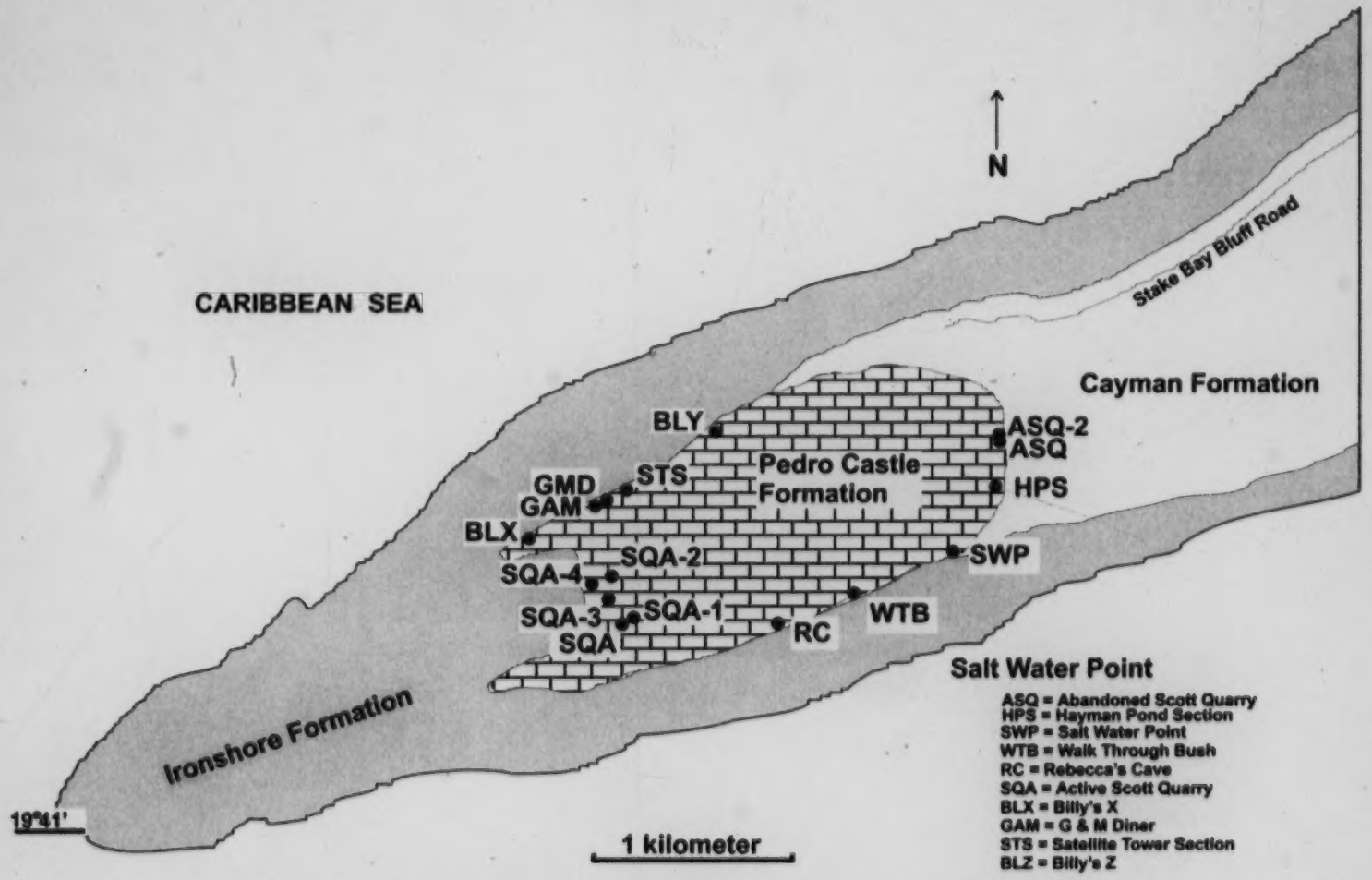

Fig. 1.5. Location of Pedro Castle Formation stratigraphic sections on Cayman Brac.

with UV fluorescent light. Selected fractured samples were sputter coated with gold (~100 angstroms thick) using a Nanotech gold coater and examined with a Jeol SM-6301 FXV scanning electron microscope. A PGT EDX system was used with the SEM to aid in the identification of calcite and dolomite.

X-ray diffraction (XRD) analyses were used to determine the carbonate mineralogy. A Rigaku Geigerflex sealed-tube X-ray generator with a Co tube, run at 40 kV and 35 mA, was used for these analyses. All samples were run in a backpacked sample container that held ~1 g of sample mixed with an internal standard of quartz. All scans were run from 29° to 38°2θ. Magnesium content in calcite was determined using the chart of Goldsmith et al. (1961). Dolomite stoichiometry was determined using peakfitting techniques (PF-XRD) (Jones et al. in press).

Carbon and oxygen stable isotopes from calcite and dolomite were systematically analyzed in the Stable Isotope Lab at the University of Alberta under the supervision of Dr. K. Muehlenbachs. A modified method of the procedure by Walters et al. (1972) was used for these analyses. Samples to be powdered for carbon and oxygen stable isotope analysis were selected from the most crystalline zones of each hand specimen. Areas that displayed leaching of corals and allochems, a chalky texture, rootcretes, or terra rossa were avoided. Samples were crushed to fine powders using a steel mortar and pestle. Splits of these powders were used for all XRD and stable isotopic analyses.

For stable isotopic analyses, the powder size range for analysis was limited to between 45 μm and 38 μm. Samples were reacted with anhydrous phosphoric acid at 25.2°C. After one hour of reaction, the produced gas was collected and considered

representative of the calcite component of the sample. Samples near the base of sections GAM and SQA-2 contained little (ie. <25%) calcite. In an attempt to avoid contamination of the calcite gas by gas produced from early dissolution of the most calcian dolomite in these samples, reaction time was reduced to 40 minutes (see Appendix 2).

For analyses of dolomite, a four hour reaction period with anhydrous phosphoric acid was allowed prior to venting the samples. Gases produced after venting were collected after 72 - 96 hours (when all remaining sample had dissolved) and considered representative of the dolomite component of the sample.

Gases were analyzed for $\delta^{13}C$ and $\delta^{18}O$ values using a Finnigan-MAT 251 Mass Spectrometer. All results are reported relative to PDB normalized to NBS-18 and the dolomite values have been corrected for the phosphoric acid fractionation factor by subtraction of 0.88 (modified from Sharma and Clayton 1965; reported in Friedman and O'Neil 1977). Correction for non-stoichiometry of the dolomite was made by addition of 0.742, following Vahrenkamp and Swart (1994).

Selected samples were analyzed for $^{87}Sr/^{86}Sr$ ratios in the Radiogenic Isotope Lab at the University of Alberta under the supervision of Dr. R. Creaser. Separation of the dolomite from the calcite was achieved by leaching the powdered samples with 5% acetic acid for a minimum of 50 minutes at room temperature. This method was established by several timed lab experiments that measured the rates of calcite and dolomite dissolution in monominerallic samples (Appendix 3). Repeated testing found that reacting a mixed sample of ~75% calcite and ~25% dolomite with 5% acetic acid for 50 minutes removed all detectable calcite by XRD. All samples

analyzed for $^{87}Sr/^{86}Sr$ contained a minimum of 25% dolomite prior to leaching, determined approximately by XRD and thin section examination.

Strontium was separated from a chloride form on a 10 cm column containing ~4 ml of 200-400 mesh AG50W-X8 resin. A second pass through a smaller column was performed to ensure low Ca contents. Purified Sr was loaded in the chloride form onto a single rhenium filament together with a tantalum activator gel. The isotopic compositions were measured on a VG 354 instrument using dynamic multi-collector routines, corrected for variable mass discrimination to $^{86}Sr/^{88}Sr = 0.1194$. Multiple runs of the SRM 987 standard gave a value of 0.7102716, so all data was normalized by 0.999963, to agree with the international value for SRM 987 of 0.710245 ±0.00002. Results were compared to high-resolution curves (Hodell et al. 1989) of $^{87}Sr/^{86}Sr$ changes in the oceans over time in the Cenozoic, in order to assign an age from the data.

Electron microprobe analysis (EMPA) with a Jeol JXA-8900 R was conducted for determination of Mg/Ca zoning in individual dolomite crystals, verification that the dolomite populations were unimodal, and for additional elemental (Sr^{2+}, Ca^{2+}, Mg^{2+}) measurements. Samples were doubly polished and coated with carbon prior to examination. Spot analyses were randomly selected and then individually adjusted to ensure analysis of dolomite crystals (adjusted to the center of each crystal when possible) rather than calcite crystals. A beam diameter of 3 μm was used. Collected data was then filtered for analyses with elemental (Na, Sr, Mg, Ca, and C) sums greater than 3.95 and less than 4.1. The stoichiometric value for dolomite should

equal 3.99 to 4.0 and analyses outside of the 3.95 to 4.1 range were considered unreliable and removed from the data set.

Chapter Two – Stratigraphy and Facies

2.0 Stratigraphy

The Pedro Castle Formation on Cayman Brac is limited to the western part of the island. Although the regional dip on the island has been estimated as ~0.5° to the west (Jones et al. 1994a), the true dip of the Pedro Castle Formation could not be determined because there are no clearly defined bedding planes that are suitable for this purpose. Stratigraphic sections previously examined (ASQ, SWQ, SQA, WTB, RC, BLX, GMD, and BLY) by Jones et al. (1994a) are included with new sections ASQ-2, SWP, HPS, SQA-1-4, GAM, and STS to further investigate the sedimentological architecture of this formation (Fig. 1.5). The Pedro Castle Formation in these sections is ~1 – 6.2 m thick. Section BLY, which lacks any of the Pedro Castle Formation, is included because it constrains the location of the erosional edge of the Pedro Castle Formation. The unconformity between the Cayman Formation and Pedro Castle Formation is present in sections WTB, SWP, HPS, ASQ, ASQ-2, SQA-2, BLX, GAM, GMD, and STS.

2.1 Cayman Formation – Pedro Castle Formation Unconformity

The Cayman Formation – Pedro Castle Formation unconformity was termed the Cayman Unconformity by Jones and Hunter (1994b) and that term is used herein. The unconformity is subtle in outcrop and commonly difficult to identify. Below the unconformity the Cayman Formation is generally tan-brown in colour whereas the overlying Pedro Castle Formation is generally white-tan in colour. This difference in colour allows recognition of the unconformity on a clean rock face (Fig. 2.1A). On

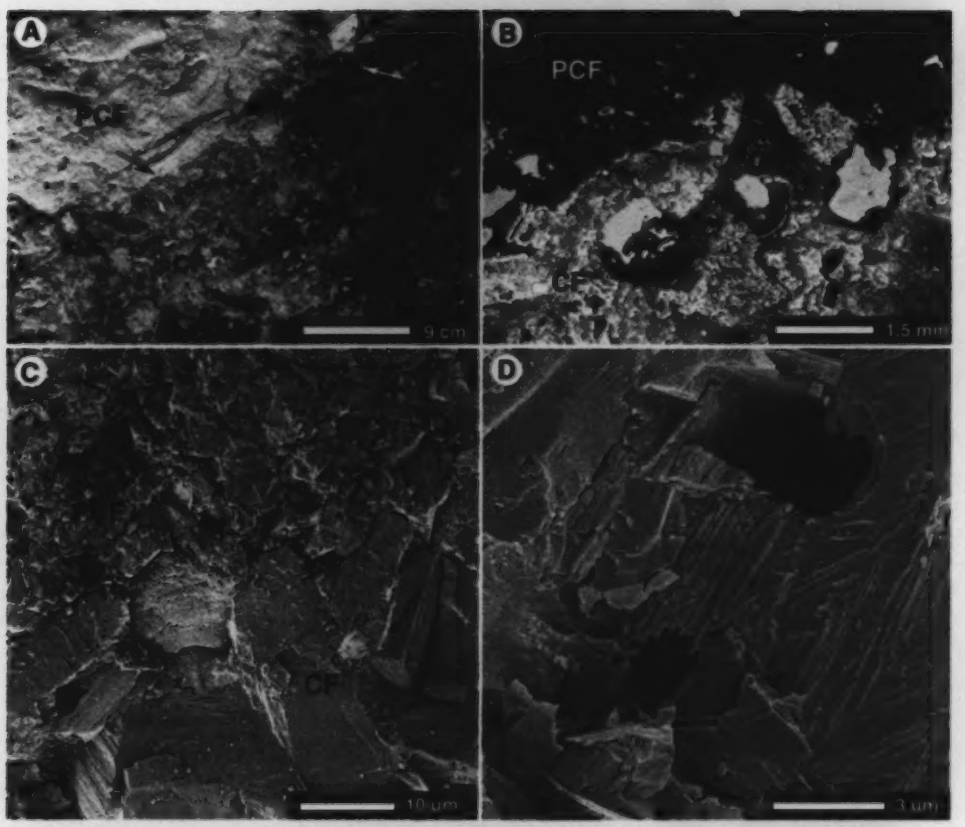

Figure 2.1. The Cayman Unconformity at section SQA-2. (CF) = Cayman Formation, (PCF) = Pedro Castle Formation. A) Unconformity near base of section SQA-2 (black arrow). White arrow indicates borings into CF at contact. B) Photomicrograph of borings (sponge?) at contact and geopetal infilling. C) SEM photomicrograph of unconformity. Note difference in dolomitization across contact. D) SEM photomicrograph of borings in CF just below unconformity.

weathered surfaces, however, the unconformity is virtually impossible to detect. In the field, lithophagid and sponge borings can be seen at the contact.

In thin section the contact between the two formations is sharp and easily identified. The style of dolomitization changes from pervasive, tight, euhedral crystalline dolomite and limpid dolomite cement of the Cayman Formation to microcrystalline dolomite with vuggy and good intercrystalline porosity of the Pedro Castle Formation (Fig. 2.1B, 2.1C). A colour change from buff-white to dark grey-brown respectively accompanies the change in dolomitization. Calcite content across the contact changes from a trace amount (<2%) in the Cayman Formation to at least 10% in the basal Pedro Castle Formation. Sponge, algal, and fungi borings found at the unconformity (Fig. 2.1D) are empty or filled with overlying sediment.

The nature of the Cayman Unconformity on Cayman Brac prior to deposition of the Pedro Castle Formation is not clearly understood (e.g. Jones and Hunter 1994a). There is no evidence of paleokarst development associated with the Cayman Unconformity on Cayman Brac, and unlike the Cayman Unconformity on Grand Cayman (Jones and Hunter 1994b), there is no evidence of extensive topographic relief. In sections GAM, SQA-2, ASQ, and ASQ-2 the Cayman Unconformity is sharp and smooth.

Jones and Hunter (1994b) concluded that at the end of the Messinian, sea level was at least 41 m below present-day sea level. If the Cayman Formation on Grand Cayman and Cayman Brac are stratigraphic equivalents, it seems reasonable that the Cayman Unconformity on Cayman Brac was also subaerially exposed during this lowstand period. Although not comparable to the topography developed at the

Cayman Unconformity on Grand Cayman (Jones and Hunter 1994b), ~2 m of relief was found at the Cayman Unconformity between sections SWP and WTB and ~4 m of relief between sections WTB and RC on Cayman Brac. The poor exposure of this unconformity on Cayman Brac may be masking its true topography.

Despite the limited data, the Cayman Unconformity on Cayman Brac is considered to be a paleokarst surface that developed at the end of the Messinian, contemporaneous with paleokarst development on Grand Cayman. Jones and Hunter (1994b) noted that transgression following karst development commonly modifies the karst surface by physical erosion and bioerosion. Erosion and surface modification related to transgression of the Cayman Unconformity on Cayman Brac may explain the lack of relief found on this contact. At the time when sediments that would later comprise the Pedro Castle Formation began to accumulate on the Cayman Unconformity, the contact was a submarine surface colonized by ahermatypic organisms and boring bivalves.

2.2 Facies

Facies descriptions of the strata in these sections summarize the lithological (pre-diagenetic) and paleontological characteristics of the deposits. As such these are consistent with the definition of *facies* by Haug (1907). Differences between the facies in these sections are subtle and defined by changes in the content of red algae, green algae, molluscs (bivalves and gastropods), benthic and planktonic foraminifera, echinoid plates, and colonial and free-living corals. Facies distinction on the basis of fossil content implies that these are biofacies (Boggs 1987). The mud content

(Dunham 1962; Embry and Klovan 1971) defines the depositional fabric of each facies but is not sufficient for facies distinction. Mineralogy and specifically dolomitization is not addressed in the facies descriptions, except where it has affected allochem preservation. There is no apparent correlation between each facies and the presence or absence of dolomite.

2.3 Facies in the Upper Part of the Cayman Formation

Sections BLX, GMD, BLY, WTB, SWQ, and ASQ include strata belonging to the Cayman Formation. Jones and Hunter (1994a) concluded that these strata represent the upper 5 – 8 m of this formation on Cayman Brac. Sections STS, GAM, SQA-2, ASQ-2, SWP, and HPS include strata of the Cayman Formation, but were not measured by Jones and Hunter (1994a). They are, however, close to the sections measured by Jones and Hunter (1994a) and have essentially the same facies architecture. Two facies (Table 2.1) are present in the Cayman Formation found in these measured sections.

Facies A. Coral Facies

This facies is dominated by massive *Porites*, *Diploria*, *Montastrea*, *Favia*, branching *Porites* and *Stylophora* (Jones and Hunter 1994a), and a matrix of skeletal wackestones and packstones. Red algae fragments, molluscs, peloids, small rhodolites (<1 cm), echinoid plates, benthic foraminifera, and coral fragments form the grain (>0.03 mm; Dunham 1962) component of the matrix. Mud content is <20%.

Coral heads up to 1 m in diameter are preserved *in situ* in sections STS and SWP. In the matrix, red algae fragments are the most abundant (~65% of allochems) skeletal component, and have been mimetically dolomitized. Echinoid plates are well preserved as single dolomite crystals, and benthic foraminifera (*Amphistegina*) have been mimetically dolomitized.

Facies B. Bioclastic – Rhodolite Facies

This facies is formed of skeletal grains derived from red algae, molluscs, echinoid plates, and benthic foraminifera. Peloids, rhodolites, and coral fragments (<1 cm) are also found in this facies. Mud content varies from <10 – 35%. The numerous red algae fragments (30 – 60% of allochems), peloids (10 - 30% of allochems), and rhodolites (≤15% of allochems) define this facies.

The small (<3 mm) and oval red algae fragments have irregular edges. Mimetic dolomite replacement has resulted in excellent preservation of their cell structures. The spherical or oval peloids are 0.25 – 1 mm in diameter. Preservation of the peloids is poor and peloidal ghosts are common. Rhodolites, 4 mm - 4 cm long, generally have irregular ovoid shapes that reflect the shape of the nuclei. In some rhodolites, coral fragments form the nucleus. The cell structure in the coralline red algae that coats the nucleus has been mimetically replaced by dolomite. As a result, excellent preservation of cell differentiation, conceptacles, and surface borings is present. Some rhodolites are fractured.

Molluscs (~10% of allochems) are inferred from the shapes of moldic porosity. Echinoid plates (<2 mm) and benthic foraminifera (*Amphistegina* and fewer *Archais*)

account for ~10% of the allochems. Branching corals are locally present in the Bioclastic – Rhodolite Facies but are isolated and do not form a framework.

2.4 Facies in the Pedro Castle Formation

Seven different facies (Table 2.1), which characterize the Pedro Castle Formation on Cayman Brac, belong to the Sandy Facies Association and the Coral Facies Association. The Sandy Facies Association includes wackestones, packstones, minor mudstones, and scattered isolated corals in some sections. The Coral Facies Association consists of a coral facies that was eventually filled and buried by sandy facies.

All of the facies in the Pedro Castle Formation developed in subtidal settings where factors such as temperature, salinity, water depth and turbidity, storm events, and changes in relative sea level controlled deposition (cf. Jones and Desrochers 1992). The mud content and biota of the different facies guide the interpretation of environmental conditions. Of greatest value from a faunal aspect are the variations in foraminifera species found in each facies. The ability to make correlations between foraminiferal assemblages and depositional environments is one of the most significant drives for the study of these organisms (Rose and Lidz 1977; Li 1997). For facies in the Pedro Castle Formation, information on the ecology of different foraminifera species (Table 2.2) is collectively important for interpretation of the depositional environments.

Amphisteginids account for ~35% of the foraminifera found in the Pedro Castle Formation. Species of this family are characteristic of marginal reef and fore-slope

Table 2.1. Facies in the upper Cayman Formation and Pedro Castle Formation on Cayman Brac.

		Facies	Fabric	Major Allochems	Minor Allochems
Pedro Castle Formation	Sandy Facies Association	1 Echinoid – Red Algae Facies	Mudstone - Wackestone	Red algae Echinoid Plates	Molluscs Amphisteginids Small (<1 cm) rhodolites
		2 Algae - Mollusc Facies	Wackestone	Red algae, Green algae Molluscs	Amphisteginids and Soritids Echinoid Plates, Peloids Coral fragments, Sponge spicules
		3 Red Algae Facies	Wackestone - Packstone	Red algae Molluscs	Amphisteginids, Soritids, Textularids, Miliolids, Globigerinids Green algae Peloids, Coral Fragments
		4 Rhodolite Facies	Wackestone	Red algae Molluscs Rhodolites	Soritids Peloids Echinoid plates
		5 Foram – Mollusc Facies	Wackestone	Red algae Peloids Molluscs Amphisteginids and Soritids	Miliolids, Globigerinids Green algae Echinoid plates
		6 Foraminifera Facies	Wackestone - Packstone	Red algae Amphisteginids, Soritids Homotrematids, Molluscs	Cibicidids, Textularids, Nodosarids Asteriginids, Miliolids, Globigerinids Peloids, Rhodolites *Porites, Stylophora*
	Coral Facies Assoc.	7 Coral Facies	Coral framestone	Framework: *Stylophora* *Porites*	*Montastrea* *Leptoseris* *Colpophyllia*
Cayman Formation		A Coral Facies	Coral framestone with skeletal wackestone – packstone matrix	Framework: *Porites, Diploria, Montastrea, Favia, Stylophora* Matrix: Red algae Molluscs	Matrix: Peloids, Small (<1 cm) rhodolites Amphisteginids, Echinoid Plates Coral Fragments
		B Bioclastic - Rhodolite Facies	Wackestone – Packstone Locally grainstone	Red algae Peloids Rhodolites	Molluscs Amphisteginids, Soritids Echinoid Plates, Coral fragments

Table 2.2. Foraminifera found in the Pedro Castle Formation on Cayman Brac and summary of their marine habitats.

Identified Foraminifera	Abundance (% of total forams)	Ecology	References
Amphisteginidae (*Amphistegina*)	~35%	Marginal reef and fore-slope environments. Not found in the interior platform unless associated with patch reefs or are transported.	Rose and Lidz (1977) Vénec-Peyré (1991) Li (1997)
Soritidae (*Archais, Peneroplis* (?))	~25%	Interior platform/ back reef environments and shallow (<2 m) waters. Strong association between these species and *Thalassia* mounds.	Rose and Lidz (1977) Hallock et al. (1986) Hallock and Peebles (1993) Li (1997)
Homotrematidae (*Homotrema*)	~20%	Encrusting foraminifera that are generally associated with hard substrates suitable for encrustation, ie. reefs and coral detrital zones.	Vénec-Peyré (1991)
Miliolidae	5 - 10%	Interior platform and some restricted interior platform environments.	Rose and Lidz (1977)
Textularidae (*Textularia, Bigenaria)*	~5%	Marginal reef and fore-slope environments.	Rose and Lidz (1977)
Globigerinacea (Globigerinidae and **Globorotaliidae)**	~5%	Planktonic foraminifera. Fore-slope and basinal environments.	Rose and Lidz (1977) Scholle (1978)
Cibicididae (*Hyalinea* (?))	≤3%	Benthic	
Nodosaridae (*Lenticulina* (?), *Alfredosilvestris* (?))	≤3%	Benthic	
Asteriginidae	≤3%	Marginal reef environments.	Rose and Lidz (1977) Li (1997)
Ataxophragmidae	≤2%	Benthic	

environments where higher energy conditions exist (e.g. Rose and Lidz 1977; Vénec-Peyré 1991; Li 1997). They are only found in lagoonal environments when associated with patch reefs or if transported and mixed with sediments (Rose and Lidz 1977; Li 1997). Soritids, which account for ~25% of the foraminifera in the Pedro Castle Formation, are characteristic of inner lagoonal environments where they are commonly associated with *Thalassia* banks in the shallow subtidal environment (Rose and Lidz 1977; Vénec-Peyré 1991; Li 1997). Homotrematids, the third most abundant type of foraminifera (~20%) in the Pedro Castle Formation, are encrusting foraminifera which are found around reefs and coral detrital zones where hard substrates suitable for encrustation exist (Vénec-Peyré 1991).

Benthic foraminifera that form <10% of the biota in the Pedro Castle Formation include miliolids, textularids, cibicidids, nodosarids, asteriginids, and ataxophragmids. Planktonic foraminifera of the superfamily globigerinacea are also present. Species of the Globigerinidae and Globorotaliidae families are characteristic of fore-slope and open marine (basinal) environments (Rose and Lidz 1977; Scholle 1978), and are only found in lagoonal environments if transported by storms or after death (Li 1997).

The faunal content and diversity in each facies of the Pedro Castle Formation can be combined with the mud content of each facies to characterize the depositional environment. The collective biota in the Pedro Castle Formation is characteristic of the biota found in normal marine conditions (Heckel 1972; Jones and Desrochers 1992) with salinity values between 30 and 40‰. Limited packstones and the absence of grainstones or rudstones indicate that sediments of the Pedro Castle Formation

were not deposited in high-energy conditions. The absence of these deposits also indicates that storm events did not contribute to the depositional history of the Pedro Castle Formation.

The original mineralogy of the organisms affected their preservation style. Aragonitic components, specifically molluscs (bivalves and gastropods) and corals, have been leached and are only recognized from the moldic porosity. Single dolomite crystals have replaced and preserved echinoid plates.

Facies 1. Echinoid – Red Algae Facies

The Echinoid – Red Algae Facies (Fig. 2.2A,B) includes echinoid plates, red algae, peloids, benthic foraminifera, molluscs, and rhodolites. The mud content varies between ~60 – 90%. The abundance of echinoid plates (~15% of allochems), red algae (~55% of allochems), and the high mud content defines this facies.

Fragments of red algae are small (<3-4 mm) and cell differentiation and conceptacles are locally preserved. Peloids up to 2 mm in diameter form ~20% of the allochems. Poorly preserved amphisteginids and molluscs constitute only a minor portion (~5%) of the allochems in this facies. Small rhodolites (<1 cm) are rare (<5% of allochems).

Interpretation

The key indicators of the depositional environment of Facies 1 are the abundant echinoid plates, peloids, and the high mud content. In most sections the depositional fabric of this facies is a mudstone or muddy (ie. >55% mud) sand. Poorly developed

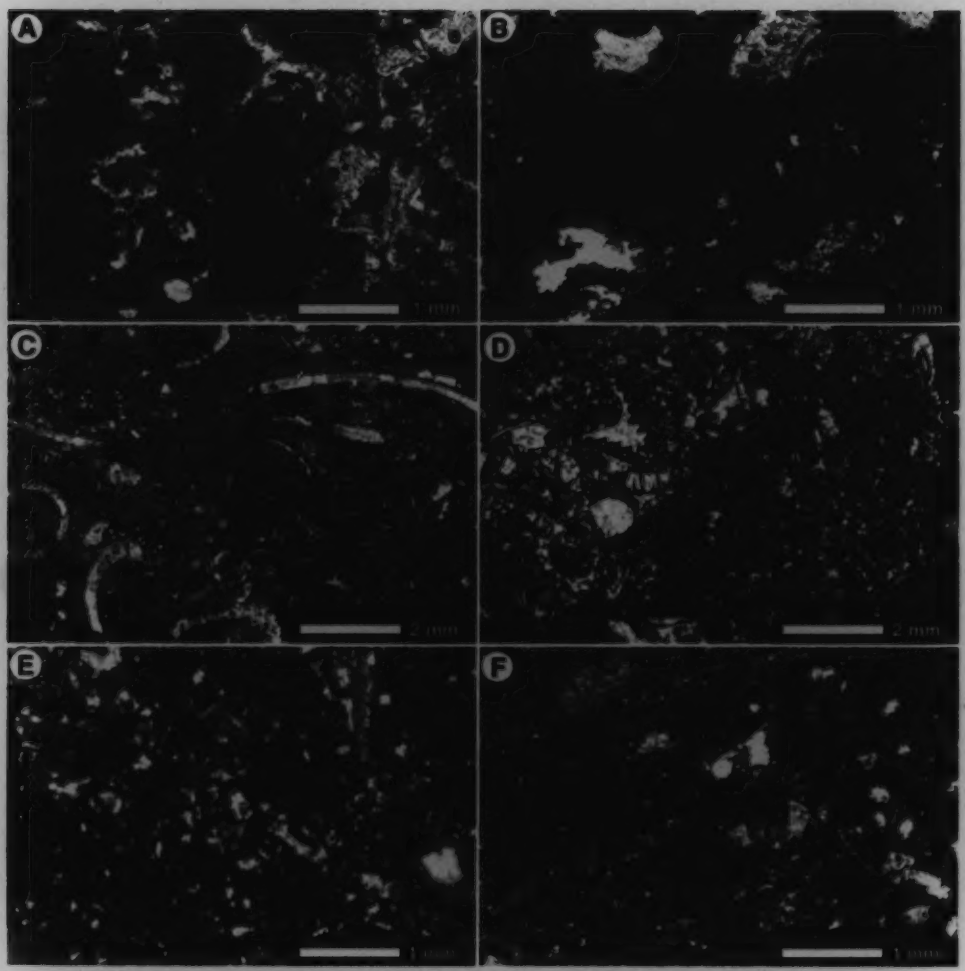

Figure 2.2. Photomicrographs of facies in the Pedro Castle Formation on Cayman Brac. Plane polarized light, e = echinoderm plate; g = green algae. All from section SQA-2. A,B) Facies 1: Echinoid - Red Algae Facies. Red algae and echinoderm plates in muddy matrix. C,D) Facies 2: Algae - Mollusc Facies. Red algae, green algae, and mollusc fragments in muddy matrix. E) Facies 3: Red Algae Facies. Red algae packstone. F) Facies 5: Foram - Mollusc Facies.

parallel sub-horizontal laminations are preserved locally and a mottled appearance indicates bioturbation.

Jones and Desrochers (1992) suggested that mudstones can be deposited in quiet environments on the lee side of islands and shoals, and in moderate to high energy environments where sea grasses (ie. *Thalassia*) and/or algal mats stabilize the substrate and bind the finer muds. This facies was probably not deposited in an environment stabilized by sea grasses. Abundant soritids and encrusting organisms (Rose and Lidz 1977; Hallock et al. 1986; Hallock and Peebles 1993; Jones and Hunter 1994; Li 1997) that are typically associated with sea grass facies are rare and the sediments that form Facies 1 are well sorted, unlike those sediments found in *Thalassia* banks (Jones and Desrochers 1992). Facies 1 was probably deposited in a low energy marine environment protected from high energy conditions. There is no clear indication of water depth for deposition of this facies.

The abundance of peloids indicates a certain degree of bioturbation, as indicated by the mottled nature of the deposit. Foraminifera are rare in this facies, and when found are characterized by amphisteginids. The presence of amphisteginids and small rhodolites indicates that moderate energy conditions capable of transporting small grains existed at least periodically.

Facies 2. Algae – Mollusc Facies

The Algae – Mollusc Facies (Fig. 2.2C, D) includes red algae, green algae, gastropods, bivalves, benthic foraminifera, echinoid plates, coral fragments, sponge spicules (~1%), and peloids. The mud content varies between 30 – 40%. The

abundant green (15 – 20% of allochems) and red algae (50 – 55% of allochems), gastropods (5 – 10% of allochems), and bivalves (5 – 10% of allochems) characterize this facies.

Red algae are present as small fragments (<3 mm). Cell structures of fragments are preserved but not exceptional in detail. The porous wall structures of circular and discoid green algae segments up to 2 mm in diameter are preserved, but minimal preservation of internal structures has taken place. Gastropods and bivalves are generally <1 cm long. Bivalve shells that originally included a calcitic component have retained that part of their shell structure (cf. Scholle 1978).

Benthic foraminifera (*Archais* and *Amphistegina*) are poorly preserved as either complete or fragmented specimens. The foraminifera and small (<2 mm) peloids constitute ~5% of the allochems in this facies. Fragments of branched coral, which form a minor part of the biota (<5%), are riddled with *Entobia* borings.

Interpretation

Facies 2 was probably deposited in shallow marine conditions (<10 m) of moderate to low energy. The abundance of green algae, red algae, and molluscs do not offer much information beyond the above interpretation. The minor amounts of coral fragments and amphisteginids suggest that some transportation and mixing of sediment from a higher energy environment contributed to the accumulation of these sediments.

Facies 3. Red Algae Facies

The Red Algae Facies (Fig. 2.2E) is dominated by red algae (up to ~70% of allochems). Green algae fragments account for <10% of allochems. Benthic foraminifera include *Archais*, *Amphistegina*, *Textularia*, and miliolid fragments. *Archais* is the most common foraminifera. Globigerinacids (planktonic foraminifera) are also present in minor (<10% of foraminifera) quantities. Foraminifera form ~5% of the allochems in this facies. Peloids (<2 mm) and skeletal grains micritized beyond identification constitute up to ~30% of the allochems. Mud content is ~10%.

Interpretation

Facies 3 was probably deposited in a shallow marine environment under higher energy conditions than Facies 2. Evidence for this suggestion includes the greater abundance of red algae relative to green algae, which is less likely to survive in a more turbid environment; a greater diversity of foraminifera including amphisteginids and globigerinids – foraminifera that are generally associated with outer-shelf environments; and a depositional fabric characterized by sandy wackestones and packstones.

Facies 4. Rhodolite Facies

The Rhodolite Facies includes rhodolites, red algae, molluscs, echinoids, and benthic foraminifera. Mud content is low (~15%). The rhodolites (~15% of allochems) are the characteristic feature of this facies. The rhodolites generally have an irregular oval shape with coral fragments (≤4 cm in length) as the nuclei. In many

rhodolites the nuclei can not be determined. Coatings around the nuclei are usually 1.5 – 2 mm thick.

Red algae fragments (<1 mm) are the most abundant allochem in this facies (~40%). Molluscs (15 – 30% of allochems) are usually <1 cm long. Echinoid plates (up to 2 mm) are well preserved and account for ~5% of the allochems. Foraminifera (*Archais*) are minor in this facies (~5%) and poorly preserved.

Interpretation

The numerous (~15% of allochems) rhodolites and low mud content (~15%) suggest that this facies was deposited in high energy conditions. The rhodolites in Facies 4 are not associated with corals, lack a mud-supported framework, and are not found with any type of foraminifera other than soritids. Collectively, this indicates considerably shallower water conditions with higher energy levels relative to Facies 1-3 and Facies 5.

Facies 5. Foram – Mollusc Facies

The Foram – Mollusc Facies (Fig. 2.2F) includes benthic and planktonic foraminifera, bivalves, gastropods, red algae, green algae, echinoid plates, and peloids. Mud content varies between 25 – 35%. The abundance of bivalves and gastropods (30 – 35% of allochems) is characteristic of this facies. The molluscs are typically <1 cm long.

Benthic foraminifera include *Amphistegina*, *Archais*, and miliolid fragments. Globigerinacids are rare (<20% of observed foraminifera). No encrusting foraminifera were found. Red algae fragments (40 – 50% of allochems) reach a

centimeter in size but are generally less than 1 mm. The wall structures of the green algae (~10% of allochems) are poorly preserved. Echinoid plates are minor (~5% of allochems) and poorly preserved due to extensive micritization of their margins. Skeletal grains micritized beyond identification are common (~30% of allochems).

Interpretation

The key indicators of the depositional environment for Facies 5 are the numerous molluscs and a greater diversity and abundance of foraminifera than in Facies 1-4. This wackestone was probably deposited in a shallow marine environment (≤10 m) with moderate to low energy conditions that allowed transportation and mixing of sediment, but was not sufficient for removing all of the finer muds.

Li (1997) conducted detailed analyses on the distribution of foraminifera on the windward and leeward sides of Grand Cayman, and found that amphisteginids and globigerinids (reef and fore-slope foraminifera) mixed with soritids (lagoonal foraminifera) was the result of intense sediment mixing. These foraminifera, found together in Facies 5, indicate that this sediment has been mixed and transported. The lack of homotrematids suggests that substrates suitable for encrustation were not present.

The lack of coral fragments indicates that either the energy conditions were not sufficient for transportation of even the smallest fragments, or that the source of transported sediment lacked coral development. The latter of these two possibilities is supported by the lack of homotrematids. The abundance of peloids suggests a certain amount of bioturbation of these sediments or the presence of grazing organisms.

Facies 6. Foraminifera Facies

The Foraminifera Facies (Fig. 2.3A-C) includes nine families of benthic foraminifera, one family of planktonic foraminifera, red algae, rhodolites, branching corals and coral fragments, molluscs, echinoid plates, and peloids. Mud content varies from <10% to 50%. The abundance (20 – 35% of allochems) and diversity of foraminifera, including numerous encrusting foraminifera are characteristic of this facies.

The benthic foraminifera in this facies include amphisteginids (*Amphistegina*), soritids (*Archais*), homotrematids (*Homotrema*), cibicidids (*Hyalinea*), textularids (*Textularia* and *Bigenaria*), nodosarids (*Lenticulina* ? and *Alfredosilvestris* ?), asterigerinids, ataxophragmids, and miliolids. Amphisteginids, soritids, and homotrematids are the most abundant foraminifera (~80% of foraminifera). The planktonic foraminifera belong to the superfamily Globigerinacea and form up to 10% of the total foraminifera. Indeterminate fragmented foraminifera are common in the facies.

Red algae fragments, which are the most abundant allochem (50-60%), are generally <0.25 mm. Larger (1 – 2 mm) fragments are locally present. Oval rhodolites up to ~7 mm long with leached or indeterminable nuclei account for ~5% of the allochems. *Homotrema* locally encrust the rhodolite edges. Locally they are overgrown and entombed by crustose red algae. Encrusting foraminifera vary from 1 to 3 layers of chambers (chamber diameter is ~ .2 mm) in thickness.

Scattered (<10%) coral fragments and *in situ* branching corals (*Porites*, *Stylophora*) are present and locally may provide a framework for this facies. Molluscs

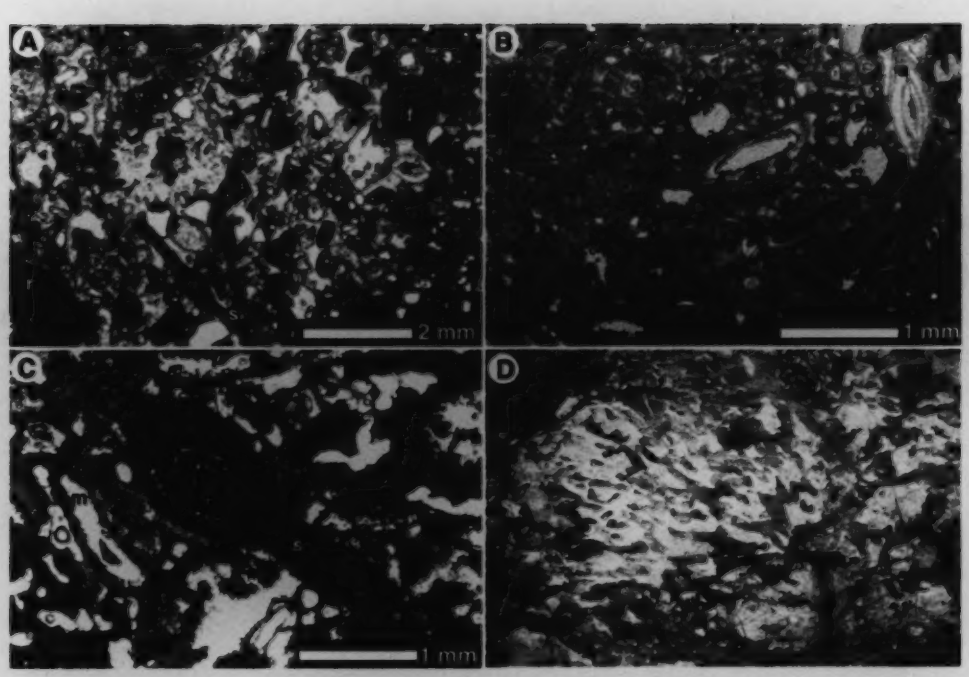

Figure 2.3. Facies in Pedro Castle Formation on Cayman Brac. All from SQA-1. Plane polarized light, s = soritid; a = amphisteginid; f = foraminifera fragment; r = rhodolite; m = micritic envelope. A,B, and C) Photomicrographs of Foraminifera Facies (Facies 6). Note abundant foraminifera and foraminifera fragments in these packstones. D) Field photograph of Coral Facies (Facies 7). Leached *Stylophora* branches of coralline thicket filled with terra rossa (dark sub-vertical branches). Hammer in lower right is ~30 cm tall.

(<1 cm) form up to ~5% of the allochems. Larger molluscs, including molds of *Strombus gigas*, are locally present in this facies. Peloids (1 – 2mm, <5% of allochems) and echinoid plates (up to 2 mm) are minor (<5% of allochems).

Interpretation

The assemblage of mixed foraminifera, abundance of fragmented foraminifera, rhodolites, and low mud content indicate that this facies is formed of mixed, transported sediments that were probably deposited in a moderate energy environment ≤10 m deep. When this facies is associated with Facies 7, or includes notable coral development, the mixed assemblage of foraminifera might be associated with the local coral development (Rose and Lidz 1977).

Unique to Facies 6 are molds of the large gastropod *Strombus gigas* in section ASQ-2. Their presence is consistent with the interpretation of shallow (≤10 m) marine conditions of moderate energy and a sandy substrate; consistent with modern lagoons around Grand Cayman and Cayman Brac.

Facies 7. Coral Facies

Branching corals (*Porites, Stylophora*) are *in situ* and served as a frame (Fig. 2.3D) for the deposition of sands that are characteristic of Facies 5, Facies 6, and transitions between the two. In the Coral Facies, mud content is low (~15 – 20%). Rare (~15% of coral) massive and free-living corals found in this facies include *Montastrea*, *Leptoseris*, and *Colpophyllia*.

Interpretation

Facies 7 was previously identified and named the *Stylophora* Coral Association by Hunter (1994) who suggested that it developed in water 10 – 20 m deep. Jones and Hunter (1994a) found that coral morphology in the Cayman Formation and Pedro Castle Formation could be correlated to substrate conditions; branching corals grew on mudstone and wackestone substrates whereas massive corals grew on packstone and grainstone substrates. They concluded that the branching morphology of *Stylophora* and *Porites* allowed the polyps to be elevated into the water column above the muddy substrate where the limited surface area prevented significant sediment accumulation. Any sediment that did accumulate could be shed by tentacular movement or cleaned from the surface by ambient currents. The association of *Stylophora* and *Porites* in this facies with sands characteristic of Facies 5, Facies 6, and transitions between the two are consistent with the conclusions of Jones and Hunter (1994a).

2.5 Facies Associations in the Pedro Castle Formation

The seven facies in the Pedro Castle Formation on Cayman Brac belong to the Sandy Facies Association and the Coral Facies Association. The Sandy Facies Association includes Facies 1-6 and lacks any coral framework development. The Coral Facies Association is limited to the Coral Facies (Facies 7).

The Pedro Castle Formation found in the north coast sections (Fig. 2.4) is characterized by the Sandy Facies Association; corals are rare. Muds and muddy sands of the Echinoid - Red Algae Facies (Facies 1) directly overlie the Cayman

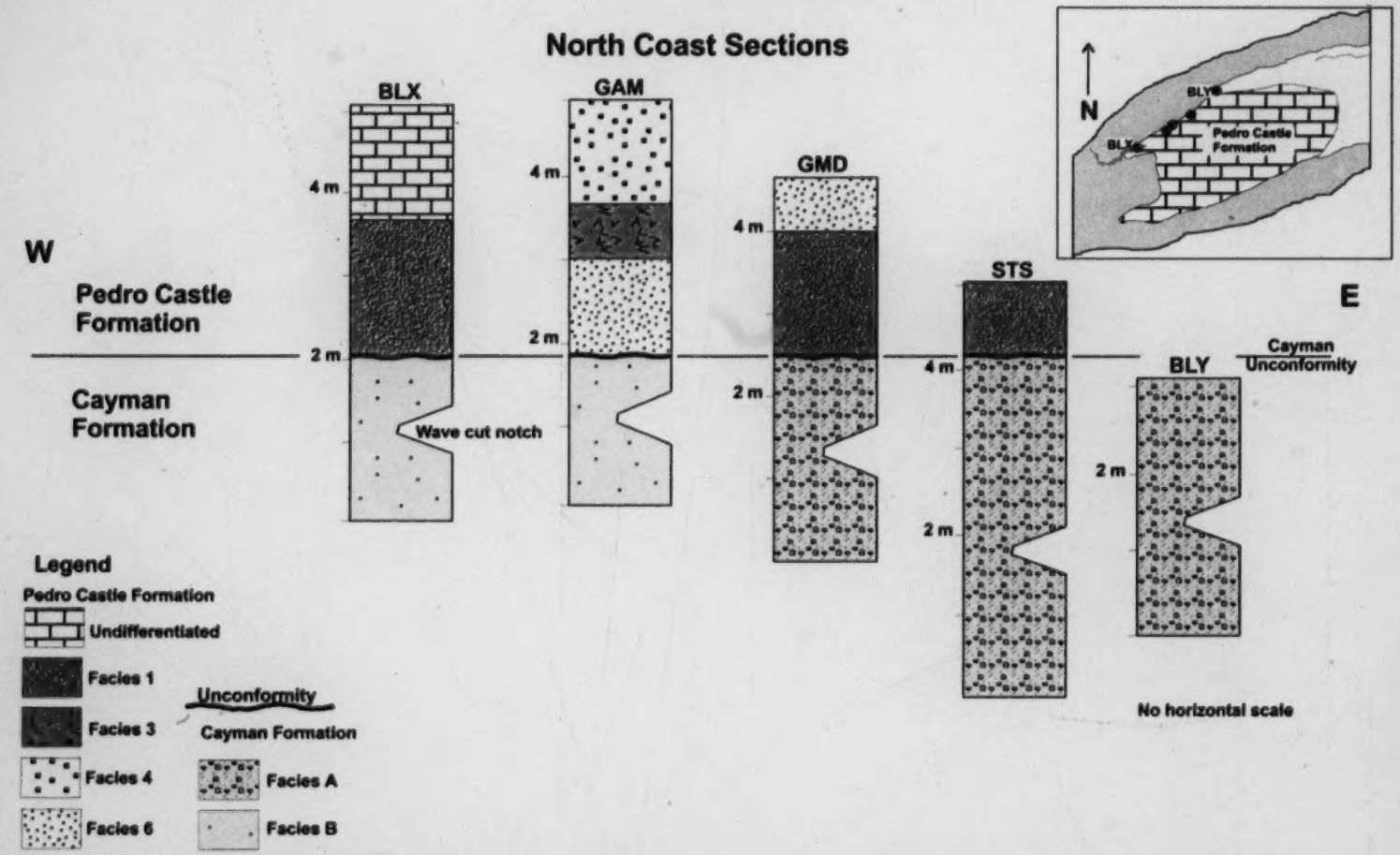

Figure 2.4. Stratigraphic sections along north coast of Cayman Brac. Sections BLX, GMD, and BLY from Jones et al. (1994a). Sections GMD and GAM are ~10 m apart. Note absence of coral development in the sections. Datum = Cayman Unconformity.

Unconformity in these sections except for GAM. The distribution of facies above Facies 1 is different in each section. Section GAM is the only locality in the Pedro Castle Formation where Facies 4 is found.

The Pedro Castle Formation in the south coast sections (Fig. 2.5) is characterized by the Sandy Facies Association but scattered corals are present in sections RC, WTB, and ASQ (Jones and Hunter 1994a). Muds and muddy sands of Facies 1 directly overlie the Cayman Unconformity in sections SWP, HPS, and ASQ-2. Wackestones overlie the Cayman Unconformity in sections RC, WTB, and ASQ. The upper part of the succession is characterized by Facies 5 and Facies 6. With the exception of Facies 1 overlying the Cayman Unconformity in three sections, there is no consistent facies distribution in these sections.

The Coral Facies Association was only found (Fig. 2.6) in the Active Scott Quarry (SQA) which is located between the north and south coast sections. In sections SQA-2, SQA-3, and SQA-4, the Coral Facies Association is up to ~2.7 m thick and overlies 1-2 m of sandy wackestones (Facies 3 or Facies 5). At section SQA (measured by Jones and Hunter 1994a) the Coral Facies Association is ~5 m thick. At the time of that study, however, excavation of the quarry floor had not exposed the facies below the Coral Facies Association, so the measurement of ~5 m is a minimum thickness. The Coral Facies Association in section SQA-1 is ~4 m thick. Similar to section SQA, however, the association extended below the excavated quarry floor at the time of study, so the true thickness can be assumed to be greater than this measured thickness.

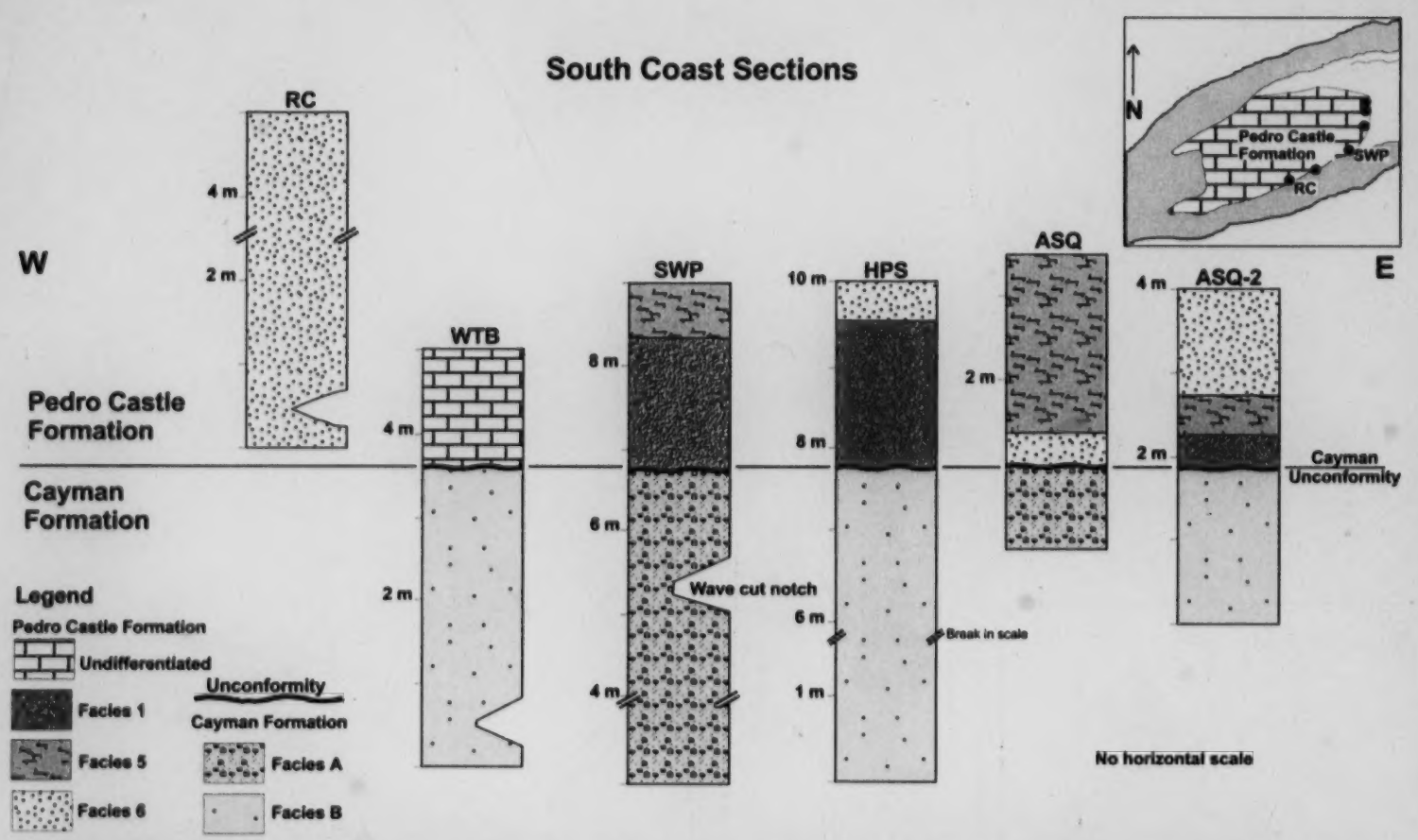

Figure 2.5. Stratigraphic sections along south coast of Cayman Brac. Datum = Cayman Unconformity. Sections RC, WTB, and ASQ from Jones et al. (1994a). Section SWP is a re-measured section (SWQ) from Jones et al. (1994a). Only sections RC, ASQ, and WTB had coral development. Coral fragments occur locally in other sections. Note that relief on Cayman Formation surface was present between sections RC, WTB, and SWP (using wave-cut notch as a structural datum).

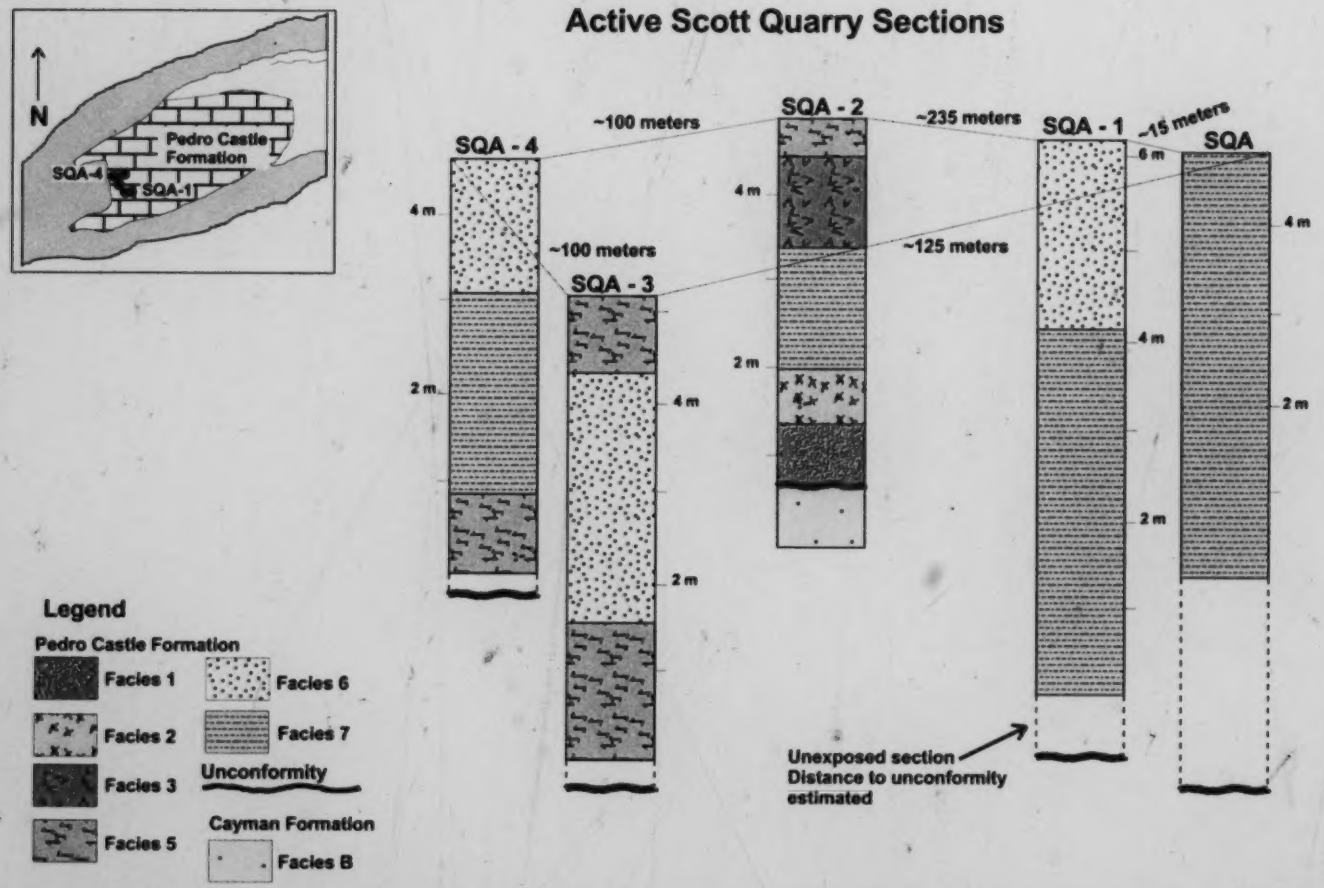

Figure 2.6. Stratigraphic sections in Active Scott Quarry (SQA). Section SQA from Jones et al. (1994a). Section SQA -2 is only section where Cayman Unconformity is visible and the Cayman Formation is exposed. The Active Scott Quarry is only area on Cayman Brac with notable coral development (Coral Facies Association) in the Pedro Castle Formation.

Allochthonous sands of Facies 3, Facies 5, and Facies 6 fill and bury the coral of the Coral Facies Association. The overlying sands (wackestones – packstones) are ~1-2 m thick and form the modern surface where chemical erosion and phytokarst development is intensive. Section SQA-1 is unique because of marine cements and a soritid – foraminifera packstone with exceptional allochem preservation not found in other sections. The lack of any dolomitization in this section is interpreted to account for the preservation of marine cements found nowhere else in the Pedro Castle Formation.

2.6 Discussion

A geographic zonation of the Coral Facies Association relative to the Sandy Facies Association is apparent on Cayman Brac (Fig. 2.7). Most of the peripheral margin of the Pedro Castle Formation is formed of the Sandy Facies Association. Along the western coast the Pedro Castle Formation is blanketed by the Ironshore Formation. Eastwards of where the formation is overlain by the Ironshore Formation, the Pedro Castle Formation is formed of the Coral Facies Association. Determination of the extent of the Sandy Facies Association from the margins, and the eastern-northeastern extent of the Coral Facies Association is limited by poor exposure. Most of the Pedro Castle Formation in the central and northwestern parts is either inaccessible or not conducive to sampling due to rugged phytokarst.

Understanding the environmental conditions in which the Coral Facies Association developed is based on information from Facies 7. Hunter (1994) concluded that this facies was probably deposited in water 10-20 m deep. The closest modern analogue in

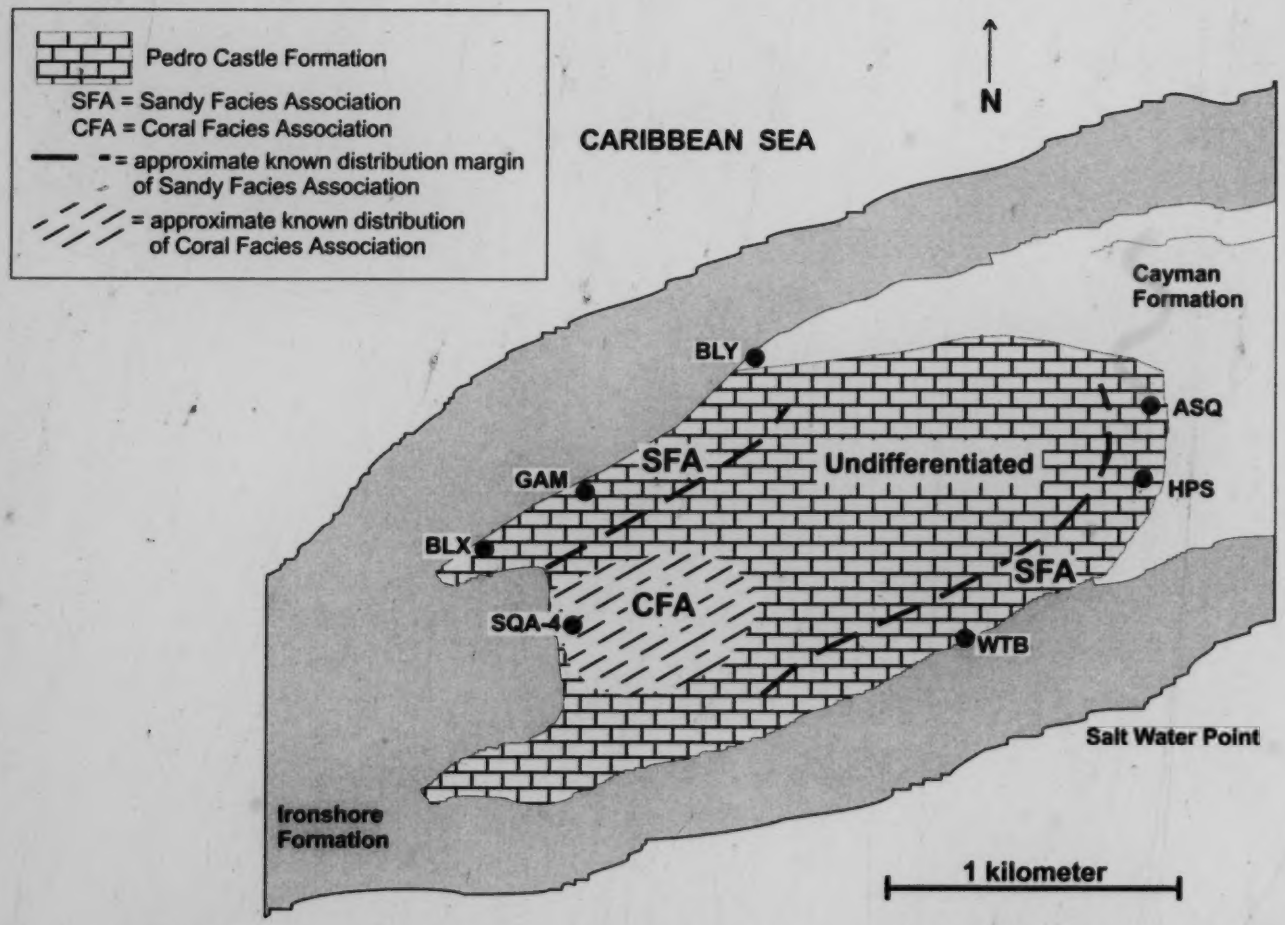

Fig. 2.7. Approximate distribution of facies associations in Pedro Castle Formation on Cayman Brac.

the Caribbean region to the thickets of branching *Stylophora* and *Porites* that characterize the Coral Facies Association are patch reefs surrounded by wackestone substrates. Rose and Lidz (1977) found that amphisteginids, homotrematids, and soritids may occur together (biocoenoses) in patch reef environments on the modern day South Florida – Bahamas platform. This implies that the presence of these foraminifera with coral development does not require sediment transport and mixing, a conclusion otherwise implied for sands where corals are absent. Amphisteginids, homotrematids, and soritids are the dominant foraminifera found associated with the Coral Facies Association. Growth in water depths between 10 and 20 m with similar environmental conditions to those around the South Florida – Bahamas patch reefs (e.g. Rose and Lidz 1977) seem probable for the Coral Facies Association.

The Sandy Facies Association (Facies 1 - 6) lacks any significant coral development. Facies 1 is only found directly above the Cayman Unconformity and represents quieter environmental conditions. The depositional environments of Facies 2 – Facies 6 vary in water depths and energy conditions (see section 2.4). The subtle differences between facies probably reflect local changes in bank morphology. This interpretation is best demonstrated in sections GAM and GMD (Fig. 2.4) which are located approximately 10 m apart. The only facies found in both sections is Facies 4, and GAM is the only section in the Pedro Castle Formation where Facies 6 is found.

2.7 Summary

Using the wave-cut notch as a structural datum, sections (Fig. 2.5) RC, WTB, and SWP along the south coast indicate that as much as 2 m of topographic relief existed

on the Cayman Unconformity when sediment accumulation began. SQA-2 is the only section in the Active Scott Quarry (Fig. 2.6) where the Cayman Unconformity is exposed. The lack of the Cayman Unconformity in the other sections in the Scott Active Quarry (the quarry floor is relatively level) indicates that topographic relief may also exist on the Cayman Unconformity at that locality. Further excavation of the floor is currently prevented by the extant water table. The Cayman Unconformity along the north coast is relatively flat. At the time when sedimentation of the Pedro Castle Formation began, the Cayman Unconformity on Cayman Brac appears to have had little topographic relief.

The Pedro Castle Formation was deposited in normal marine conditions in relatively shallow water depths (<20 m) under moderate to low energy conditions. Most of the deposits are wackestones with a variable biota of algae, foraminifera, molluscs, and echinoids. The Sandy Facies Association reflects rapid spatial changes in the bank morphology. Branching *Stylophora* and *Porites* are the most abundant corals in the Coral Facies Association, and grew as thickets in the area of the bank where the Active Scott Quarry now exists.

Chapter Three – Diagenesis and Dolomite Petrography

3.0 Introduction

The diagenetic history of the rocks in the Pedro Castle Formation on Cayman Brac is complex and records the transition from the Pliocene seafloor environment through to the modern vadose environment. The history can be divided into four stages, the third of which is variable dolomitization. The two most important features affecting the degree of dolomitization appear to have been the height above the Cayman Unconformity and the mineralogy of the precursor carbonate.

3.1 Diagenesis Stage I; Seafloor diagenesis

Dolomitization and meteoric diagenesis has destroyed or altered the earliest diagenetic fabrics in most sections. Section SQA-1, however, is an exception because it lacks dolomitization. The marine cements and excellent preservation of skeletal grains found in this section offer important information about the earliest marine diagenetic fabrics in the Pedro Castle Formation.

Micritization of skeletal grains in the Pedro Castle Formation was intensive and included development of micritic envelopes (Fig. 3.1A) around skeletal grains and aggrading recrystallization of biogenic calcite. The septal walls of foraminifera (soritids) and foraminifera fragments in section SQA-1 (Fig. 3.1B,C) were recrystallized to subhedral micrite, ~1 μm long. Similar recrystallization of soritids from the seafloor realm, documented elsewhere (cf. Reid and MacIntyre 1998), has been attributed to taphonomic and micritization processes that include aggrading recrystallization.

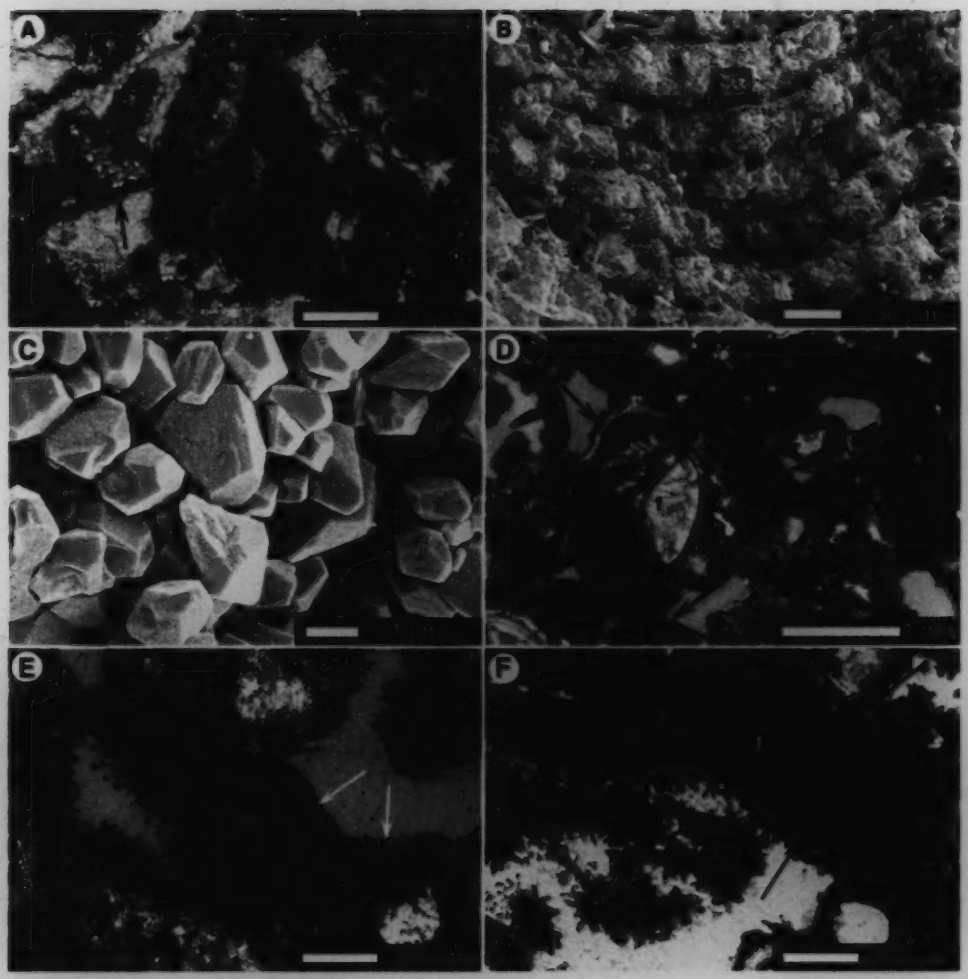

Figure 3.1. Early marine diagenesis and cementation of Pedro Castle Formation on Cayman Brac. All from SQA-1A) Photomicrograph of well-developed micritic envelopes (black arrows) around skeletal grains. B,C) Recrystallization of biogenic calcite in soritid septal wall. Box in B indicates view in C. D-F) Stubby bladed calcite marine cements (arrows); f = foraminifera.

At least two types of bladed calcite cement are present in the Pedro Castle Formation at SQA-1. An early "stubby" bladed cement is rare and commonly difficult to separate from later "coarser" bladed cement that is well developed. The presence and details of the stubby bladed cement is viewed best with fluorescence microscopy. This cement (Fig. 3.1D-F) forms isopachous but discontinuous rinds ~20-25 μm thick. Individual crystals display similar morphology to the "Roman Sword" shape described by James and Ginsburg (1979), where the crystal increases in width lengthwise away from its origin, to a maximum, and then terminates in an obtuse pyramid. These crystals in the Pedro Castle Formation, however, are much smaller than the bladed "Roman Sword" cements described elsewhere (e.g. James and Ginsburg 1979; Aissaoui 1988). The cement is developed best around micritic envelopes and lining small intergranular pore spaces.

Coarse bladed cements (Fig. 3.2) partially fill intergranular porosity and are always developed on the stubby bladed cement, indicative of the paragenetic sequence of cementation. Individual crystals, 4 – 10 μm at the base and 30 – 50 μm long, display an elongate triagonal shape with sharp edges. Crystal growth, is perpendicular to, or at a high angle to the substrate, and individual crystals display straight extinction. Bundles of the blades or radial arrangements are not found, and superimposed layers of coarse bladed cement are not present.

The original mineralogy of the bladed cements is not clear. The crystal morphology of these cements may, however, be compared to documented examples of HMC and aragonitic marine cements, in an attempt to delineate their original mineralogy. Bladed HMC cements, as described from Belize (James et al. 1976;

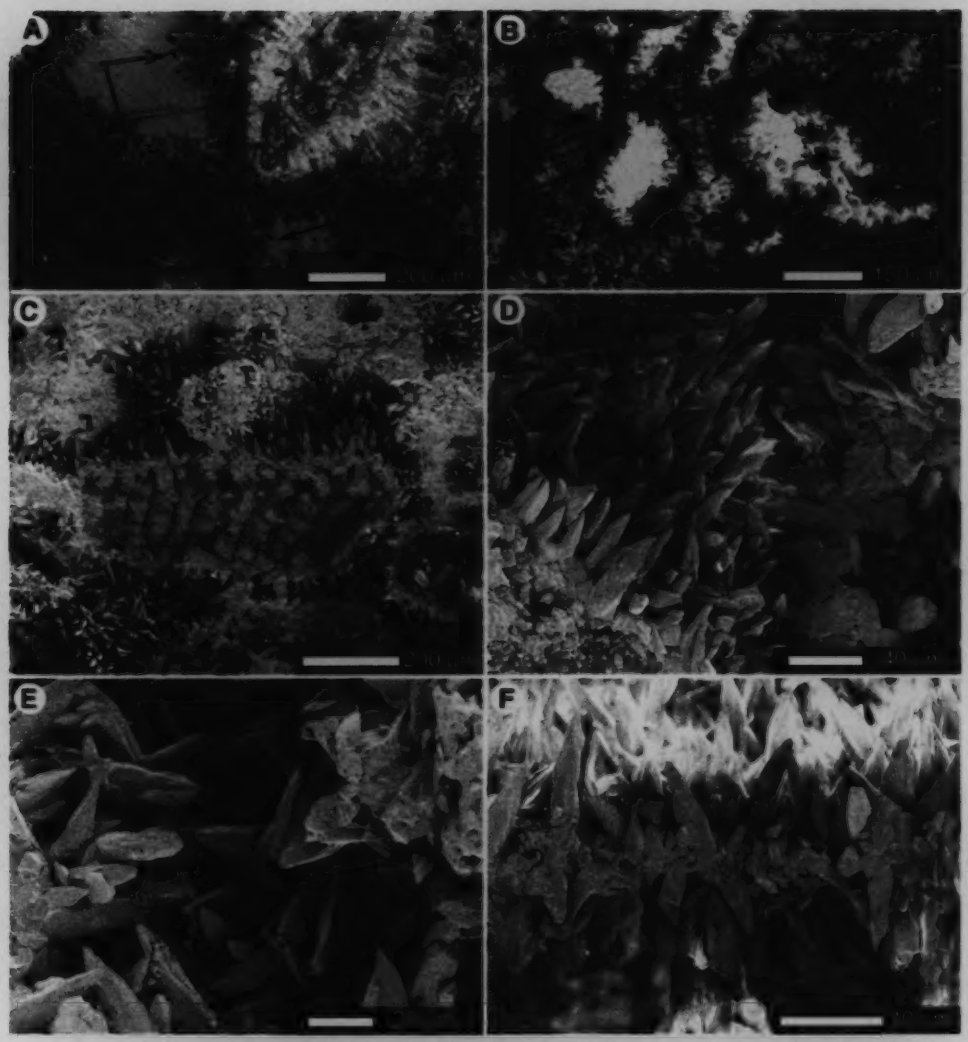

Figure 3.2. Coarse bladed marine calcite cements in Pedro Castle Formation on Cayman Brac. All samples from SQA-1. A) Cement filling (arrows) intergranular porosity. B) Cement filling intergranular porosity around micritic envelopes. The original grains have since been selectively leached. C) Scanning electron micrograph of coarse bladed cements filling intergranular porosity around soritid foraminifera. D) Coarse bladed cement. E) Coarse bladed cement filling intergranular porosity showing general crystal relationships. F)Coarse bladed cement.

James and Ginsburg 1979), Mururoa Atoll (Aissaoui 1988) and in general (eg. James and Choquette 1990b; Tucker and Wright 1990) are formed of larger crystals (10-50 μm wide, average length ~400 μm) and commonly have the "Roman sword" morphology (James and Ginsburg 1979). Both types of bladed cements in the Pedro Castle Formation are considerably smaller than these HMC bladed cements, although the stubby bladed cements share the same morphology. The "Roman sword" morphology is a rare shape of the coarse bladed cements. Isopachous rinds of bladed cements (e.g. Ginsburg et al. 1971; Aissaoui 1986), or rinds of spherulites or splays cumulating to form isopachous rinds are also not found in the Pedro Castle Formation.

Documented aragonitic cements commonly include needle meshes, fibrous crystals, and botryoidal aragonite (e.g. James and Ginsburg 1979; Aissaoui et al. 1986; James and Choquette 1990a). None of these crystal morphologies are similar to the cements in the Pedro Castle Formation. The only similarity of the Pedro Castle Formation cements with aragonitic cements is the lack of well-defined growth orientation, although the early stubby bladed cement forms discontinuous isopachous rinds. Based on these morphological characteristics of HMC and aragonitic cements, the cements in the Pedro Castle Formation share the greatest similarities with marine HMC cements. The most significant difference is the contrast in crystal size between these cements and the "typical" HMC cements described above.

The earliest diagenesis of the Pedro Castle Formation can be summarized as recrystallization of biogenic calcite (cf. Reid and MacIntyre 1998), development of micritic envelopes, and growth of an early stubby bladed cement followed by growth

of coarse bladed cements. The original mineralogy of the bladed cements is not clear, but morphological similarities to HMC cements suggest that the cements were originally of a high- Mg^{2+} content.

3.2 Diagenesis Stage II; Pre-Dolomitization Diagenesis

Most aragonitic allochems (green algae, bivalves, gastropods, corals) were selectively leached from the matrix. Their presence is now indicated by moldic porosity and micritic envelopes. The shell structure of bivalve fragments is only rarely preserved. Molds of coral skeletons are given detail by dolomitized linings of interstitial muds. The paucity of aragonitic components that were preserved and/or replaced by dolomite indicates that the sediments were flushed by fluids undersaturated with respect to aragonite prior to dolomitization (cf. Sibley 1980; Ward and Halley 1985; Pleydell et al. 1990; Meyers et al. 1997).

3.3 Diagenesis Stage III; Dolomitization

Dolomitization appears to have taken place after dissolution of the aragonitic components (Stage II) but before extensive meteoric diagenesis. Two types of replacement dolomite, termed here Types I and II, are found in the Pedro Castle Formation. Type I is a microcrystalline, texture preserving but non-mimetic replacement dolomite, similar to the crystalline, non-mimetic dolomite described from Niue Atoll by Wheeler et al. (1999). Type II is a microsucrosic replacement dolomite that poorly preserves the pre-existent texture, similar to the microsucrosic dolomite also from Niue Atoll, described by Wheeler et al. (1999). Moldic porosity

and intergranular porosity in the Pedro Castle Formation is lined with limpid and cloudy centered clear rimmed dolomite cements. Mapping the distribution of dolomite in the Pedro Castle Formation indicates lateral variation in the degree of dolomite replacement. The extent of dolomite replacement tends to decrease with height above the Cayman Unconformity.

Dolomite Petrography

Dolomite in the Pedro Castle Formation has selectively replaced and moderately preserved the texture of the micritic component of the original limestones and micritic envelopes. Type I replacement dolomite is non-mimetic but texture preserving. The crystals are microcrystalline subhedral rhombs 0.4-1.6 μm long, and can only be viewed in detail with scanning electron microscopy (Fig.3.3). The edges and corners of the crystals are dull to rounded. Crystals do not interlock and good intercrystalline porosity exists.

Type II replacement dolomite poorly preserves the pre-existing texture and is micro-sucrosic (cf. Dawans and Swart 1988). The crystals consist of euhedral cloudy rhombs, generally 15-35 μm long, and have sharp edges and corners (Fig. 3.4). Type I dolomite may occur by itself or with Type II dolomite. Type II dolomite is never found by itself.

Two types of dolomite cement are found in the Pedro Castle Formation. Clear dolomite cement is found as overgrowths on Type II dolomite (Fig. 3.5). Similar dolomite cement has been described from the Bahamas (Dawans and Swart 1988), Bonaire (Sibley 1980, 1982), and Mururoa Atoll (Aissaoui et al. 1986), where the

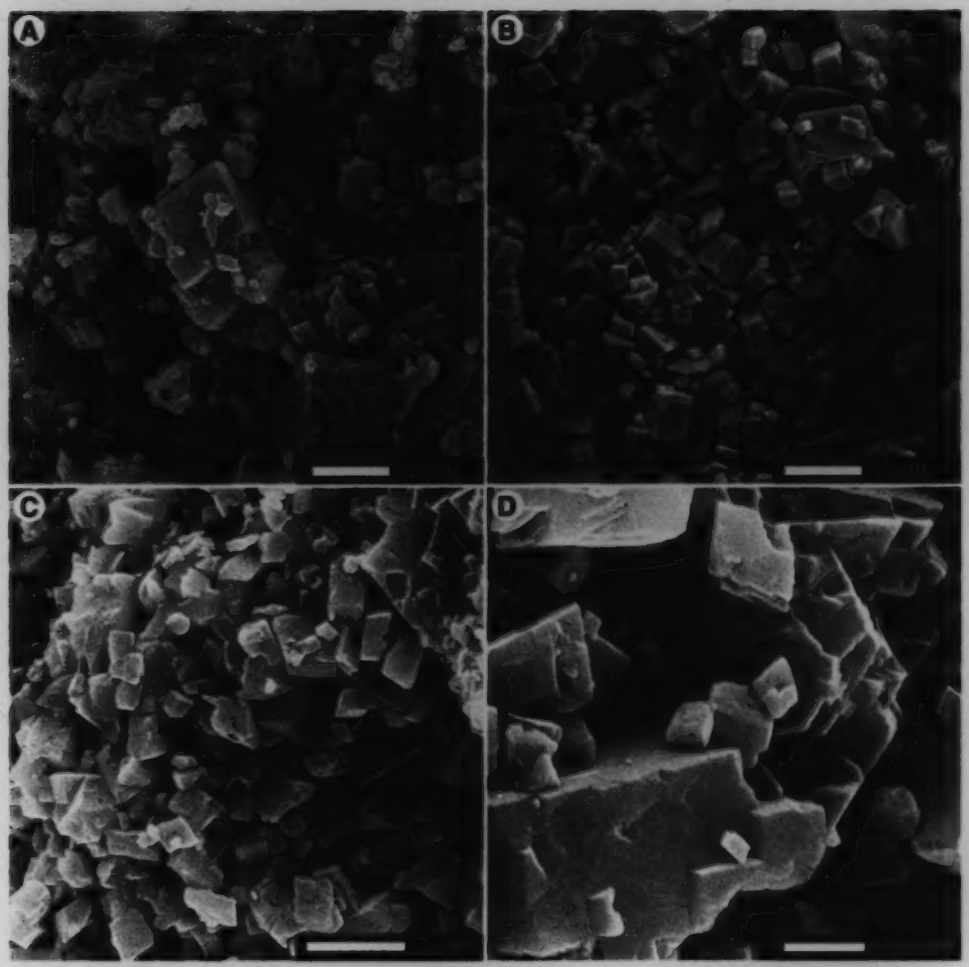

Figure 3.3. Scanning electron micrographs of Type I dolomite in Pedro Castle Formation. A) Sub-micrometer rhombs of dolomite and slightly larger 1-2 micrometer euhedral and subhedral rhombs. Microcrystalline calcite (c) as amorphous bodies are also in matrix. (Section SQA-2). B) Subhedral and lesser euhedral rhombs. (Section SQA-2). C) Subhedral and lesser euhedral rhombs. Note rounded and worn, poorly formed corners and edges of individual crystals. Crystals do not generally interlock and moderate to good intercrystalline porosity exists. (Section GAM). D) Enlarged view of rhombs. (Section GAM).

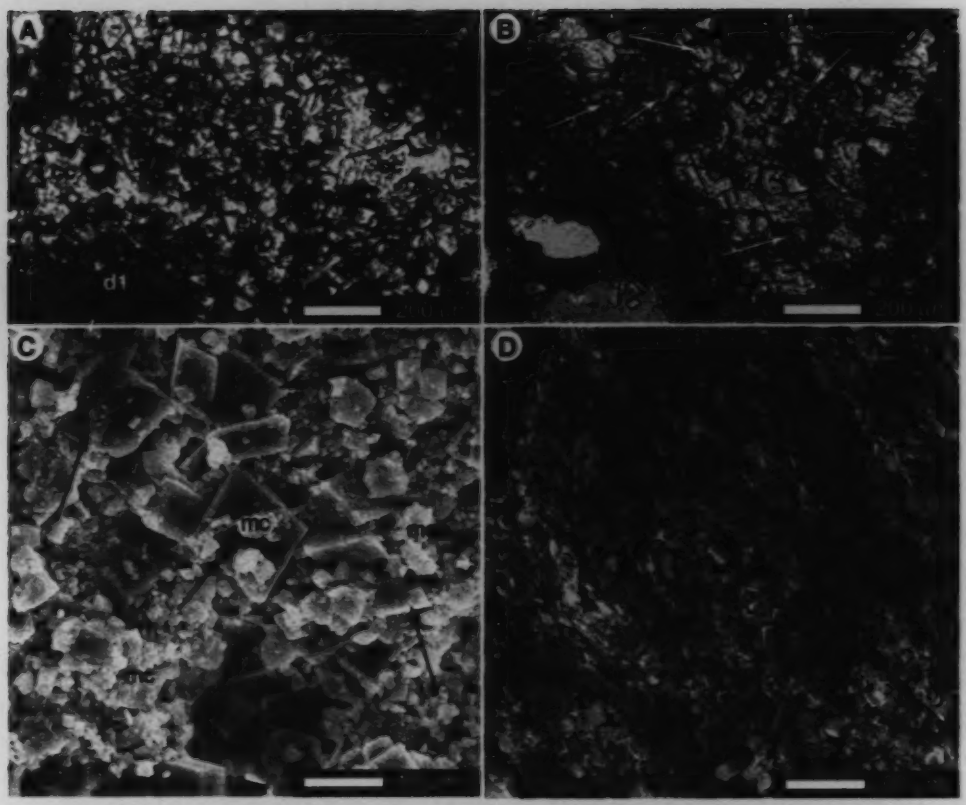

Figure 3.4. Type II dolomite in Pedro Castle Formation. A) Photomicrograph of matrix material with cloudy Type II rhombs (arrows) and microcrystalline Type I dolomite (d1). Porosity filled by dolomite cement (ce) and coarse calcite (cc). (Section SQA-2). B) Photomicrograph of Type II dolomite (arrows) and porosity filled by coarse calcite cement (cc). (Section SQA-2). C) Scanning electron micrograph of Type II dolomite (arrows) and microcrystalline calcite (mc). (Section GAM). D) Scanning electron micrograph of matrix composed of Type I (d1) and Type II (arrows) dolomite. (Section GAM).

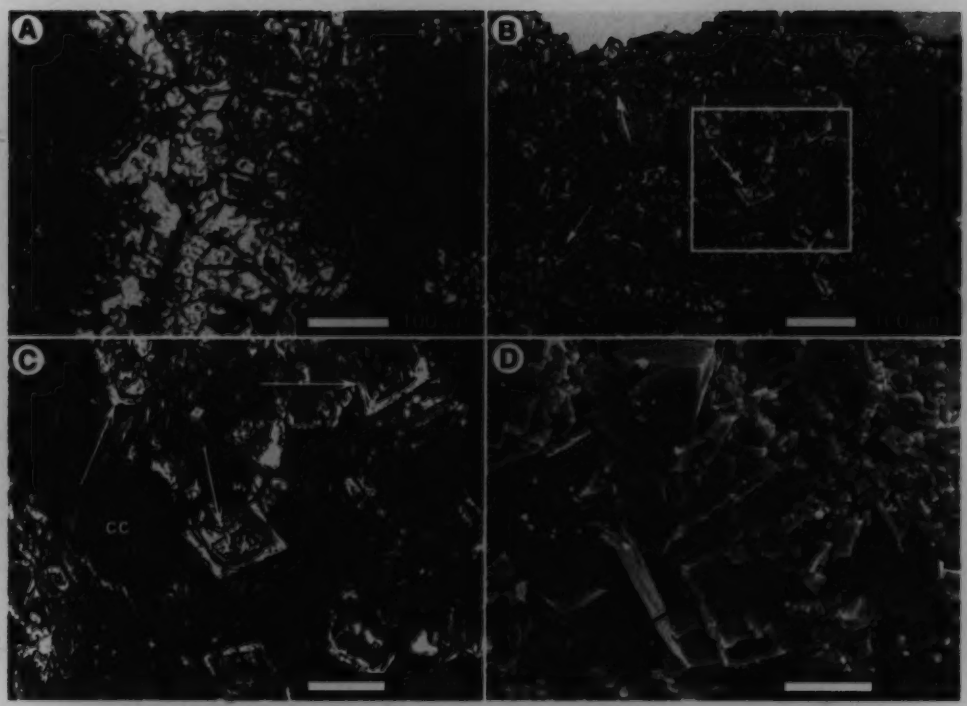

Figure 3.5. Cloudy-centered clear-rimmed dolomite cement (arrows) in Pedro Castle Formation on Cayman Brac. All samples from SQA-2. A) Dolomite cement and coarse calcite (cc) cement. B) Box highlights view in C. C) Dolomite cement and later coarse calcite cement (cc). D) Scanning electron micrograph of cloudy centered clear rimmed dolomite cement. Note gap (arrow) between replacement rhomb and cement overgrowth.

clear rims have been interpreted as cement overgrowths. The second type of dolomite cement is limpid dolomite. The euhedral limpid dolomite crystals, 5-35 μm long, line intergranular porosity, micritic envelopes, and moldic porosity (Fig. 3.6). Limpid dolomite has not previously been recognized in the Pedro Castle Formation (eg. Jones and Hunter 1994a).

Different types of skeletal grains have been affected by dolomitization in different manners. Mimetic dolomitization is rare in the Pedro Castle Formation, and echinoderm plates are the only type of skeletal grain that are consistently mimetically replaced. Syntaxial dolomite cement overgrowths are found on some echinoderm plates (Fig. 3.7A,B). Dolomitization of red algae fragments is rarely mimetic (Fig. 3.7C-F). Instead, dolomite replaced the sides of the conceptacle walls and grew inwards. The walls therefore are either preserved as microcrystalline calcite or were leached out after dolomitization, leaving a mold (Fig. 3.7E,F). Alternatively, Type I dolomite may replace red algae fragments, but in a non-mimetic manner (Fig. 3.7D). Foraminifera were replaced by texture preserving but non-mimetic Type I dolomite, preserved as microcrystalline calcite, or leached. Replacement of foraminifera by dolomite is generally incomplete.

Grains of an original aragonitic composition (ie. bivalves, gastropods, green algae, and coral) have generally been completely leached from the matrix and their original presence can only be recognized from moldic porosity. Such pores may be lined by dolomite cement. Interstitial micritic muds in the coral skeletons resisted leaching and were generally replaced by Type I dolomite, and acted as a substrate for limpid dolomite cement. Bivalve fragments are, in some rare exceptions, found partially

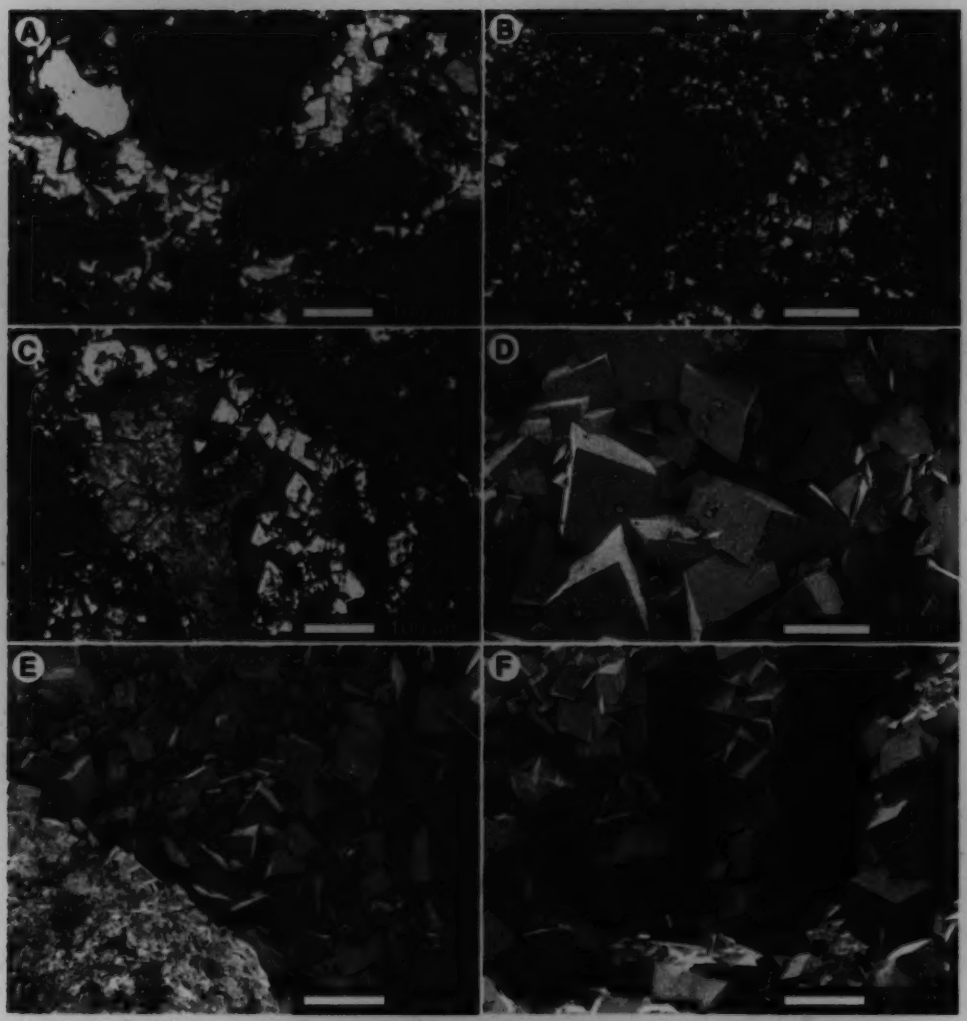

Figure 3.6. Limpid dolomite in Pedro Castle Formation on Cayman Brac. All samples from section SQA-2. A-C) Limpid dolomite growing into porosity from substrate. In B and C, coarse calcite cement (cc) precipitated after limpid dolomite, completely filling remaining porosity. D-F) Scanning electron micrographs of limpid dolomite. Note well defined euhedral crystals and interlocking relationships.

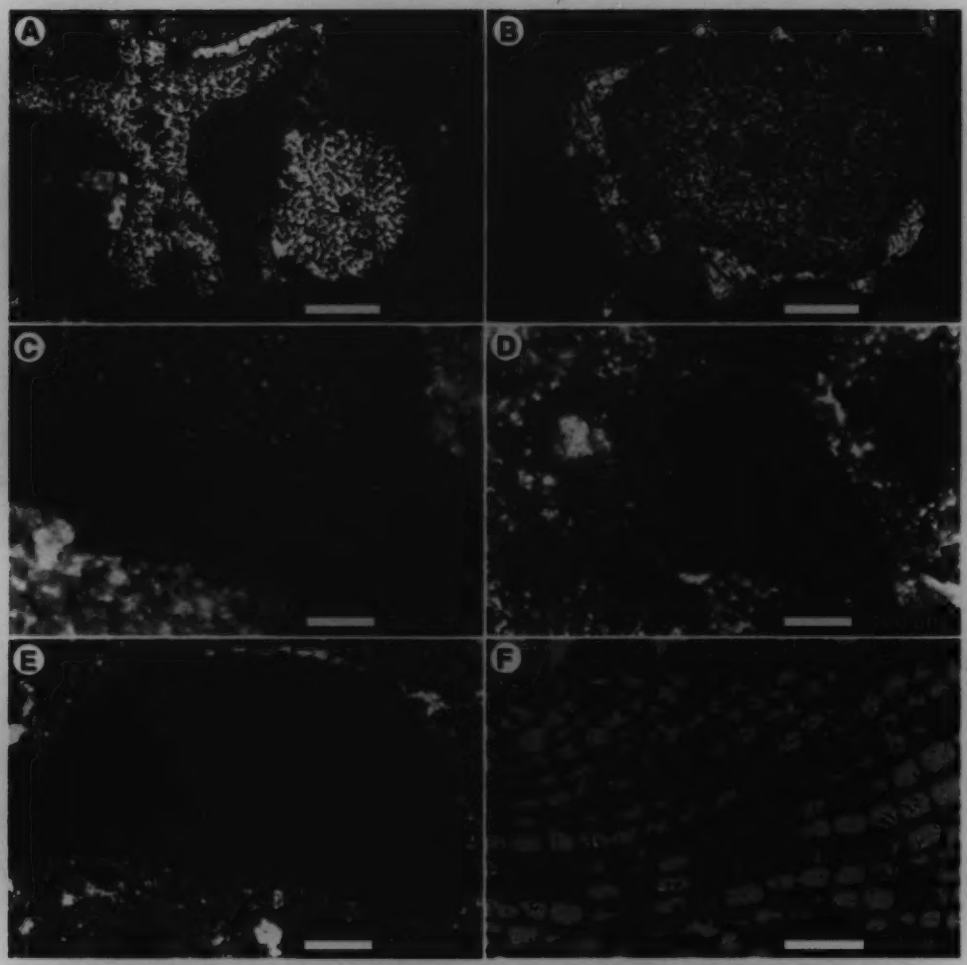

Figure 3.7. Skeletal grains and different degrees of replacement dolomitization in Pedro Castle Formation. A,B) Mimetic dolomitization of echinoderm plates and syntaxial cement overgrowths. (Section SQA-2). C) Red algae fragment (calcite) that has not been replaced, although surrounding matrix is pervasively replaced by Type I dolomite. (Section SQA-2). D) Non-mimetic partial replacement of red algae fragment by Type I dolomite. (Section GAM). E) Poor replacement of red algae fragment by Type I dolomite. Blue stain in epoxy (not obvious in photomicrograph) highlights moldic porosity formed after selective leaching of cell walls. (Section GAM). F) Electron microprobe image. White = calcite, grey = dolomite, and black = porosity. Note how walls were lined with dolomite that grew into conceptacles, and that subsequent leaching of calcitic walls resulted in moldic porosity. (Section GAM).

preserved and these may or may not have been replaced by texture preserving Type I dolomite.

Pattern of Dolomitization

The degree of dolomitization decreases vertically as the distance from the Cayman Unconformity increases. This is reflected in the degree of dolomite replacement of skeletal grains, and the completeness of matrix replacement. Dolomite replacement of red algae fragments is only found near the base of the formation (ie. basal 1 m) where the matrix has been pervasively replaced. The best replacement of foraminifera is also near the base of the formation.

In the Pedro Castle Formation on Cayman Brac, the basal dolostone (>75% replacement dolomite) grades upwards over 1 – 2 m into dolomitic limestone (20-75% replacement dolomite). The upper exposures of the formation is either dolomitic limestone or limestone.

The lateral distribution of dolomite in the Pedro Castle Formation is also variable (Fig. 3.8). Sections along the north coast (BLX, GAM, GMD, and STS) are composed of dolostone that grades upwards into dolomitic limestone. This trend continues to the south, and is present in the northern half of the Active Scott Quarry. Sections SQA and SQA-1, the southern most sections in the quarry, however, are formed of limestone. The sharp lateral transition from sections of dolostone and dolomitic limestone to sections of limestone in the Active Scott Quarry indicates a very sharp edge to the dolomitization front.

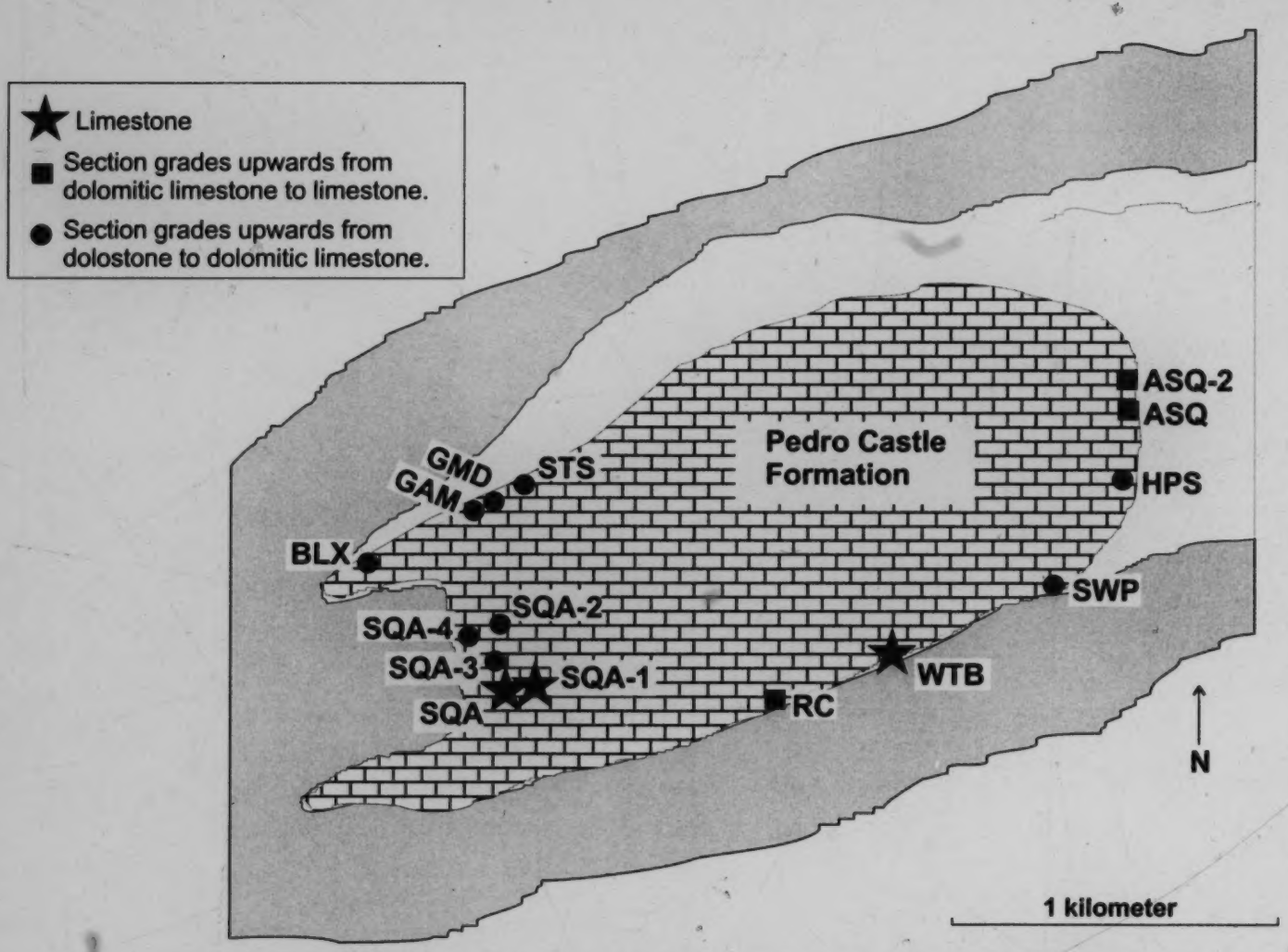

Fig. 3.8. Distribution of dolostone and limestone in the Pedro Castle Formation.

The pattern of dolomite distribution along the eastern and southern edge of the Pedro Castle Formation is more varied. Sections ASQ and ASQ-2 are dolomitic limestones at the bases of the sections, and grade over less than a meter into limestones. These sections, however, show evidence of intensive meteoric alteration and recrystallization, which may have destroyed the dolomitization. Sections HPS and SWP are composed of dolostone and dolomitic limestone. Section WTB is limestone and section RC is dolomitic limestone and limestone (Jones and Hunter 1994a).

3.4 Diagenesis Stage IV; Meteoric Diagenesis

Intense diagenesis of the Pedro Castle Formation has taken place in the meteoric realm resulting in numerous micro- and macroscopic features. The most prevalent diagenetic feature from the meteoric phreatic zone has been cementation by coarse calcite. Coarse calcite cement and drusy calcite (Fig. 3.9A) fill or partially occlude all types of porosity in the Pedro Castle Formation. Calcite crystals with scalenohedron terminations are found in some pores where cementation has not been complete, indicating that the pore space was filled with fluid at the time of cement growth. The coarse calcite spar and drusy calcite are interpreted to have been precipitated in the meteoric phreatic zone, based on the lack of pendant or meniscus type cements. This conclusion is consistent with a number of other studies that have reviewed calcite cements (Land 1970, 1971; Friedman and Kolesar 1971; Jones et al. 1984; Harris et al. 1985; Aissaoui et al. 1986; James and Choquette 1990b; Quinn 1991).

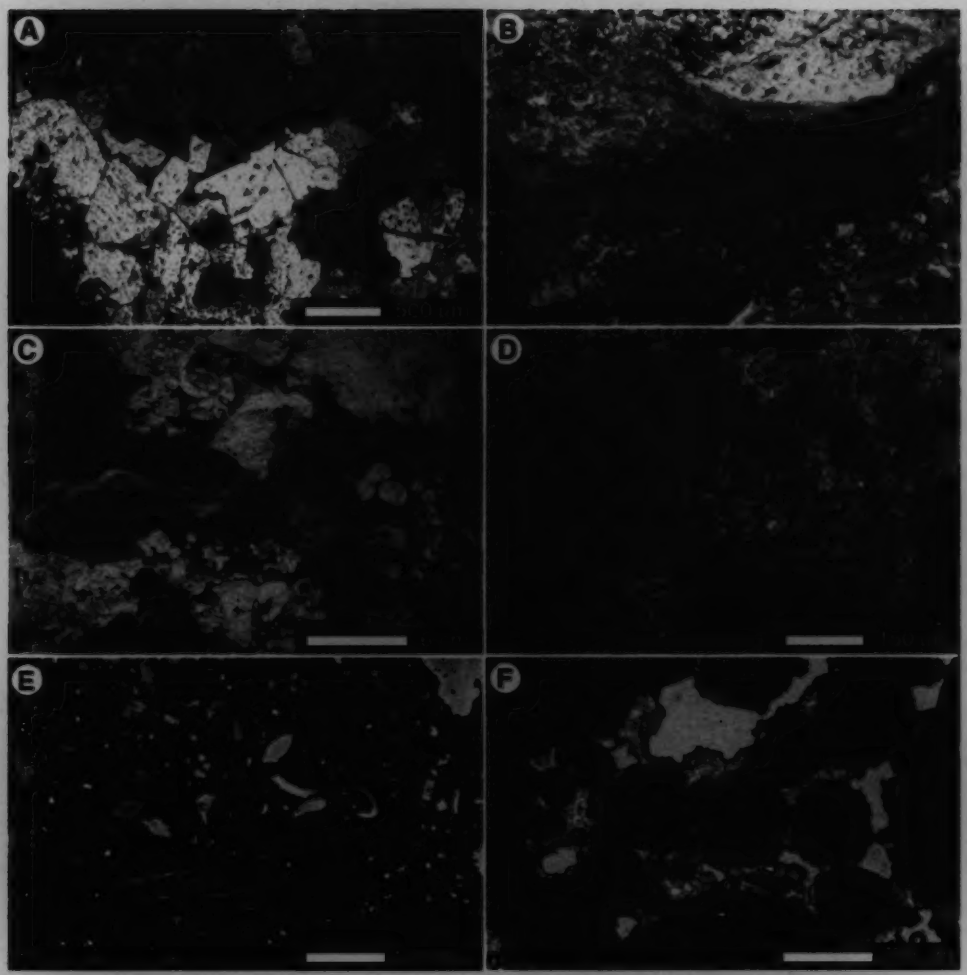

Figure 3.9. A) Drusy calcite (crossed-nichols)(Section SQA-2). B) Horizontal cave with stalactites and flowstone in Active Scott Quarry (Section SQA-1). Hammer (left of center) is ~30 cm tall. C) Rubble breccia associated with rhizoconcretion. Terra rossa and calcite rinds partially fill the cavity. (Section SWP). D) Scanning electron micrograph of fungal hyphae coated with calcite in recrystallized matrix. (Section SQA-2). E) Chalky texture produced by leaching of coarse calcite cement from matrix. Good intergranular/ intercrystalline and moldic porosity. (Section SQA-2). F) Vadose pisoids. (Section SQA-4).

Diagenesis in the vadose zone is exemplified by intensive phytokarst development. Carbonate dissolution widened joints and fractures and produced small subsurface karst features. Two horizontal, discoid shaped caves are present in the Active Scott Quarry (Fig. 3.9B). These caves are approximately 0.75 m high and 3 m long. Speleothems found in the caves include stalactites, stalagmites, and flowstone. The shape of the caves suggests that they developed at a paleo-water table level (cf. James and Choquette 1990b). On a microscale, where dissolution in the vadose zone of the coarse calcite cement has been most intense (Fig. 3.9E), a chalky, mottled appearance can be observed in hand sample.

Maroon-coloured and rusty yellow-coloured terra rossa partially lines and fills voids in the Pedro Castle Formation. Rhizoconcretions (Fig. 3.9C) from the microscopic to centrimetric scale, which are abundant in the Pedro Castle Formation, are most common within two meters of the modern exposure surface. Rhizoconcretions, however, are also found at deeper stratigraphic levels of three and four meters (ie. Section SQA-3 and SWP). In thin section, alveolar structures and fungal hyphae (Fig. 3.9D) are found with the rhizoconcretions.

Vadose cements are only found associated with pisoliths and terrestrial oncoids hosted in terra rossa that is filling cavities (Fig. 3.9F). Spectacular meniscus cements are found within these infilling sediments; pendant or gravitational cements are less common. Microstalactites and cement rinds that are best described as microscale flowstone deposits are found in large pore spaces.

3.5 Summary

Diagenesis of the Pedro Castle Formation significantly altered many of the original limestones. Following micritization and cementation on the seafloor and during shallow burial, a change in the ambient fluids caused selective dissolution of most aragonitic components. Later, dolomitization selectively replaced the remaining micritic component of the limestone, micritic envelopes, and certain skeletal components. Mimetic dolomite replacement of red algae or foraminifera is rare in the Pedro Castle Formation. Post-dolomitization, coarse low-Mg^{2+} calcite cements precipitated in the meteoric phreatic zone and filled or partially filled remaining porosity. Diagenesis in the meteoric vadose zone has resulted in wholesale dissolution and development of surface and sub-surface karst features and increased net porosity and permeability in the formation.

Chapter Four – Isotopic Geochemistry of Calcite

4.0 Introduction

Limestones and dolomitic limestones in the Pedro Castle Formation contain matrix calcite, sparry meteoric calcite cements, biogenic calcite, and marine cements (limited to section SQA-1). The modal abundance of the different types of calcite is highly variable. Very finely crystalline (generally < 20μm) dolomite is found in the matrix, and its small size precluded physical separation of the calcite from the dolomite for isotopic analyses. Bulk samples for isotopic analyses were prepared so that large allochems and visible patches of sparry calcite were avoided. Nonetheless, sparry calcite cements, especially when filling intercrystalline porosity, were unavoidable and probably included in the analyzed samples. Consequently, the $\delta^{13}C$ and $\delta^{18}O$ isotope values for the calcite in the Pedro Castle Formation, reflect all four types of calcite found in the formation.

4.1 Results of Calcite Isotopic Analyses

Calcite in the Pedro Castle Formation (Table 4.1) yielded $\delta^{13}C$ values that range from -8.40‰ to -2.25‰ and $\delta^{18}O$ values from -6.18‰ to -2.41‰. Cross-plotting of $\delta^{13}C$ and $\delta^{18}O$ values (Fig. 4.1) defines a covariant trend. The average $\delta^{18}O$ value is -4.33‰. Strontium isotopic ratios (n = 3) (Appendix 2) in calcite, determined from samples collected from SQA-1 and SQA-2, range from 0.709070 ±0.000011 to 0.709093 ±0.000015, and average 0.709081 ±0.000015.

In sections SQA-2, SQA-4, HPS, GAM, STS, and ASQ-2, the $\delta^{13}C$ values are highly variable (Table 4.1, Fig. 4.2). Trends of the $\delta^{18}O$ values between sections are

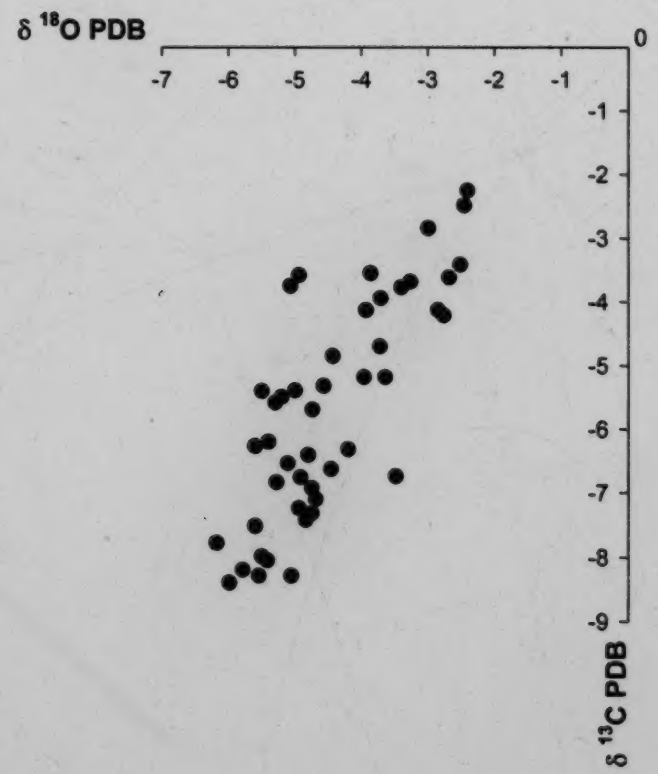

Fig. 4.1. $\delta^{18}O$ and $\delta^{13}C$ isotopic composition of calcite in Pedro Castle Formation on Cayman Brac (n = 46).

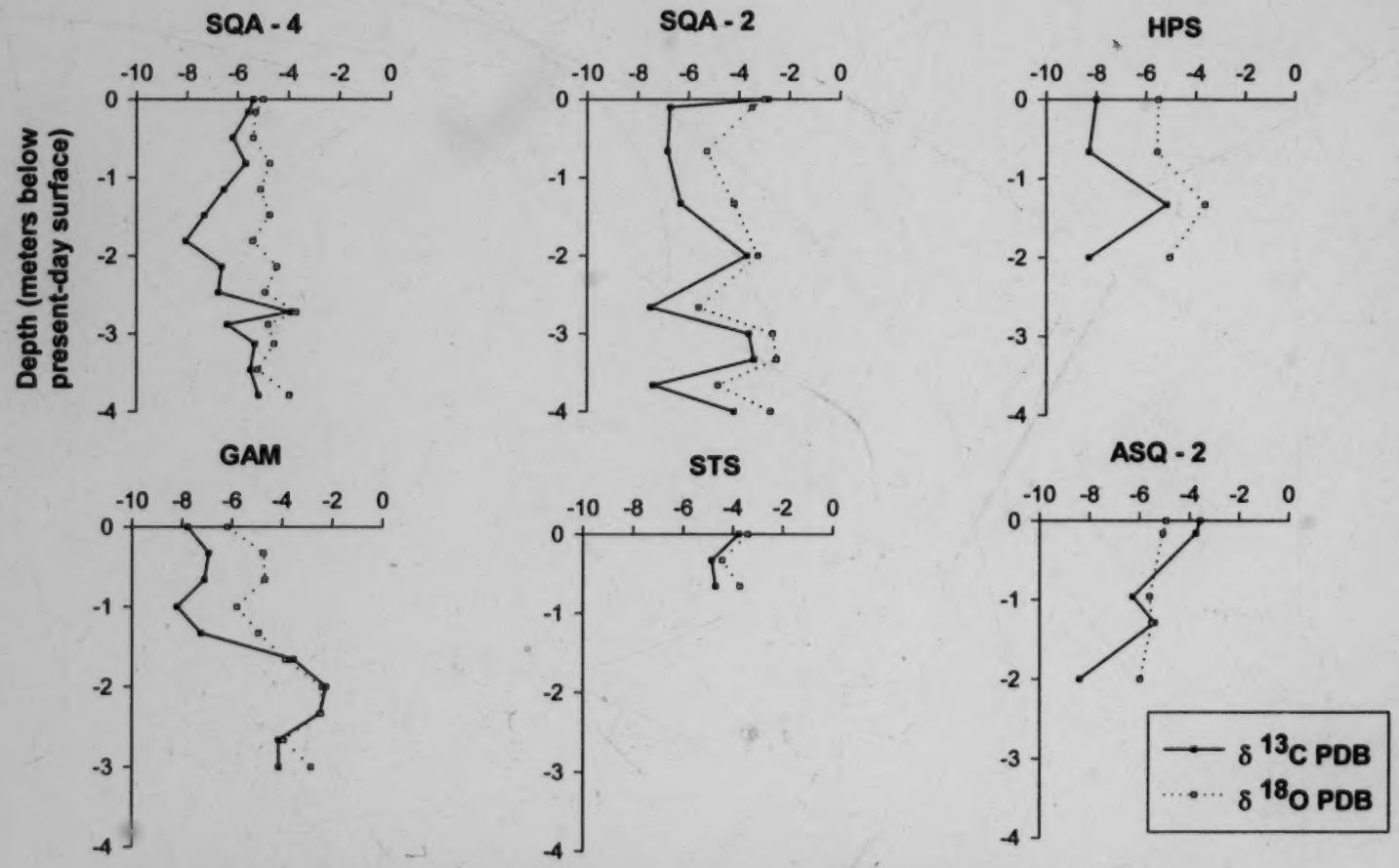

Fig. 4.2. Isotopic composition of calcite in Pedro Castle Formation from six representative sections. Section SQA - 4 is best example of invariable $\delta^{18}O$ values coupled with variable $\delta^{13}C$ values. Sections SQA - 2 and GAM have variable $\delta^{18}O$ values with depth.

not consistent. In sections SQA-2 and GAM, the $\delta^{18}O$ value is variable with depth (Fig. 4.2). Section SQA-4, however, displays a relatively invariable $\delta^{18}O$ trend with depth. The $\delta^{18}O$ values in sections HPS, STS, and ASQ-2 also show little change with depth. This however, may be a reflection of the limited thickness of the Pedro Castle Formation at those localities.

Table 4.1. Carbon and oxygen stable isotopes of calcite in the Pedro Castle Formation on Cayman Brac. Depth (m) was measured from modern day surface. (*) indicate samples considered contaminated with CO_2 from calcian dolomite (see discussion).

Section/Sample	Depth (m)	‰ $\delta^{13}C$ (PDB)	‰ $\delta^{18}O$ (PDB)	Section/Sample	Depth (m)	‰ $\delta^{13}C$ (PDB)	‰ $\delta^{18}O$ (PDB)
GAM-15	-0.05	-7.78	-6.18	SQA-2 (5012.2)	-0.05	-2.84	-2.99
GAM-14	-0.33	-6.93	-4.75	SQA-2 (5011)	-0.10	-6.74	-3.48
GAM-13	-0.66	-7.10	-4.69	SQA-2 (5010)	-0.66	-6.84	-5.28
GAM-12	-1.0	-8.20	-5.79	SQA-2 (5009)	-1.33	-6.32	-4.20
GAM-11	-1.33	-7.24	-4.94	SQA-2 (5008)	-2.00	-3.68	-3.26
GAM-10	-1.66	-3.55	-3.86	SQA-2 (5007)	-2.66	-7.52	-5.60
GAM-9*	-2.00	-2.28	-2.41	SQA-2 (5006)*	-3.00	-3.62	-2.68
GAM-8*	-2.33	-2.51	-2.45	SQA-2 (5005)*	-3.33	-3.41	-2.51
GAM-7	-2.66	-4.17	-3.93	SQA-2 (5004)	-3.66	-7.42	-4.84
GAM-6*	-3.0	-4.16	-2.85	SQA-2 (5003.2)*	-4.00	-4.21	-2.76
HPS-15	-0.05	-7.99	-5.50	SQA-4 (5042)	-0.05	-5.39	-5.00
HPS-14	-0.66	-8.29	-5.55	SQA-4 (5041)	-0.16	-5.58	-5.30
HPS-13	-1.33	-3.64	-3.64	SQA-4 (5040)	-0.49	-6.20	-5.40
HPS-12	-2.00	-5.06	-5.06	SQA-4 (5039)	-0.82	-5.69	-4.74
STS-15	-0.05	-3.40	-3.40	SQA-4 (5038.2)	-1.15	-6.54	-5.11
STS-14	-0.33	-4.43	-4.43	SQA-4 (5037)	-1.48	-7.32	-4.75
STS-13	-0.66	-3.72	-3.72	SQA-4 (5036)	-1.81	-8.05	-5.42
ASQ-2 (5057)	-0.05	-4.94	-4.94	SQA-4 (5035)	-2.14	-6.63	-4.46
ASQ-2 (5060)	-0.16	-5.07	-5.07	SQA-4 (5034)	-2.47	-6.76	-4.92
ASQ-2 (5054)	-0.96	-5.60	-5.60	SQA-4 (5033)	-2.72	-3.94	-3.71
ASQ-2 (5053)	-1.29	-5.50	-5.50	SQA-4 (5032.2)	-2.88	-6.41	-4.80
ASQ-2 (5051)	-2.00	-5.99	-5.99	SQA-4 (5031)	-3.13	-5.32	-4.57
				SQA-4 (5030)	-3.46	-5.49	-5.20
				SQA-4 (5029)	-3.79	-5.18	-3.96

4.2 Discussion

The stable isotopic signatures are averages of three types of calcite, and, in the case of section SQA-1, additional marine calcite cements. X-ray diffraction, however, demonstrates that all calcite in the Pedro Castle Formation is low magnesium calcite (mean = 2.5-3% $MgCO_3$), indicating compositional stabilization of the calcite. Associated with this process is an exchange of isotopes with the diagenetic fluid (Allan and Matthews 1982; Lohmann 1988). Numerous investigations have associated calcite stabilization with the meteoric phreatic environment (e.g. Land 1970; Allan and Matthews 1982; Harris et al. 1985; James and Choquette 1990b; Quinn 1991). The same change is assumed for the marine calcites in the Pedro Castle Formation. The coarse, sparry calcite cements probably formed by precipitation in the meteoric phreatic zone (e.g. Land 1970, 1971; Friedman and Koselar 1971; Jones et al. 1984; Harris et al. 1985; Aissaoui et al. 1986; James and Choquette 1990b; Quinn 1991). It is therefore assumed that stabilization of the original marine calcite phases, and any residual aragonite that was not leached, and precipitation of the sparry calcite cements probably took place in the meteoric phreatic environment, possibly simultaneously. This implies that the four types of calcite should all have similar isotopic signatures because they were all altered or precipitated from the same fluid in more or less the same diagenetic environment. There is no evidence that the Pedro Castle Formation has been subjected to more than one event of post-dolomitization meteoric diagenesis.

Diagenetic products in the meteoric realm should reflect highly variable $\delta^{13}C$ values and relatively invariable $\delta^{18}O$ values (e.g. Allan and Matthews 1982; Lohmann

1988; James and Choquette 1990b; Quinn 1991). Lohmann (1988) defined this trend as the *meteoric calcite line.* In an ideal situation, the meteoric calcite line is vertical and defines the $\delta^{18}O_{calcite}$ value. Lohmann (1988) noted, however, that the trend may deviate in response to (a) cumulative rock-water interaction resulting in more positive $\delta^{13}C$ values with depth and possibly a shift towards more positive $\delta^{18}O$ values or (b) intense surface evaporation resulting in positive $\delta^{18}O$ shifts coupled with very depleted $\delta^{13}C$ values (due to soil gas at the surface). The latter of these should be accompanied by caliche development.

The trend of data for calcite in the Pedro Castle Formation (Fig. 4.1) is not a normal trend for diagenesis and precipitation in the meteoric environment. Separation of these data by each respective section helps to resolve the isotopic trends. The trends in sections (Fig. 4.2) SQA-4, HPS, STS, and ASQ-2 are consistent with meteoric diagenesis (cf. Lohmann 1988). Sections SQA-2 and GAM are problematic because the oxygen isotopic trend in those sections becomes variable with depths below ~2 m, not typical of trends reflecting meteoric diagenesis (cf. Lohmann 1988). The data in these two sections accounts for the unexpected trend of the collective data plotted irrespective of location (Fig. 4.1). The variability with depth in sections SQA-2 and GAM is produced by an enrichment of ^{18}O with depth (Fig. 4.3), for which there are three possible explanations.

a) The calcite reflects an increase in water salinity, consistent with the upper meteoric phreatic – marine phreatic mixing zone. The saline waters are contributing ^{18}O which results in more positive $\delta^{18}O$ values.

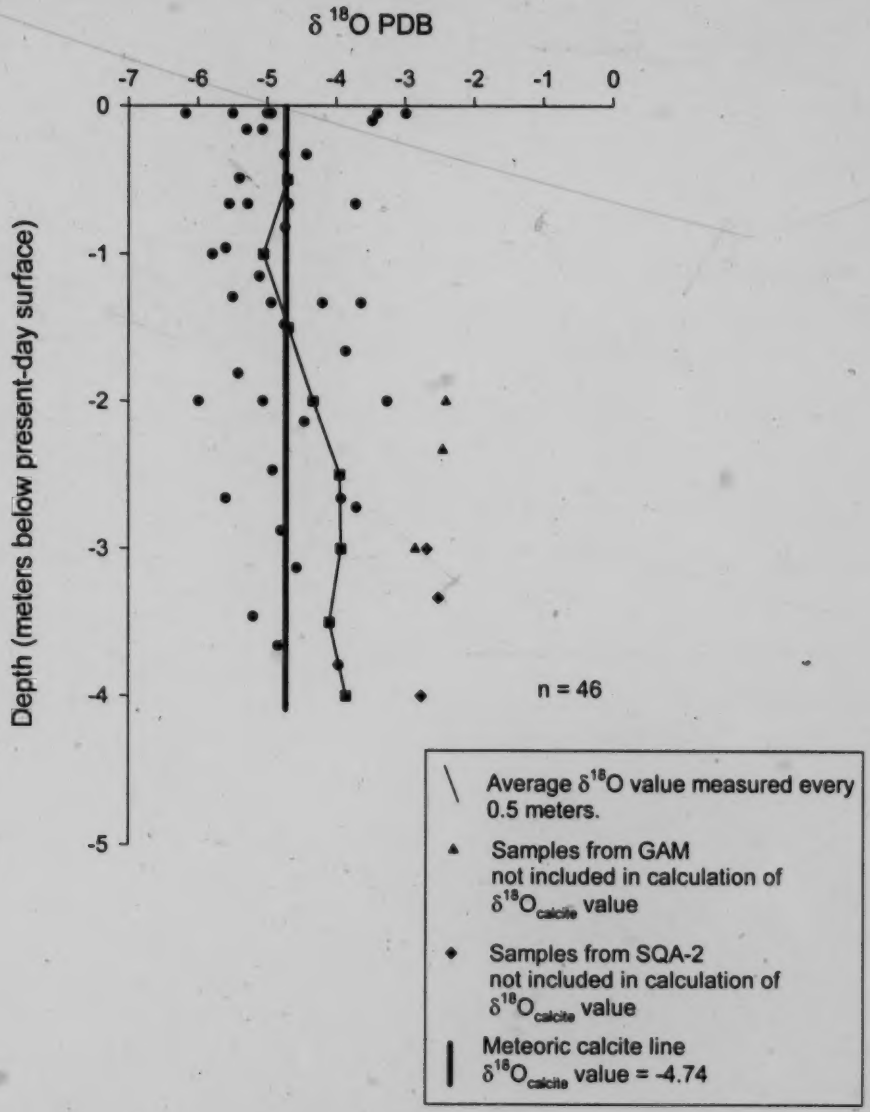

Fig. 4.3. $\delta^{18}O$ (PDB) values of calcite in Pedro Castle Formation plotted against depth (m) irrespective of location. Note that range of $\delta^{18}O$ values increases with depth, affecting overall average of the $\delta^{18}O_{calcite}$ value. The meteoric calcite line produced if the values below 2 m depth and heavier than -3 parts per mil (n = 6, from sections SQA-2 and GAM) are not included is plotted.

b) Increased rock-water interaction with depth caused the precipitation of cements of equivalent isotopic composition to dissolving meta-stable phases (Lohmann 1988). The result is a trend to more positive, marine $\delta^{18}O$ values.

c) A laboratory error factor. Contamination of the calcite CO_2 gas samples with CO_2 produced by simultaneous dissolution of the most calcian dolomite phases may cause shifts towards more positive $\delta^{18}O$ values.

There are two indications that the cause of enriched $\delta^{18}O$ values with depth in sections SQA-2 and GAM is not due to a mixing-zone or marine influence. First, section SQA-4, located only ~100 m from SQA-2, shows no variability in the $\delta^{18}O$ value with depth (Fig. 4.2). Second, the carbon signatures in sections SQA-2 and GAM are typical of meteoric signatures without a mixing-zone or marine influence (Machel and Burton 1994).

The primary cause of variability in the $\delta^{18}O$ signature with depth in sections SQA-2 and GAM is probably due to contamination of the calcite gas sample with CO_2 produced by simultaneous dissolution of the most calcian dolomite phases (see Appendix 2). The contamination coincides with more pervasive dolomitization near the base of the sections, and is unavoidable without a process of calcite microsampling.

Accepting that a significant increase in dolomitization at depths below 2 m caused unavoidable contamination of some samples in sections GAM and SQA-2, the isotopic trend of calcite in the Pedro Castle Formation can be reconsidered. Samples from depths below 2 m with $\delta^{18}O$ values heavier than - 3‰ (Table 4.1, Fig. 4.3) are

suspected of partial contamination and removed from the data set. This reduced range of $\delta^{18}O$ values is more consistent with a trend of meteoric diagenesis (cf. Allan and Matthews 1982; Lohmann 1988; James and Choquette 1990b). A reasonable meteoric calcite line can now be defined. The $\delta^{18}O_{calcite}$ value is measured from this line as -4.74‰.

Establishment of the $\delta^{18}O_{calcite}$ value (-4.74‰) is important for evaluating the water chemistry and temperature of fluids that mediated alteration and precipitation of calcite in the Pedro Castle Formation. Using data (Table 4.2) on the water chemistry for the Cayman Islands (Ng 1990) and measured subsurface aquifer temperatures (Ng 1990), the possibility of sea water, highly (>15% sea water) brackish, lightly (<15% sea water) brackish, and fresh ground water as the diagenetic fluid can be evaluated using the equation (Friedman and O'Neil 1977):

$$10^3 \ln\alpha = (2.78)(10^6)(T^{-2}) - 2.89 \qquad [1]$$

Where $\alpha = [1000 + \delta^{18}O_{(calcite)}‰ \text{ SMOW} / 1000 + \delta^{18}O_{(water)}‰ \text{ SMOW}]$ and T = °K. Conversions between the standards PDB and SMOW are expressed by equations [2a] and [2b] (Kyser 1987).

$$\delta^{18}O_{V\text{-}SMOW} = (1.03091)(\delta^{18}O_{PDB}) + 30.91 \qquad [2a]$$

$$\delta^{18}O_{PDB} = (0.97002)(\delta^{18}O_{V\text{-}SMOW}) - 29.98 \qquad [2b]$$

The standards Vienna Standard Mean Oceanic Water (V-SMOW) and SMOW are considered identical (Kyser 1987).

The calculated temperatures of highly brackish (39.7°C) and sea water (44.5°C) parent fluids for calcite in the Pedro Castle Formation (Table 4.2) are not reasonable without some unknown thermal source. The temperature calculated for a fresh ground water (16.7°C) parent fluid for calcite in the Pedro Castle Formation is also lower than expected for a tropical island. Ng (1990) found that the average temperature of shallow subsurface mixing-zones in the Cayman Islands is ~27-30°C and 25-27°C for deeper, saline waters. Consideration of these measured temperatures with the range of temperatures for possible parent fluids (Table 4.2) indicates that the $\delta^{18}O$ of calcite was in equilibrium with "lightly brackish fluids" to near "highly brackish fluids" in the meteoric phreatic – marine phreatic mixing zone.

Table 4.2. Different types of water found in the phreatic zone on Cayman Brac. All terms and data except the calculated temperature of calcite formation are from Ng (1990).

Water type	Average isotopic composition (SMOW)	Salinity	Calculated temperature of calcite formation
Fresh ground water	-4.54‰	<1.01 ppt	16.7°C
Lightly brackish water	-4.16‰	<15% sea water	18.4°C
Highly brackish water	0.14‰	>15% sea water	39.7°C
Sea water	0.5 – 1.0‰	~35 ppt	44.5°C

Ng (1990) reached a similar conclusion that waters ranging from fresh to mixed with up to 45% sea water could account for the diagenesis of calcite in the Cayman Formation and Pedro Castle Formation on Grand Cayman. These conclusions, however, are in contrast to the general interpretation that coarse calcite cements are

produced in the meteoric phreatic zone (Land 1970, 1971; Friedman and Koselar 1971; Jones et al. 1984; Harris et al. 1985; Aissaoui et al. 1986; James and Choquette 1990b; Quinn 1991) and that the mixing zone is generally a zone of intense dissolution, not precipitation or incongruent alteration (Plummer 1975; Lohmann 1988; James and Choquette 1990b).

For calcite in the Pedro Castle Formation on Cayman Brac, the unusual water chemistry suggested by the stable isotopes may be related to the method of whole-rock sampling. As Quinn (1991) noted, whole-rock sampling results in the physical mixing of chemical end-members; an event reflected in the final data. It is therefore possible that the $\delta^{18}O_{calcite}$ value of -4.74‰ is an intermediate between the true meteoric phreatic signal and the marine calcite isotopic signal. Interpretation of the $\delta^{18}O_{calcite}$ value as an intermediate value would account for the calculated brackish fluid composition that is in contrast to the expected result of a fresh ground water composition.

Based on previous conclusions about the water chemistry and calcite saturation conditions in mixed waters by Plummer (1975), fabrics of meteoric phreatic cements on Grand Cayman by Jones et al. (1984), calcite cement fabrics by Harris et al. (1985), and both fabrics and geochemistry of meteoric cements by Aissaoui et al. (1986), Lohmann (1988), James and Choquette (1990b), and Quinn (1991), it is concluded that calcite in the Pedro Castle Formation was altered and cements precipitated in the meteoric phreatic zone. The evidence for waters of brackish composition is based on the use of the $\delta^{18}O_{calcite}$ value, which is considered to be

problematic due to a non-quantifiable $\delta^{18}O$ sea water contribution related to the method of bulk sampling.

4.3 Analogy

The data presented here parallels the study of meteoric diagenesis on Enewetak Atoll by Quinn (1991). In that investigation whole-rock sampling was conducted and a $\delta^{18}O_{calcite}$ value of -4.66‰ was defined. If this value is used in equation [1] with a value of –4.00‰ SMOW for meteoric water (Quinn 1991) the same mixed water chemistry is apparent. Furthermore, the data collected by Quinn (1991) do not fit the expected meteoric calcite line produced by theoretical modeling. Quinn (1991) concluded that the diagenesis, however, was meteoric phreatic and the isotopic data was a mix of chemical end members. This conclusion was based on modeling chemical variations, petrographic evidence, and previous studies. Similar to the comments of Quinn (1991), only a method of microsampling could further clarify the relationship between the measured isotopic signal of calcite in the Pedro Castle Formation and the calculated chemistry of the diagenetic fluid.

Chapter Five – Dolomite Geochemistry

5.0 Introduction

It is generally accepted that the only reasonable source of the Mg^{2+} required for formation of island dolomites (cf. Budd 1997) is seawater (Machel and Mountjoy 1986; Budd 1997). Seawater or a modified form of seawater (ie. evaporated seawater or seawater mixed with meteoric water) must therefore be used in any model of dolomitization. Potentially, the geochemistry of dolomite, particularly the oxygen, carbon, and strontium isotopic ratios, can be used to determine the nature of these fluids (e.g. Pleydell et al. 1990; Budd 1997).

The apparent inability to precipitate dolomite at surface conditions in the laboratory has limited the knowledge of isotopic fractionation and distribution coefficient values for dolomite (see Budd 1997 for review). The result is that interpretation of the geochemistry from a given set of dolomite may be complex and interpretation is subject to the values used by researcher. The stoichiometry of the dolomite has also been shown to be an important control on isotopic fractionations and strontium distributions (e.g. Vahrenkamp and Swart 1990, 1994). It is therefore important that dolomite geochemistry be used as a tool that compliments petrography and observed field relationships, and not be used alone to draw conclusions.

Dolomite in the Pedro Castle Formation has a geochemical signature similar to most other island dolomites (cf. Budd 1997), especially those thought to have formed from mixed seawater and meteoric fluids. Close examination of the data, however, and consideration of the petrography and style of dolomite replacement of the precursor limestone, provides an alternative conclusion. It is found that dolomite in

the Pedro Castle Formation formed from slightly modified seawater and that it replaced limestone that had experienced at least some meteoric alteration.

5.1 Analysis of Dolomite Population

Imperative to any geochemical investigation of dolomite is knowledge of how many compositional populations are present in the samples (e.g. Budd 1997; Jones et al. in press). If more than one compositional population exists, a method of microsampling must be used; otherwise the data will reflect physical mixing of the populations (Banner and Hanson 1990; Wheeler et al. 1999).

Petrographically, the dolostone in the Pedro Castle Formation (chapter 3) is formed of two types of replacement dolomite and two types of dolomite cement. XRD and EMPA of these dolostones, however, indicated that they are compositionally unimodal (Fig. 5.1, 5.2). EMPA of dolomite (n = 615) from seven samples in section SQA-2 indicated that the dolomite ranged in %Ca (%Ca following use by Lumsden and Chimahusky 1980) from 53.34% to 61.59%, and is calcian with a mean of 57.41 ±1.23 %Ca. XRD analyses of samples from sections GAM, HPS, STS, and SQA-4 indicated that dolomite in these sections is also unimodal in composition and are equivalent in %Ca to those samples from section SQA-2.

5.2 Carbon, Oxygen, and Strontium Results

Dolomite in the Pedro Castle Formation (Table 5.1) yielded $\delta^{13}C$ values of -1.81‰ to 1.42‰ and $\delta^{18}O$ values of -0.22‰ to 2.02‰. The mean $\delta^{13}C$ value (n = 36) was 0.29 ±0.70‰ and the mean $\delta^{18}O$ value was 1.09 ±0.53‰. Cross-plotting of these

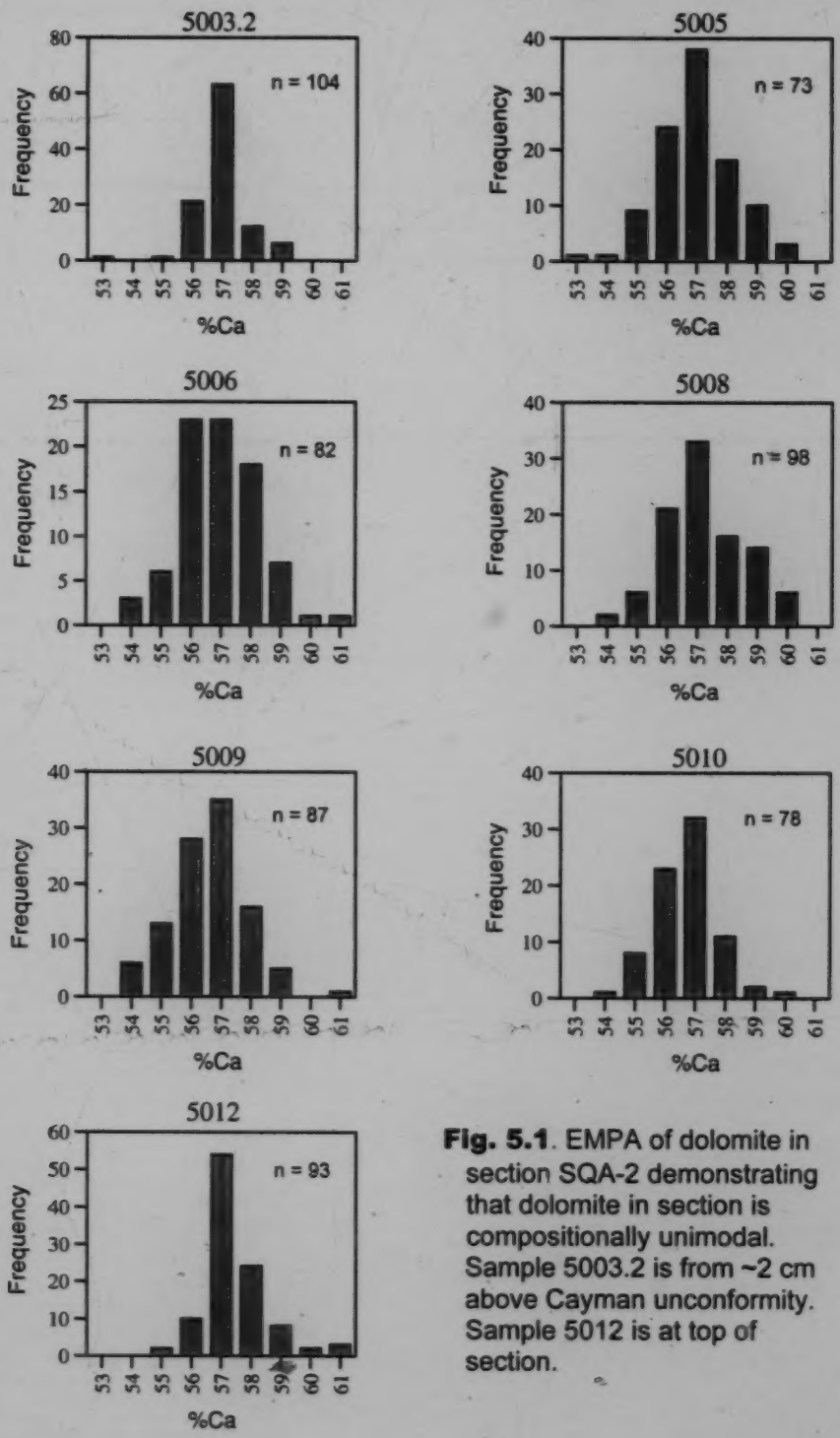

Fig. 5.1. EMPA of dolomite in section SQA-2 demonstrating that dolomite in section is compositionally unimodal. Sample 5003.2 is from ~2 cm above Cayman unconformity. Sample 5012 is at top of section.

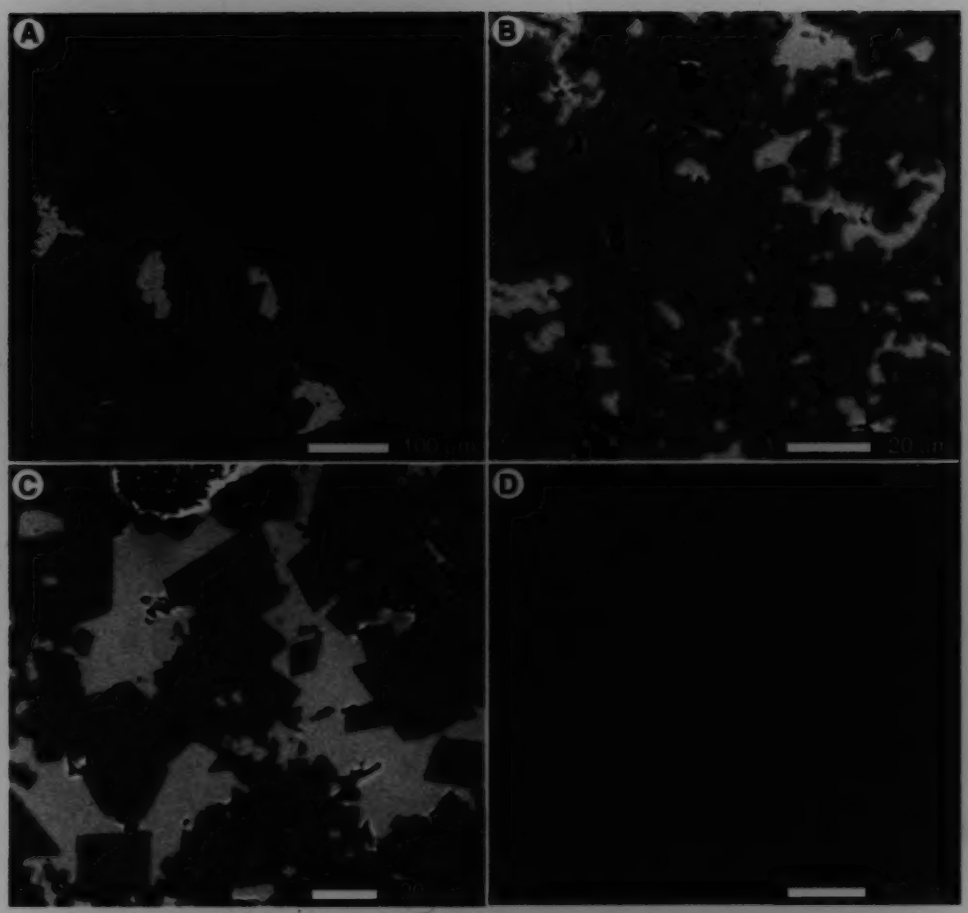

Figure 5.2. Electron microprobe backscattered electron images. Grey = dolomite, white= calcite, black = porosity. Samples A-C are from Pedro Castle Formation. A) Homogeneous dolomite in matrix around red algae fragment that has been leached. (Section SQA). B,C) Homogeneous dolomite in Section GAM. D) For comparison, mottled grey colour indicative of a heterogeous dolomite population in the Cayman Formation (Jones et al. in press). (Section SQA).

values (Fig. 5.3) produces a steeply positive co-variant to near vertical trend. Plotting the data for sections STS, GAM, SQA-2, and SQA-4 against depth (Fig. 5.4) shows a slight increase in the carbon isotopic ratios with depth. The oxygen isotopic trend is not consistent between sections.

The average strontium content (Table 5.2) in seven samples of Pedro Castle Formation dolomite from section SQA-2 is 358.49 ±22.92 ppm (n = 607). The average Sr/Ca ratio for dolomite in the Pedro Castle Formation is 0.00141 ±0.00009. Strontium isotopic ratios in dolomite from the Pedro Castle Formation (n = 14) range from 0.709032 ±0.000017 to 0.709108 ±0.000014 (Appendix 2).

Table 5.1. Carbon and oxygen stable isotopes of dolomite in the Pedro Castle Formation (PCF).

Section/ Sample	‰ $\delta^{13}C$ (PDB)	‰ $\delta^{18}O$ (PDB)	Section/ Sample	‰ $\delta^{13}C$ (PDB)	‰ $\delta^{18}O$ (PDB)
GAM-14	0.55	1.38	SQA-2 (5007)	-1.81	0.35
GAM-13	0.50	1.13	SQA-2 (5006)	0.63	0.94
GAM-12	-1.34	-0.22	SQA-2 (5005)	0.70	1.20
GAM-11	0.46	1.41	SQA-2 (5004)	0.52	1.25
GAM-10	0.63	0.86	SQA2(5003.2)	1.42	1.44
GAM-9	0.88	1.32	SQA-4 (5042)	-0.41	0.46
GAM-8	1.07	1.58	SQA-4 (5041)	-0.69	-0.06
GAM-7	0.78	0.91	SQA-4 (5040)	-0.35	0.29
GAM-6	0.76	1.49	SQA-4 (5039)	0.21	0.93
GAM-5.5A	1.16	1.61	SQA-4 (5038)	0.14	1.37
STS-15	0.92	1.43	SQA-4 (5037)	0.21	1.65
STS-14	1.06	1.38	SQA-4 (5036)	-0.37	0.99
STS-13	0.96	1.23	SQA-4 (5035)	0.49	1.07
SQA-2 (5012)	-0.21	1.97	SQA-4 (5034)	0.17	1.02
SQA-2 (5011)	0.17	2.02	SQA-4 (5033)	0.34	0.93
SQA-2 (5010)	-0.95	0.24	SQA-4 (5032)	0.39	1.34
SQA-2 (5009)	-0.07	1.38	SQA-4 (5031)	0.48	1.37
SQA-2 (5008)	0.75	1.38	SQA-4 (5029)	0.34	0.32

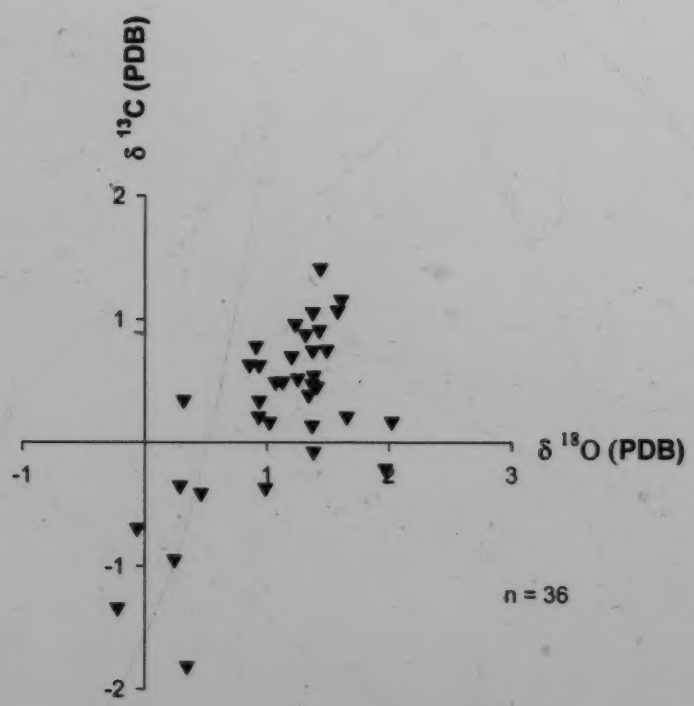

Fig. 5.3. Stable isotopic composition of dolomite in the Pedro Castle Formation, Cayman Brac.

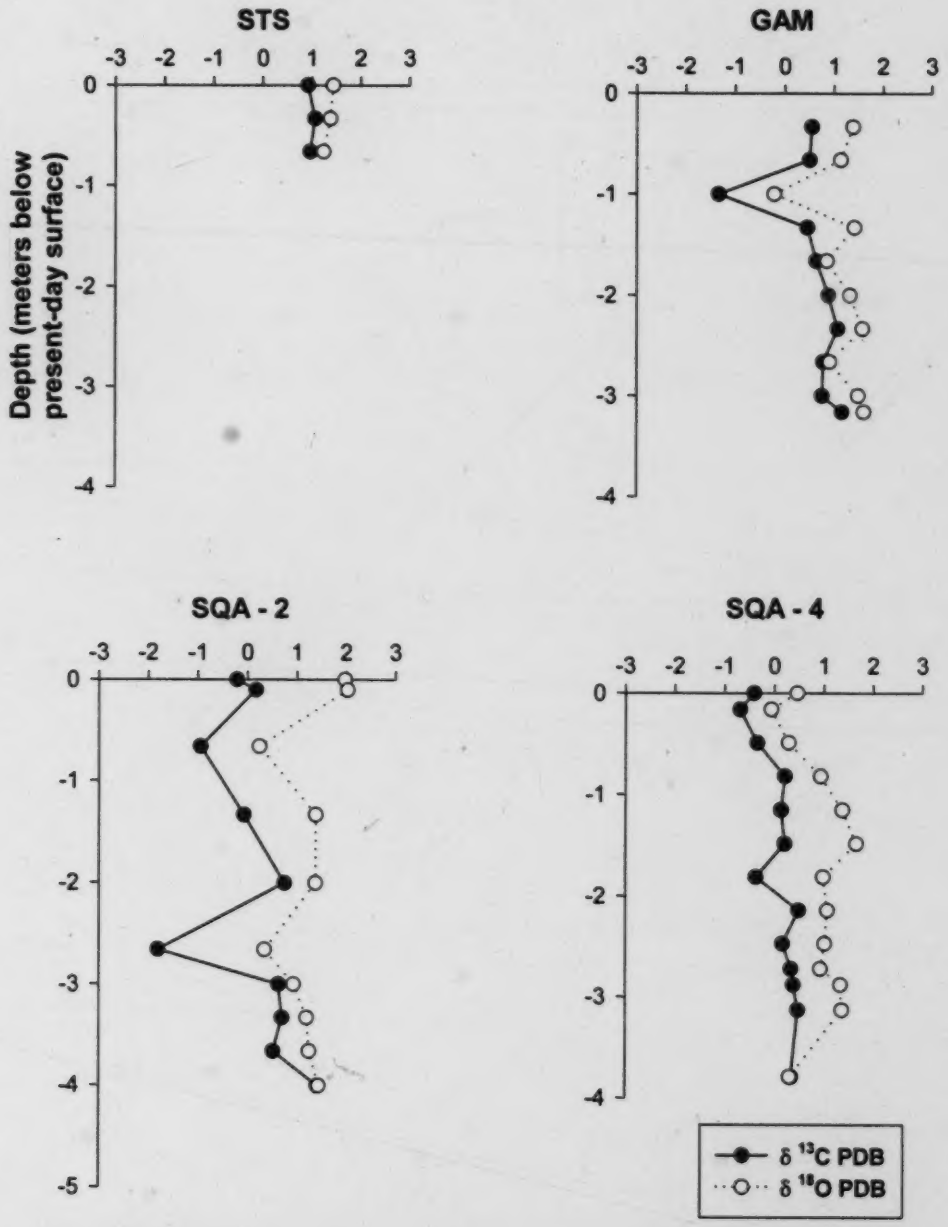

Fig. 5.4. Stable isotopic signature of dolomite in sections STS, GAM, SQA-2, and SQA-4. The oxygen isotopic signature in sections STS and GAM remains relatively unchanged with depth. In section SQA-2 a slight decrease in the oxygen isotopic signature occurs with depth. In section SQA-4 a slight increase in the oxygen isotopic signature occurs with depth. The carbon isotopic signature increases with depth in all sections.

5.3 Discussion

Dolomite stoichiometry:

Dolomite in the Pedro Castle Formation is calcian (average 57.41 %Ca) and comparable in stoichiometry to most island dolomites (cf. Budd 1997; Jones et al. in press). There is no evidence from any section of a second population of compositional dolomite in the Pedro Castle Formation on Cayman Brac. Increasing strontium content (Fig. 5.5) in the dolomite is found to correlate with increasing calcium content. This is consistent with the idea that Sr substitutes almost exclusively for Ca (Vahrenkamp and Swart 1990; Banner 1995; Budd 1997), and an increase in the Ca content facilitates more substitutions. A correlation between %Ca and $\delta^{18}O$ values (Fig. 5.6) (cf. Vahrenkamp and Swart 1994; Budd 1997) is poorly defined in the Pedro Castle Formation samples. No correlation is found in sections GAM or SQA-2. In section SQA-4, however, the $\delta^{18}O$ values become heavier with decreasing %Ca. It is possible that the range of %Ca in the dolomite population is too narrow to express any clear correlation with the oxygen isotopic signature.

Parent fluid to dolomitization:

The oxygen isotopic signature of dolomite in the Pedro Castle Formation is consistent with the oxygen isotopic signature of dolomite precipitated by seawater or a mix of seawater and meteoric water (Budd 1997). The range is not consistent with dolomitization by either evaporated seawater (Budd 1997) or brines mixed with meteoric water (cf. Gill et al. 1995; Meyers et al. 1997). The probability of seawater or a mixed seawater – meteoric water composition being the parent fluid to the

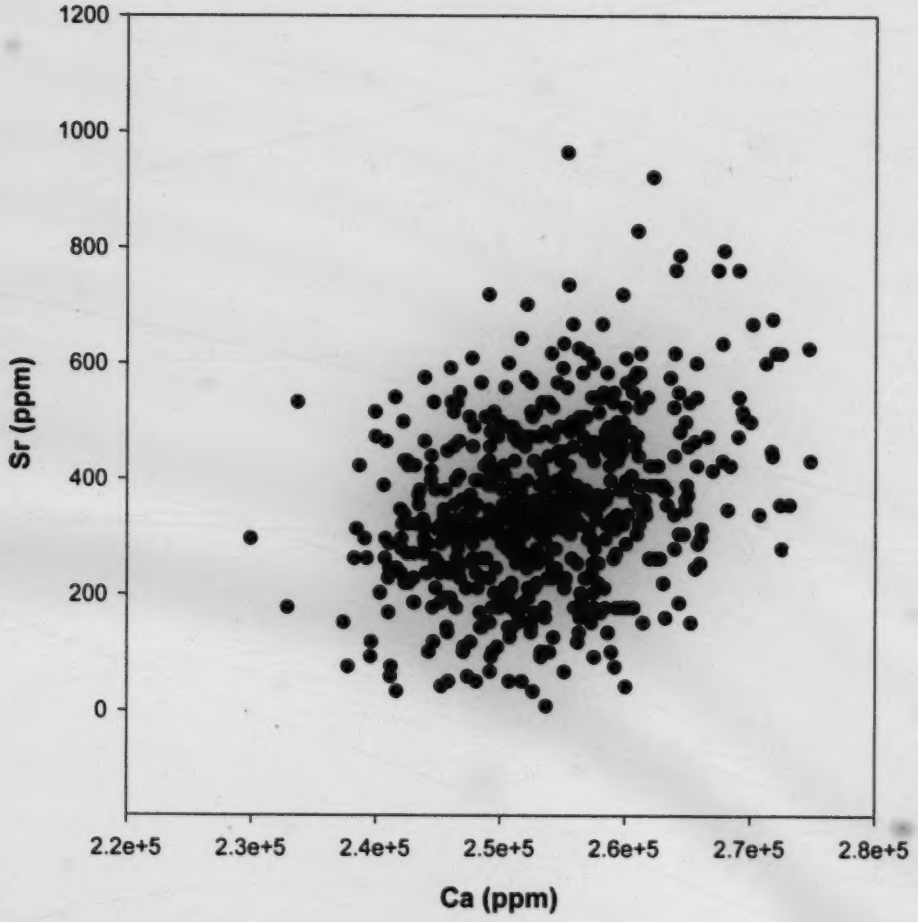

Fig. 5.5. Strontium versus calcium content (n = 604) in dolomite from Pedro Castle Formation. All data from section SQA-2 (7 samples).

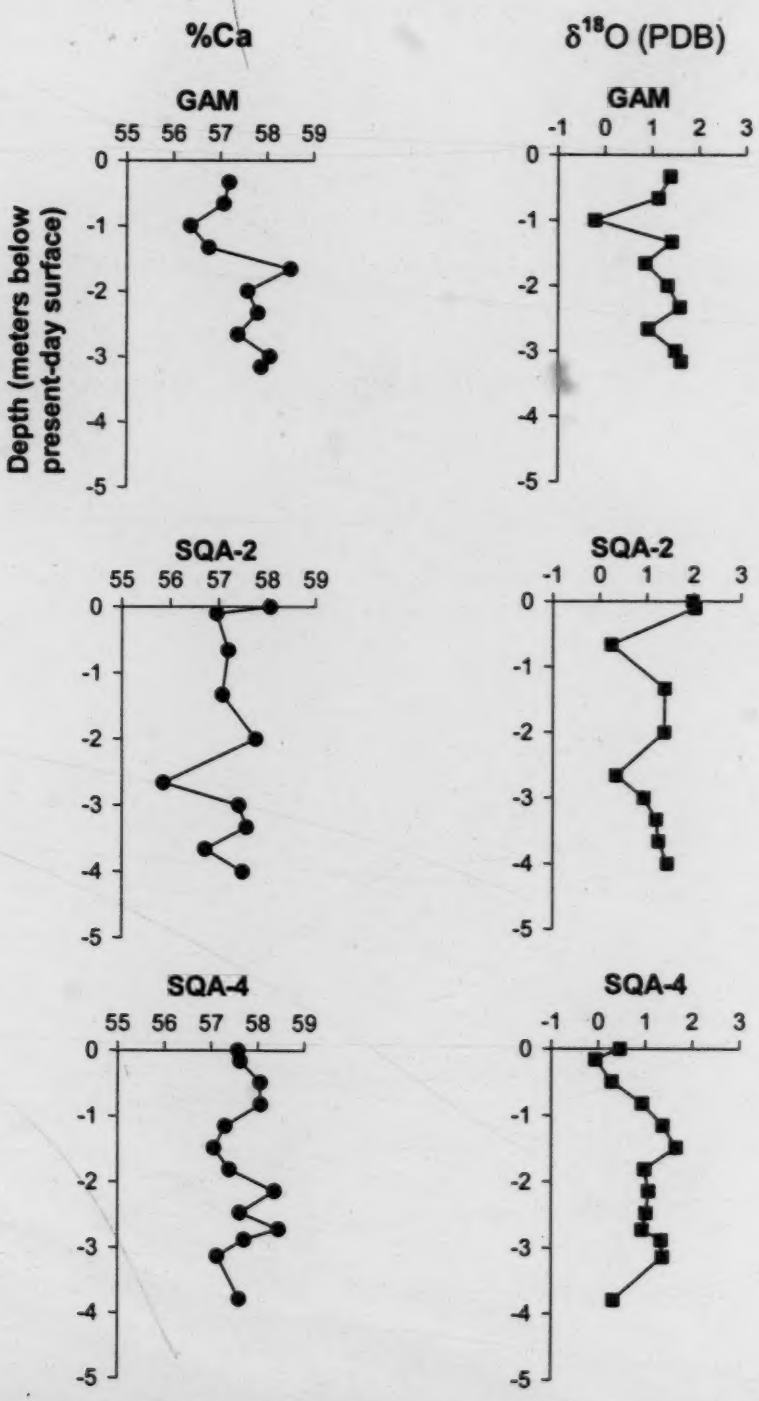

Fig. 5.6. Comparison of %Ca against depth to $\delta^{18}O$ against depth for sections GAM, SQA-2, and SQA-4.

dolomite may be evaluated (Table 5.3) with the equation by Friedman and O'Neil (1977) for the equilibrium precipitation of calcite (equation 1, Chapter 4) from water. This requires assuming a $\Delta_{calcite\text{-}dolomite}$ of 3‰ (Land 1985, 1991; Machel and Burton 1994; Vahrenkamp and Swart 1994; Swart and Melim 2000) and equilibrium precipitation. The method is mathematically equivalent to using the equation of Fritz and Smith (1970) for the isotopic fractionation between dolomite and water, which is based on extrapolations from high temperature experiments.

Table 5.2. Calculation (using oxygen isotopes) of the temperature from which dolomite might have grown, using data of different water compositions from the Cayman Islands (Ng 1990).

Water type	Average isotopic composition (SMOW)	Salinity	Calculated temperature of dolomite formation
Fresh groundwater	-4.54‰	<1.01 ppt	4.9°C
Lightly brackish water	-4.16‰	<15% seawater	6.3°C
Highly brackish water	0.14‰	>15% seawater	25°C
Seawater	0.5-1.0‰	~35 ppt	27.6-30.0°C

Modern oceanic waters at low latitudes are believed to be equivalent in temperature to oceanic waters at low latitudes in the Pliocene (Krantz 1991; Cronin and Dowsett 1993). This allows for comparison of modern measured temperatures to the theoretical temperatures calculated from the oxygen isotopic data. Shallow subsurface mixing-zone water on Grand Cayman has a temperature of 27-30°C, whereas the deep saline zone is 25-27°C (Ng 1990). Shallow lagoonal waters have a temperature of 27-34°C. The temperature of 25°C calculated (Table 5.2) for dolomite

precipitated from "highly brackish water" is cooler than measured modern mixing-zone temperatures. This temperature, however, is within a reasonable amount that it might be considered as a potential parent fluid to dolomitization. The temperature range from 27.6-30.0°C calculated for dolomite precipitated from seawater is in best agreement with the modern subsurface and surface temperatures measured by Ng (1990). The temperatures calculated for equilibrium precipitation of dolomite from "lightly brackish water" or fresh groundwater are unreasonable for a tropical island, even at depth (eg. Saller 1984, Whitaker et al. 1994). The agreement between the calculated temperature for seawater and the measured temperatures of seawater around the Cayman Islands favours seawater as the parent fluid for dolomitization.

The carbon isotopic signature of dolomite in the Pedro Castle Formation on Cayman Brac is not characteristic of dolomite replacing a marine carbonate precursor (cf. Ward and Halley 1985; Machel and Burton 1994; Vahrenkamp and Swart 1994; Banner 1995; Budd 1997). Depleted carbon isotopic signatures in dolomite may be caused by several different possibilities including ^{12}C enriched seawater resulting from the oxidation of organics (e.g., Machel and Burton 1994; Humphrey 2000), meteoric waters enriched in ^{12}C from vadose soil zones mixed with seawater (Lohmann 1988; Meyers et al. 1997), meteoric recrystallization of dolomite (Budd 1997; Meyers et al. 1997; Chafetz et al. 1999), or partial retention of a carbon signature from a precursor that experienced meteoric alteration (Vahrenkamp and Swart 1994; Budd 1997).

The first possibility is unlikely because the most negative carbon value is –1.81‰, significantly heavier than the extremely depleted values expected if oxidized organics

(ie. oxidation of methane) had contributed carbon to the system (cf. Machel and Burton 1994). The phenomenon of dolomite recrystallization at the near surface is poorly understood (Budd 1997), and is not likely the cause of depleted carbon values in the Pedro Castle Formation. If dolomite recrystallization had taken place, it would be expected that negative shifts in the oxygen isotopic signature would also occur, reflecting the meteoric signature (Lohmann 1988; Meyers et al. 1997). This is not a trend found in the Pedro Castle Formation. Recrystallization of dolomite should also change the dolomite stoichiometry to more ideal Ca/Mg ratios (Land 1985; Budd 1997; Meyers et al. 1997; Chafetz et al. 1999). The dolomite in the Pedro Castle Formation, however, is calcian dolomite.

Carbon derived from meteoric fluids when mixed with seawater will dominate the carbon isotopic signature of the hybrid fluid (Lohmann 1988). The result is a hyperbolic trend in the data defined by the depleted meteoric end member values (see chapter 4) and the heavier marine end member (2-4‰ PDB) value. This trend in the carbon signature is present in the Pedro Castle Formation, and is consistent with the possibility that mixed meteoric and marine waters mediated dolomitization.

The alternative to the mixed fluid possibility is that the precursor carbonate experienced some degree of meteoric alteration. Partial retention of the depleted carbon signature caused by this pre-dolomitization diagenesis would account for the carbon isotopic trend in the Pedro Castle Formation. An important consideration for this argument is that the rock:water ratio for porous carbonates relative to carbon is in excess of 10,000 (Budd 1997) making it very difficult for dolomitizing fluids to alter the precursor signature (Land 1980; Banner and Hanson 1990; Land 1991; Banner

1995; Budd 1997). The carbon isotopic signature of dolomite may therefore be inherited from the precursor, not the dolomitizing fluid.

The style of dolomite replacement in the Pedro Castle Formation is consistent with the possibility that a certain amount of meteoric diagenesis altered the sequence prior to dolomitization. Petrographic evidence indicative of pre-dolomitization diagenesis include the following:

a) Most aragonitic skeletal elements were selectively leached from the matrix prior to dolomitization, as indicated by the lack of dolomitized aragonitic skeletons and moldic porosity lined with limpid dolomite cements. This indicates that the sediments were flushed with a fluid undersaturated with respect to aragonite prior to dolomitization, such as meteoric waters (cf. Sibley 1980; Ward and Halley 1985; Pleydell et al. 1990; Meyers et al. 1997).

b) The cloudy nature of replacement dolomite, a common feature of island dolomites (Budd 1997), is thought to be caused by solid LMC inclusions of the precursor that resisted replacement (Sibley 1980, 1982; Dawans and Swart 1988; Pleydell et al. 1990; Budd 1997). The presence of LMC in a carbonate sequence is commonly the result of meteoric diagenesis (Sibley 1982; James and Choquette 1990b).

c) Mimetic replacement of red algae and foraminifera in the Pedro Castle Formation is rare. Rather, dolomite has lined the outer walls of red algae conceptacles and grown inwards. Most of the walls have not been replaced, and the remaining calcitic component has either been preserved or selectively leached, resulting in partial moldic porosity. This is significant because it indicates that the red algae

skeletal composition resisted replacement. Partial stabilization to LMC is the only explanation for the nature of this replacement (cf. Sibley 1982; Bullen and Sibley 1984; Pleydell et al. 1990; Meyers et al. 1997).

d) The stable isotopic signature of calcite in the Pedro Castle Formation (chapter 4), and the stabilization of calcite to LMC, are consistent with meteoric diagenesis of the formation.

Selective dissolution of aragonitic components prior to and concurrent with dolomitization is a common feature in island dolomites (Budd 1997). The resistance of red algae, and to a lesser extent foraminifera, to mimetic dolomite replacement, is however, rare (Budd 1997). Examples of this have been described from the Seroe Domi Formation in the Netherland Antilles (Sibley 1980, 1982) and in Upper Miocene carbonates from Nijar, Spain (Meyers et al. 1997). In both examples the non-mimetic replacement was attributed to partial stabilization to LMC prior to dolomitization, as a result of meteoric diagenesis.

Pre-dolomitization diagenesis that took place in the Pedro Castle Formation was probably in the mixing-zone, based on the lack of meteoric calcite cements that pre-date the dolomitization. Plummer (1975) demonstrated that aragonite dissolution without calcite precipitation in the mixing-zone can be modeled, and documented cases of this include examples from Enewetak (Goff 1979) and Jamaica (O'Neil 1974). Land (1973) noted the lack of cements in the Pleistocene Falmouth Formation of Jamaica that was interpreted to have experienced pre-dolomitization meteoric

diagenesis, and Kaldi and Gidman (1982) noted the same for carbonates from Little Bahama Bank.

The isotopic signature of dolomite in the Pedro Castle Formation, in view of the petrographic evidence and the high rock:water ratios relative to carbon found in porous carbonate sequences, probably reflects partial retention of the carbon signature from the precursor limestone. The implication of this argument is that seawater could have mediated dolomitization; there is no need to invoke fluids of mixed seawater-meteoric composition. Negative trends in the carbon isotopic signature of dolomites from San Salvador and Little Bahama Bank have been shown to directly correlate with subaerial exposure surfaces, and interpreted as the result of depletion of the precursor carbon signature due to pre-dolomitization meteoric diagenesis (Vahrenkamp and Swart 1994; Budd 1997). This affect of pre-dolomitization diagenesis has therefore been documented on other islands.

The strontium content in dolomite from the Pedro Castle Formation indicates that the seawater that mediated dolomitization was slightly modified with respect to its Sr^{2+}/Ca^{2+} ratio. A distribution coefficient value ($D_{Sr}^{Dolomite}$) of 0.0407 for Sr^{2+} into the non-stoichiometric dolomite of the Pedro Castle Formation on Cayman Brac is calculated using the method of Vahrenkamp and Swart (1990). This value is similar to a $D_{Sr}^{Dolomite}$ value (0.048) calculated from a high temperature experiment by Jacobson and Usdowski (1976), and falls within the range for $D_{Sr}^{Dolomite}$ (0.039-0.048) values calculated by Saller (1984) for dolomite from Enewetak Atoll.

The following equation (Banner 1995) relates the Sr/Ca ratio of the dolomite to the $D_{Sr}^{Dolomite}$ value and the Sr^{2+}/Ca^{2+} ratio of the dolomitizing fluid:

$$(Sr/Ca)_{Dolomite} = (D_{Sr}^{Dolomite})(Sr^{2+}/Ca^{2+})_{fluid} \quad [5.1]$$

Using the average $(Sr/Ca)_{Dolomite}$ value of 0.00141 and the $D_{Sr}^{Dolomite}$ value of 0.0407, the $(Sr^{2+}/Ca^{2+})_{fluid}$ value is 0.03464. This value is enriched relative to end-member $(Sr^{2+}/Ca^{2+})_{fluid}$ values for normal seawater (0.01874; Vahrenkamp and Swart 1990; Ng 1990) and meteoric waters collected from Grand Cayman (0.00667; this study).

There are two processes associated with meteoric diagenesis that can cause elevated Sr^{2+}/Ca^{2+} levels in diagenetic fluids, and possibly result in increased Sr content in precipitated dolomite. These are aragonite dissolution and concurrent calcite precipitation (Budd 1988; Humphrey 2000; Swart and Melim 2000) and the stabilization of calcite (Mucci and Morse 1983). If one or both of these processes did affect dolomitization in the Pedro Castle Formation, the possibility that seawater with a meteoric component mediated dolomitization should be re-evaluated.

Petrographic evidence indicates that the affect of aragonite dissolution and concurrent calcite precipitation on dolomitization in the Pedro Castle Formation was probably negligible. Humphrey (1988, 2000) demonstrated that associated with this process is a significant increase in the dolomite Sr content, beyond the range of dolomite in the Pedro Castle Formation. Dolomite replacement of aragonitic components is also expected with this process, a feature not found in the Pedro Castle Formation. Also, there is no evidence of pre-dolomitization meteoric cementation.

Partial stabilization of HMC to LMC will release extraneous Sr^{2+} into the pore fluids (Mucci and Morse 1983), and might have contributed to the fluids that mediated dolomitization. A number of factors with unknown parameters, however,

including the extent of rock:water interaction and the rate of fluid flow through the system, would have exerted important controls on the influence of this extraneous Sr^{2+} on dolomitization in the Pedro Castle Formation (cf. Budd 1997; Swart and Melim 2000). Without knowledge of these specific controls, modeling of the affect of partial stabilization of HMC and how it might have contributed to the chemistry of dolomite in the Pedro Castle Formation is open to debate.

The overall value of the strontium content data is therefore limited to indicating that the dolomitizing fluid had a Sr^{2+}/Ca^{2+} value greater than that of normal seawater or meteoric water; the cause of this enrichment is not apparent. There is no evidence that contradicts the suggestion that dolomitization in the Pedro Castle Formation was mediated by seawater. The strontium content data indicate slight modification of this fluid to weakly enriched Sr^{2+}/Ca^{2+} values. Strontium derived from aeolian clays (terra rossa) in the underlying Cayman Formation may have contributed to at least a portion of the elevated strontium levels.

5.4 Summary

The geochemical evidence indicates that dolomitization of the Pedro Castle Formation was mediated by slightly modified seawater. The oxygen isotopic data indicates that the fluids from which dolomite grew were equivalent in temperature to modern seawater and subsurface waters in the Cayman Islands. Petrographic evidence indicates that partial stabilization of the precursor limestone took place prior to the dolomitization event, and at least partial retention of the modified carbon signature from this diagenesis explains the depleted carbon values in the dolomite. Consistent

with this theory is the slight increase in carbon isotopic values with depth (Fig. 5.4) – a possible trend of carbonates that have experienced meteoric diagenesis (see chapter 4). The strontium content of the dolomite indicates that dolomite precipitated from waters with elevated Sr^{2+}/Ca^{2+} levels.

Chapter Six – Discussion and Summary

6.0 Introduction

An understanding of the geological history of the Pedro Castle Formation on Cayman Brac requires study of its sedimentology, stratigraphy, diagenesis, and dolomitization. Distribution of facies associations, integrated with the depositional environments of each facies, provides a detailed insight into the bank morphology of Cayman Brac in the Pliocene. Petrography and geochemistry provide the information necessary for understanding the mineralogic, petrographic, and chemical characteristics and changes in the formation. From all of this information, a model of the evolution of the Pedro Castle Formation on Cayman Brac can be developed.

Tectonic movement of the island and changes in eustatic sea level were the greatest controls on the depositional history of the Pedro Castle Formation. The eastern end of the island has been uplifted to ~45 m and tilted to the west, giving the island a wedge shape. Global warming at the end of the Miocene and in the Pliocene resulted in warmer oceanic temperatures at higher latitudes, glacial retreat, and three third-order sea level highstands. The relative influence of tectonic movement and eustatic sea level change on how the Pedro Castle Formation formed, however, is difficult to measure without knowing the specific tectonic history of the island or the time within the Pliocene when deposition took place.

6.1 Tectonic Setting of Cayman Brac in the Pliocene

The tectonic setting of Cayman Brac in the Pliocene is important when considering a number of questions about the geological history of the Pedro Castle Formation. The age of the uplift of Cayman Brac is unresolved, other than the fact

that it post-dated deposition of the Cayman Formation and pre-dated deposition of the Ironshore Formation. This is concluded from the regional dip of the Cayman and Brac Formations of 0.5° to the west (Jones and Hunter 1994a). The lack of internal bedding planes in the Pedro Castle Formation precludes measurement of the attitude of its strata. If the formation is horizontal, uplift was pre- and/or syn-depositional and the Cayman Unconformity is angular. If the formation has the same regional dip as the Cayman Formation and Brac Formation, island uplift must have been post-deposition of the Pedro Castle Formation.

Pre-depositional uplift and tilting of the island implies that the Pedro Castle Formation was deposited as an onlapping sequence at the western end while the eastern end was subaerially exposed. This is similar to the Pleistocene Ironshore Formation and modern sediment deposition around the island. Subaerial exposure is expected because the facies in the Pedro Castle Formation are consistent with a shallow marine origin (<20 m), and the difference in elevation between the region where these facies exist and the eastern end of the island is greater than 20 m.

To date, a wave-cut notch that formed during deposition of the Pedro Castle Formation has not been found. A wave-cut notch that correlates with the Sangoman highstand in the Pleistocene is evident around the island (Jones and Hunter 1994a; Jones et al. 1994a), and modern wave action is cutting a notch at the present sea level. It is possible that a wave-cut notch from the Pliocene has not been preserved; the eastern end of the island has had cliff failure and rock slides.

The model for evolution of the Pedro Castle Formation on Cayman Brac therefore makes an assumption that initiation of uplift and tilting of the island might have taken

place while sediment was being deposited in the Pliocene. The major event of uplift and tilting, however, is believed to have taken place some time after deposition had been terminated.

6.2 Pliocene Sea Level

Global warming at the end of the Miocene resulted in retreat of glacial ice sheets and three sea level highstands in the Pliocene (Fig. 6.1) (Vail et al. 1977; Dowsett and Cronin 1990; Cronin and Dowsett 1993). The initial highstand in the Pliocene (H1) reached its maximum at 4.6 Ma, with estimated rises in sea level of 29-36 m (Wardlaw and Quinn 1991) and 75 m (Pickard et al. 1988) above present sea level. A second highstand (H2), at 4.0 Ma, fell at approximately 3.8 Ma (Arts 2000). A third highstand (H3) occurred at ~3.5 Ma. Evidence from the eastern coastal United States indicates that sea level rose 35 ±18 m (Dowsett and Cronin 1990) during that highstand. The first two highstands in the Pliocene (H1 and H2) were of greater magnitude and duration than the third highstand in the Middle Pliocene.

Attempting to correlate deposition in the Pedro Castle Formation to one of these highstands is difficult. Arts (2000) argued that deposition of the Pedro Castle Formation on Grand Cayman probably took place during the first highstand, although it was noted that there was no conclusive evidence. It was also noted, using average sedimentation rates on carbonate banks, that the duration of any of the three highstands was sufficient for deposition of the Pedro Castle Formation. Any of the three highstands could therefore have led to deposition of the sediment that now forms the Pedro Castle Formation on Cayman Brac.

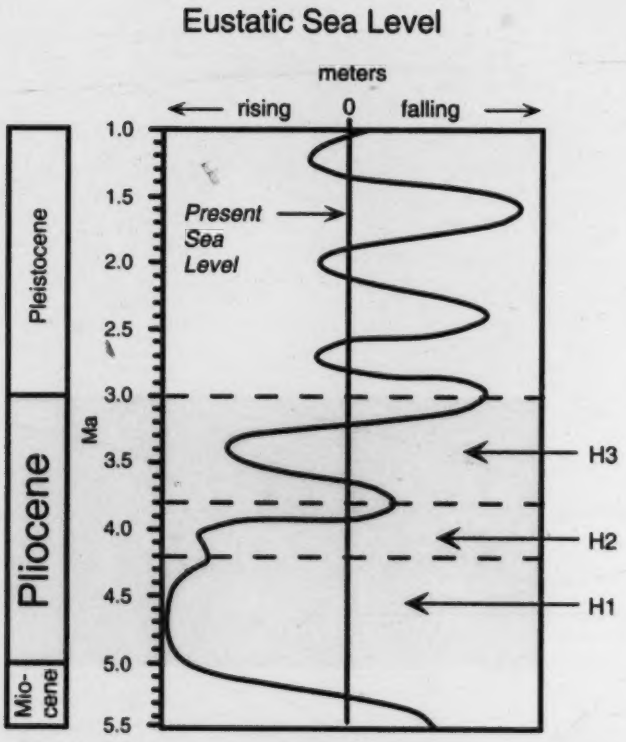

Figure 6.1. Third order sea level curves for the Pliocene (modified from Haq *et al.* 1987; Krantz 1991; copied from Arts 2000).

The minimum rise in sea level associated with deposition of the Pedro Castle Formation on Grand Cayman is 30-35 m (Arts 2000). On Cayman Brac, the Pedro Castle Formation outcrops at maximum heights of ~12 m above present sea level. The unknown amount of tectonic movement of the island, however, makes it impossible to estimate the amount of sea level rise in the Pliocene. The estimated sea level rise of 30-35 m from Grand Cayman (Arts 2000) is in close agreement to estimates of 29-36 m of rise in the Early Pliocene (Wardlaw and Quinn 1991) and 35 m in the Middle Pliocene (Dowsett and Cronin 1990). A rise of this magnitude, for a period of duration of any of the three Pliocene highstands, could have deposited the Pedro Castle Formation. The model of evolution for the formation on Cayman Brac therefore does not require specific correlation to any of the specific highstands. The role of tectonic movement of the island, discussed above, is also not known.

6.3. Bank Morphology and Depositional History of the Pedro Castle Formation

Any model developed to explain deposition of the sediments that formed the Pedro Castle Formation must address the following observations:

a) The Cayman Unconformity appears to have little topographic relief on Cayman Brac. Prior to deposition of sediment, transgression of the bank must have planed most of this surface.

b) Muds and muddy sands appear at the base of the formation in most sections. A change in environments from one that erodes to one in which quiet water sediments can accumulate must have taken place.

c) The muds and muddy sands at the base of the formation grade upwards to higher-energy sandy facies.

d) Coral development was limited to the area that now includes the Active Scott Quarry. This coral development was eventually filled in and buried by transported sands, indicative of some change in depositional conditions.

The model can be described in five phases, followed by diagenetic alteration and post-depositional dolomitization. Changes in sea level, whether by eustatic fluctuations or tectonic movement of the island, also controlled the later diagenetic events and dolomitization.

Phase 1: Pre-sediment accumulation

The Cayman Unconformity (see chapter 2) on Cayman Brac is considered to be a paleokarst surface that developed at the end of the Messinian, contemporaneous with paleokarst development on Grand Cayman. Sea level rise of ~30 m above present sea level, flooding of the bank, and erosion at the Cayman Unconformity (Fig. 6.2.A.) prior to accumulation of sediment accounts for the subdued topography at this contact. The actual depth of water across the bank, however, is not known. The sea level rise does not necessarily equate with depth on the bank because early tectonic movement of the island may have lowered or raised the Cayman Unconformity relative to sea level. Trace fossils on the Cayman Unconformity indicate that a community of algae, fungi, sponges, and boring molluscs was established on this

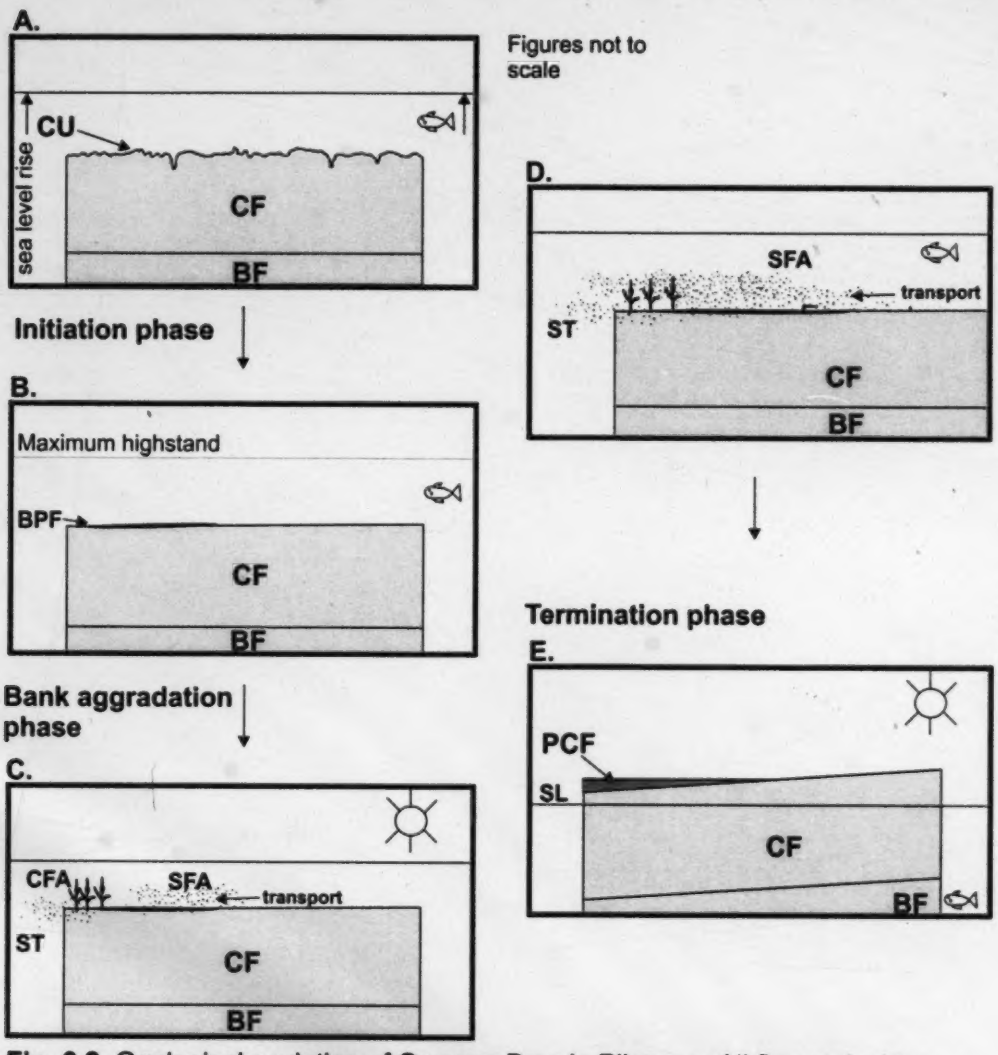

Fig. 6.2. Geological evolution of Cayman Brac in Pliocene. All figures looking north. CF = Cayman Formation. BF = Brac Formation. CU = Cayman Unconformity. ST = sediment transport off-bank. CFA = Coral Facies Association. SFA = Sandy Facies Association. BPF = muds and muddy sands at base of Pedro Castle Formation. SL = Sea level. A. Flooding of bank and erosion at Cayman Unconformity. Any sediment produced is swept from surface. B. Muds and muddy sands (BPF) deposited in deeper waters during maximum highstand. C. Water depth over bank decreases due to sediment build-up and/or tectonic subsidence of island and/or falling sea level. Deposition of sandy facies. CFA develops in slightly deeper (15-20 m) water at western end. Sediment produced at eastern end (windward side) is probably either transported off-bank or westwards to lee side of island. D. Burial of Coral Facies Association by Sandy Facies Association. E. Termination of deposition on the bank in Pliocene. Either a drop in eustatic sea level and/or tectonic uplift exposed the Pedro Castle Formation.

surface prior to the onset of sedimentation. This community was probably established during the early stages of the transgression.

Phase 2: Initiation of sediment deposition

Muds and muddy sands were the first sediments to accumulate as indicated in sections BLX, GMD, STS, SQA-2, SWP, HPS, and ASQ-2 (Fig. 6.2B). These appear to have been deposited in relatively deeper (possibly 25-30 m), quiet waters. The lack of coral development in the early stages of sediment accumulation might have been related to substrate conditions.

Phase 3: Bank aggradation

During Phase 3 (Fig. 6.2C) the bank was probably in the zone of maximum carbonate production (cf. Schlager 1981). Shallower water conditions than in Phases 1 or 2 existed across the bank, due to sediment build-up and/or tectonic movement of the island and/or a change in sea level. Sediments produced over most of the island were probably either transported to the western end or off-bank, leaving a continually bare surface over much of Cayman Brac (cf. Goldberg 1983; Glasner and Droxler 1991). Alternatively, they did accumulate but have since been removed by erosion.

At the leeward, west end, sediments accumulated on the bank. Most of these facies belong to the Sandy Facies Association and were deposited in normal marine conditions in water depths ~10 m. The decrease in mud content from the base of the formation is attributed to an increase in energy across the bank due to shallower conditions.

Facies in the sands changed rapidly, reflecting local depth variations, variations in wave and current energies, bedforms, and variations in the production and transport of sediment (ie. Triffleman et al. 1992). Mixed foraminiferal assemblages, including planktonic species associated with open-marine conditions, and amphisteginids mixed with soritids support interpretation that sediment mixing and transport were intense.

Water depth across the bank was not, however, uniform. The deepest waters (~15-20 m) appear to have been in the area where the Active Scott Quarry now exists. In that area, thickets of branching *Stylophora* and *Porites* developed and other corals including *Montastrea*, *Leptoseris*, and *Colpophyllia* existed. This is where the Coral Facies Association developed. Associated with the coral development were communities of amphisteginids, soritids, and homotrematids and some other minor foraminifera species. Sands that locally accumulated included grains of these foraminifera and bivalves, gastropods, red algae, echinoderms, and green algae.

Phase 4: Burial of the Coral Facies Association

Coral growth and development in the western region of the bank was terminated during the latest stages of bank evolution by sediment that filled and eventually buried the coral framework (Fig. 6.2.D). The cause for the change from an environment that supported coral growth and development to one that became filled with sandy facies is open to different interpretations. Three explanations include:

a) Accumulation of sands to the east of the Coral Facies Association surpassed the budget that could be maintained for the amount of cross-bank circulation, and sediment re-distribution occurred, transporting sands westwards into the corals.

b) Energy across the bank increased, possibly due to a change in sea level or bank subsidence, and this resulted in increased sediment transport to the west and off-bank. Sediment transport resulted in burial of the corals.

c) Carbonate production exceeded the rate of sea level rise or bank subsidence, and the sands that filled and buried the coral are part of the resultant shallowing-upwards cycle.

Any of these possibilities, or a combination of them, may be used to explain the eventual burial of the corals at the Active Scott Quarry. Common to all of them is that the bank was an effective carbonate producer.

Phase 5: End of deposition in the Pliocene and pre-dolomitization diagenesis

Termination of sediment deposition on Cayman Brac in the Pliocene was probably a rapid event caused by eustatic sea level drop, tectonic uplift, or a combination of the two (Fig. 6.2.E). The thickness of the formation, or its extent over the island at that time is not known. Prior to partial dolomitization of the formation, a certain amount of diagenesis took place (chapters 3 and 5), probably within a mixing-zone of meteoric and marine waters.

6.3 Dolomite Genesis

Dolomitization in the Pedro Castle Formation was entirely post-depositional. Type I dolomite is cloudy in appearance, a feature that on other carbonate islands has been interpreted to be the result of inclusions of the precursor carbonates (Sibley 1980,

1982; Dawans and Swart 1988; Vahrenkamp and Swart 1994; Budd 1997), indicating that such dolomite is truly replacive. The style of dolomite replacement was also fabric selective, and was probably controlled by the calcite Mg^{2+} composition (cf. Sibley 1980; Pleydell et al. 1990). LMC was not replaced, and skeletal calcite partially stabilized to LMC (ie. red algae and foraminifera grains) was poorly replaced.

What triggered the onset of dolomitization in the Pedro Castle Formation is not clear. In attempting to determine the pumping mechanism that promoted the event, the fluid chemistry, the geometry of the dolomite body, and the local geology must be considered. The geochemistry (chapter 5) of dolomite has indicated that slightly modified seawater mediated dolomitization. The geometry of the dolomite body in the Pedro Castle Formation is wedge-shaped; the degree of dolomitization decreases in a south, south-east direction from the north coast. Sections SQA, SQA-1, and WTB are limestone. A spatial relationship between the degree of dolomitization and distance from the north coast may therefore have existed. Whether or not this dolomitization event caused further dolomitization or overprinting of dolomite in the underlying Cayman Formation is not known. If it did, the Cayman Formation, at least in its upper parts, has at least two compositional populations of dolomite; one that pre-dates deposition of the Pedro Castle Formation (based on petrographic evidence) and one that is genetically related to the replacement dolomite in the overlying Pedro Castle Formation.

Based on these limited data, tidal pumping (cf. Saller 1984; Buddemeier and Oberdorfer 1986; Land 1991; Hein et al. 1992; Wheeler and Aharon 1997) of

seawater and/or entrainment of seawater by flow from a meteoric lens (cf. Land 1991; Vahrenkamp et al. 1991; Wheeler and Aharon 1997) are two possible dolomitization mechanisms that might have taken place in the Pedro Castle Formation. Both of these mechanisms are capable of pumping seawater or a modified form of seawater (consistent with the conclusion that slightly modified seawater mediated dolomitization) through a carbonate sequence (cf. Kaufman 1994; Budd 1997) and can produce wedge-shaped bodies of dolomite (Wheeler and Aharon 1997).

Critical to concluding that any mechanism was responsible for dolomitization of the Pedro Castle Formation, more data needs to be collected. Knowledge of what happens below the Cayman Unconformity, with respect to any dolomite that is genetically related to dolomite in the Pedro Castle Formation, is essential. With the limited current data, tidal pumping of slightly modified seawater or entrainment of slightly modified seawater by flow from a meteoric lens may provide the mechanism for dolomitization in the Pedro Castle Formation.

6.4 Post-dolomitization Diagenesis

Following partial dolomitization of the formation, island uplift and/or a drop in sea level caused a change in the hydrogeology of the island and the Pedro Castle Formation moved within the meteoric realm. Fabrics and types of alteration typical of meteoric diagenesis in wet, tropical climates (cf. James and Choquette 1990b) have since formed in the Pedro Castle Formation. The amount of the formation that has been removed by wholesale dissolution in the vadose zone is not known.

6.5 The Age of Events

The time within the Pliocene when the Pedro Castle Formation was deposited on Cayman Brac is not known because diagenetic alteration of calcite may re-set the isotopic ratios and provide inaccurate ages for the time of deposition. The values, however, do provide a minimum age of deposition and alteration. The strontium isotopic ratios from calcite (n = 3; Chapter 4) in the Pedro Castle Formation provide a minimum age of late Late Pliocene to earliest Pleistocene for the age of deposition and alteration. Strontium isotopic ratios from dolomite (n = 14; Chapter 5) in the Pedro Castle Formation correspond to an age of late Late Pliocene to earliest Pleistocene, and indicate that it was in this time frame that the dolomitization event took place.

6.6 Summary

The depositional and diagenetic history (Fig. 6.4) of the Pedro Castle Formation on Cayman Brac is complex. A number of issues remain unresolved, including the depositional age within the Pliocene of the Pedro Castle Formation, the cause of enriched Sr/Ca values in the dolomite, and whether or not the late Late Pliocene, earliest Pleistocene dolomitization event overprinted dolomite in the underlying Cayman Formation. This may have implications on the mechanism invoked for the dolomite formation.

Detailed study of the petrography and geochemistry of the dolomite has concluded that slightly modified seawater was the fluid that mediated dolomitization. There is also evidence that the formation underwent a certain amount of pre-dolomitization

diagenesis which affected the style of replacement and the carbon isotopic signature in the dolomite. Tidal pumping and/or entrainment of seawater by flow of meteoric water from an overlying lens may have been the "pump" that drove dolomitization.

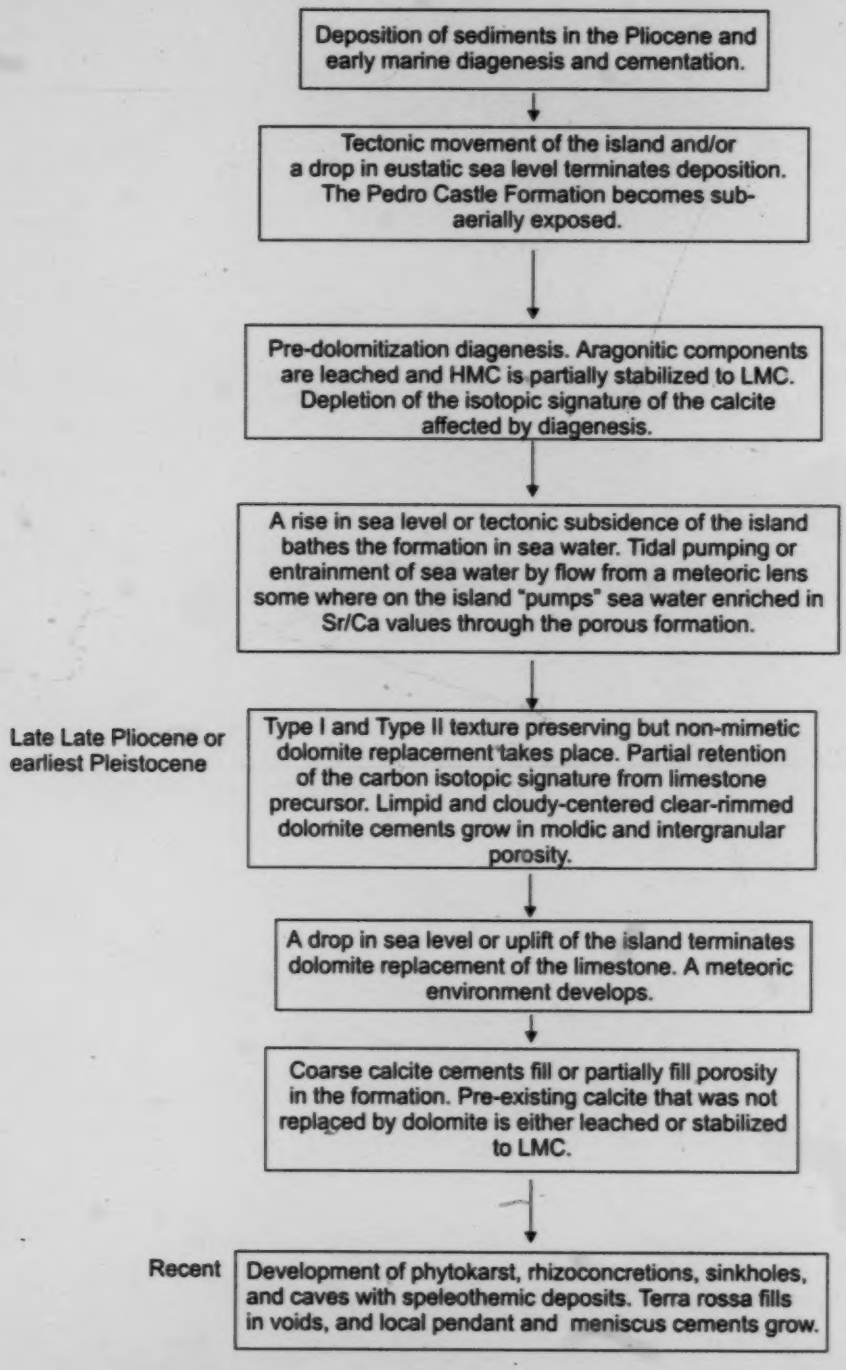
Deposition of sediments in the Pliocene and early marine diagenesis and cementation.
Tectonic movement of the island and/or a drop in eustatic sea level terminates deposition. The Pedro Castle Formation becomes sub-aerially exposed.
Pre-dolomitization diagenesis. Aragonitic components are leached and HMC is partially stabilized to LMC. Depletion of the isotopic signature of the calcite affected by diagenesis.
A rise in sea level or tectonic subsidence of the island bathes the formation in sea water. Tidal pumping or entrainment of sea water by flow from a meteoric lens some where on the island "pumps" sea water enriched in Sr/Ca values through the porous formation.
Late Late Pliocene or earliest Pleistocene
Type I and Type II texture preserving but non-mimetic dolomite replacement takes place. Partial retention of the carbon isotopic signature from limestone precursor. Limpid and cloudy-centered clear-rimmed dolomite cements grow in moldic and intergranular porosity.
A drop in sea level or uplift of the island terminates dolomite replacement of the limestone. A meteoric environment develops.
Coarse calcite cements fill or partially fill porosity in the formation. Pre-existing calcite that was not replaced by dolomite is either leached or stabilized to LMC.
Recent
Development of phytokarst, rhizoconcretions, sinkholes, and caves with speleothemic deposits. Terra rossa fills in voids, and local pendant and meniscus cements grow.

Fig. 6.3. Paragenetic sequence of events in Pedro Castle Formation on Cayman Brac.

References

Aissaoui, D.M. 1988. Magnesian calcite cements and their diagenesis: dissolution and dolomitization, Mururoa Atoll. Sedimentology, **35**, 821-841.

Aissaoui, D.M., Buigues, D., and Purser, B.H. 1986. Model of Reef Diagenesis: Mururoa Atoll, French Polynesia. *In* Reef Diagenesis. *Edited by* J.H. Schroeder and B.H. Purser. Springer-Verlag, pp 27-52.

Allan, J.R. and Matthews, R.K. 1982. Isotope signatures associated with early meteoric diagnesis. Sedimentology, **29**, 797-817.

Arts, A. 2000. Sedimentology and stratigraphy of the Pedro Castle Formation, Grand Cayman. Unpublished M.Sc. Thesis, University of Alberta.

Banner, J.L. 1995. Application of the trace element and isotope geochemistry of strontium to studies of carbonate diagenesis. Sedimentology, **42**, 805-824.

Banner, J.L. and Hanson, G.N. 1990. Calculation of simultaneous isotopic and trace element variations during water – rock interaction with application to carbonate diagenesis. Geochimica et Cosmochimica Acta, **54**, 3123-3137.

Boggs, S., Jr. 1987. Principles of Sedimentology and Stratigraphy. Merrill Publishing Company, 784 pp.

Bowin, C.O. 1968. Geophysical study of the Cayman Trough. Journal of Geophysical Research, **73**, 5159-5173.

Budd, D.A. 1988. Aragonite-to-calcite transformation during fresh-water diagenesis of carbonates: Insights from pore-water chemistry. Geological Society of America Bulletin, **100**, 1260-1270.

Budd, D.A. 1997. Cenozoic dolomites of carbonate islands: their attributes and origin. Earth Science Reviews, **42**, 1-47.

Buddemeier, R.W., and Oberdorfer, J.A. 1986. Internal hydrology and geochemistry of coral reefs and atoll islands: key to diagenetic variations. *In* Reef Diagenesis. *Edited by* J.H. Schroeder and B.H. Purser. pp. 91-110.

Bullen, S.B. and Sibley, D.F. 1984. Dolomite selectivity and mimic replacement. Geology, **12**, 655-658.

Carballo, J.D., Land, L.S., and Miser, D.E. 1987. Holocene Dolomitization of Supratidal Sediments By Active Tidal Pumping, Sugarloaf Key, Florida. Journal of Sedimentary Petrology, **57**, 153-165.

Case, J.E., MacDonald, W.D., and Fox, P.J. 1990. Caribbean crustal provinces; seismic and gravity evidence. *In* The Caribbean Region. *Edited by* G.Dengo and J.E. Case. *In* The Geology of North America, **H**, 15-36.

Chafetz, H.S., Imerito-Tetzlaff, A.A., and Zhang, J. 1999. Stable isotope and elemental trends in Pleistocene sabkha dolomites: Descending meteoric water vs. sulfate reduction. Journal of Sedimentary Research, **69**, 256-266.

Cronin, T.M. and Dowsett, H.J. 1993. PRISM: Warm climates of the Pliocene. Geotimes, **11**, 17-19.

Darbyshire, J., Bellamy, I., and Jones, B. 1976. Part III Results of the investigations into the physical oceanography. Cayman Islands Natural Resources Study. 121 pp.

Dawans, J.M. and Swart, P.K. 1988. Textural and geochemical alternations in Late Cenozoic Bahamian dolomites. Sedimentology, **35**, 385-403.

Dowsett, H.J. and Cronin, T.M. 1990. High eustatic sea level during the Middle Pliocene: Evidence from the southeastern U.S. Atlantic coastal plain. Geology, **18**, 435-438.

Dunham, R.J. 1962. Classification of carbonate rocks according to depositional textures. *In* Classification of Carbonate Rocks. *Edited by* W.E. Ham. American Association Petroleum Geologists Memoir 1, 108-121.

Embry, A.F. and Klovan, J.E. 1971. A Late Devonion reef tract on the northeastern Banks Island, N.W.T. Bulletin of Canadian Petroleum Geology, **19**, 730-781.

Emery, K.O. and Milliman, J.D. 1980. Shallow water limestones from slope off Grand Cayman Island. Journal of Geology, **88**, 483-488.

Friedman, G.M. and Koselar, P.T. 1971. Freshwater carbonate cements. *In* Carbonate Cements. *Edited by* O.P. Bricker. 122-126.

Friedman, I. and O'Neil, J.P. 1977. Compilation of stable isotope fractionation factors of geochemical interest. United States Geological Survey Professional Paper, 440KK, 12 pp.

Fritz, P. and Smith, D.G.W. 1970. The isotopic composition of secondary dolomite. Geochimica et Cosmochimica Acta, **34**, 1161-1173.

Gill, I.P., Moore, C.H. Jr., and Aharon, P. 1995. Evaporitic Mixed-Water Dolomitization On St. Croix, U.S.V.I.. Journal of Sedimentary Research, **A65**, 591-604.

Ginsburg, R.N., Shinn, E.A., and Schroeder, J.H. 1971. Recent synsedimentary cementation in subtidal Bermuda reefs. *In* Carbonate Cements. *Edited by* O.P. Bricker. 54-59.

Glasner, K.S., and Droxler, A.W. 1991. High production and highstand shedding from deeply submerged carbonate banks, northern Nicaraguan Rise. Journal of Sedimentary Petrology, **61**, 128-142.

Goff, S.K. 1979. Early carbonate cementation and diagenesis as related to the present surficial water regime, Engebi Island, Enewetak Island. Unpublished M.Sc. Thesis, Louisiana State University.

Goldberg, W.M. 1983. Cay Sal Bank: biologically impoverished physically controlled environment. Atoll Research Bulletin, **271**, 1-19.

Goldsmith, J.R., Graf, D.L., and Heard, H.C. 1961. Lattice constraints of the calcium magnesium carbonates. American Mineralogist, **46**, 453-457.

Hallock, P. and Peebles, M.W. 1993. Foraminifera with chlorophyte endosymbionts: Habitats of six species in the Florida Keys. Marine Micropaleontology, **20**, 277-292.

Hallock, P., Cottey, T.L., Forward, L.B., and Halas, J. 1986. Population biology and sediment production of *Archais angulata* (Foraminiferida) in Largo Sound, Florida. Journal of Foraminiferal Research, **16**, 1-8.

Haq, B.V., Hardenbol, J., and Vail, P.R. 1987. Chronology of fluctuating sea levels since the Triassic. Science, **235**, 1156-1167.

Harris, P.M., Kendall, C.G.St.C., and Lerche, I. 1985. Carbonate cementation – a brief review. *In* Carbonate Cements. *Edited by* N. Schneidermann and P.M. Harris. Society of Economic Paleontologists and Mineralogists Special Publication 36, pp. 79-96.

Haug, E. 1907. Traité de géologie. Colin, Paris. 2 volumes.

Heckel, P.H. 1972. Recognition of ancient shallow marine environments. *In* Recognition of ancient sedimentary environments. *Edited by* J.K. Rigby and W.K. Hamblin. Society of Economic Paleontologists and Mineralogists, Special Publication 16, 226-286.

Hein, J.R., Gray, S.C., Richmond, R.M. and White, L.D. 1992. Dolomitization of Quaternary reef limestone, Aitutaki, Cook Islands. Sedimentology, **39**, 645-662.

Hodell, D.A., Mueller, P.A., McKenzie, J.A., and Mead, G.A. 1989. Strontium isotope stratigraphy and geochemistry of the late Neogene ocean. Earth and Planetary Science Letters, **92**, 165-178.

Holcombe, T.L., Vogt, P.R., Matthews, J.E., and Murchison, R.R. 1973. Evidence for sea-floor spreading in the Cayman Trough. Earth and Planetary Science Letters, **20**, 357-371.

Holcombe, T.L., Ladd, J.W., Westbrook, G.K., Edgar., N.T., and Bowland, C.L. 1990. Caribbean marine geology; ridges and basins of the plate interior. *In* The Caribbean Region. *Edited by* G. Dengo and J.E. Case. *In* The Geology of North America, **H**, 231-260.

Humphrey, J.D. 2000. New geochemical support for mixing-zone dolomitization at Golden Grove, Barbados. Journal of Sedimentary Research, **70**, 1160-1170.

Hunter, I.G. 1994. Coral associations of the Cayman Islands. Unpublished PhD Thesis, University of Alberta.

Jacobson, R.L., and Usdowski, H.E. 1976. Partitioning of strontium between calcite, dolomite, and liquids. Contributions to Mineralogy and Petrology, **59**, 171-185.

James, N.P., and Ginsburg, R.N. 1979. The Seaward Margin of Belize Barrier and Atoll Reefs. Special Publication Number 3 of the International Association of Sedimentologists. Blackwell Scientific Publications. 191 pp.

James, N.P., and Choquette, P.W. 1990a. Limestones – The sea floor diagenetic environment. *In* Diagenesis. *Edited by* I.A. McIlreath and D.W. Morrow. Geoscience Canada Reprint Series 4, Geological Association of Canada, pp.13-34.

James, N.P., and Choquette, P.W. 1990b. Limestones – The meteoric diagenetic environment. *In* Diagenesis. *Edited by* I.A. McIlreath and D.W. Morrow. Geoscience Canada Reprint Series 4, Geological Association of Canada, pp.35-74.

James, N.P., Ginsburg, R.N., Marszalek, D.S., and Choquette, P.W. 1976. Facies and fabric specificity or early subsea cements in shallow Belize (British Honduras) reefs. Journal of Sedimentary Petrology, **46**, 523-544.

Jones, B. 1988. The influence of plants and micro-organisms on diagenesis in caliche: example from the Pleistocene Ironshore Formation on Cayman Brac, British West Indies. Bulletin Canadian Petroleum Geology, **36**, 191-201.

Jones, B.1989. Calcite rafts, peloids, and micrite in cave deposits from Cayman Brac, British West Indies. Canadian Journal of Earth Sciences, **26**, 654-664.

Jones, B. 1991. Genesis of terrestrial oncoids, Cayman Islands, British West Indies. Canadian Journal of Earth Sciences, **28**, 382-397.

Jones, B. 1992a. Caymanite, a cavity-filling deposit in the Oligocene- Miocene Bluff Formation of the Cayman Islands. Canadian Journal of Earth Sciences, **29**, 720-736.

Jones, B.1992b. Void filling deposits in karst terrains of isolated oceanic islands: a case study from Tertiary carbonates of the Cayman Islands. Sedimentology, **39**, 857-876.

Jones, B. and Hunter, I.G. 1989. The Oligocene-Miocene Bluff Formation on Grand Cayman. Caribbean Journal of Science, **25**, 71-85.

Jones, B. and Desrochers, A. 1992. Shallow platform carbonates. *In* Facies Models. *Edited by* R.G. Walker and N.P. James. Geological Association of Canada, 277-301.

Jones, B. and Hunter, I.G. 1994a. Evolution of an Isolated Carbonate Bank during Oligocene, Miocene, and Pliocene Times, Cayman Brac, British West Indies. Facies, **30**, 25-50.

Jones, B. and Hunter, I.G. 1994b. Messinian (Late Miocene) Karst on Grand Cayman, British West Indies: An Example of an Erosional Sequence Boundary. Journal of Sedimentary Research, **B64**, 531-541.

Jones, B., Lockhart, E.B., and Squair, C.A. 1984. Phreatic and vadose cements in the Tertiary Bluff Formation of Grand Cayman Island, British West Indies. Bulletin of Canadian Petroleum Geology, **32**, 382-397.

Jones, B., Pleydell, S.M., Ng, K.-C., and Longstaffe, F.J. 1989. Formation of poikilotopic calcite-dolomite textures in the Oligocene-Miocene Bluff Formation of Grand Cayman, British West Indies. Bulletin of Canadian Petroluem Geology, **37**, 255-265.

Jones, B., Hunter, I.G., and Kyser, K. 1994a. Stratigraphy of the Bluff Formation (Miocene-Pliocene) and the Newly Defined Brac Formation (Oligocene), Cayman Brac, British West Indies. Caribbean Journal of Science, **30**, 30-51.

Jones, B., Hunter, I.G., and Kyser, K. 1994b. Revised Stratigraphic Nomenclature for Tertiary Strata of the Cayman Islands, British West Indies. Caribbean Journal of Science, **30**, 53-68.

Jones, B., Luth, R. and MacNeil, A. *in press*. Powder X-ray diffraction analysis of homogeneous and heterogeneous sedimentary dolostones. Journal of Sedimentary Research.

Kaldi, J. and Gidman, J. 1982. Early diagenetic dolomite cements: examples from the Permian Lower Magnesium Limestone of England and Pleistocene carbonates of the Bahamas. Journal of Sedimentary Petrology, **52**, 1073-1086.

Kaufman, J. 1994. Numerical models of fluid flow in carbonate platforms: Implications for dolomitization. Journal of Sedimentary Research, **A64**, 128-139.

Krantz, D.E. 1991. A chronology of Pliocene sea level fluctuations: The U.S. middle Atlantic coastal plain record. Quaternary Science Reviews, **10**, 163-174.

Kyser, K.T. 1987. Equilibrium fractionation factors for stable isotopes. *In* Stable isotope geochemistry of low temperature processes. *Edited by* K.T. Kyser. Mineralogical Association of Canada Short Course Handbook 13. 1-84.

Land, L.S. 1970. Phreatic versus vadose meteoric diagenesis of limestones: evidence from a fossil water table. Sedimentology, **14**, 175-185.

Land, L.S. 1971. Submarine lithification of Jamaican reefs. *In* Carbonate Cements. *Edited by* O.P. Bricker. 59-62.

Land, L.S. 1973. Holocene meteoric dolomitization of Pleistocene limestones, North Jamaica. Sedimentology, **20**, 411-424.

Land, L.S. 1985. The Origin of Massive Dolomite. Journal of Geological Education, **33**, 112-125.

Land, L.S. 1991. Dolomitization of the Hope Gate Formation (north Jamaica) by seawater: Reassessment of mixing-zone dolomite. *In* Stable Isotope Geochemistry: A Tribute to Samuel Epstein. *Edited by* H.P. Taylor Jr., J.R. O'Neil, and I.R. Kaplan. The Geochemical Society, Special Publication 3, pp. 121-133.

Li, C. 1997. Foraminifera: their distribution and utility in the interpretation of carbonate sedimentary processes around Grand Cayman, British West Indies. Unpublished PhD Thesis, University of Alberta.

Lohmann, K.C. 1988. Geochemical patterns of meteoric diagenetic systems and their applications to studies of paleokarst. *In* Paleokarst. *Edited by* P.W. Choquette and N.P. James. Springer, pp. 55-80.

Lumsden, D.N. and Chimahusky, J.S. 1980. Relationship between dolomite nonstoichiometry and dolomite facies parameters. *In* Concepts and Models of Dolomitization. *Edited by* D.H. Zenger, J.B. Dunham, and R.L. Ethington. Society of Economic Paleontologists and Mineralogists Special Publication 28, 123-137.

MacDonald, K.C., and Holcombe, T.L. 1978. Inversion of magnetic anomalies and sea-floor spreading in the Cayman Trough. Earth and Planetary Science Letters, **40**, 407-414.

Machel, H.G. and Mountjoy, E.W. 1986. Chemistry and Environments of Dolomitization – A Reappraisal. Earth Science Reviews, **23**, 175-222.

Machel, H.G. and Burton, E.A. 1994. Golden Grove Dolomite, Barbados: Origin From Modified Seawater. Journal of Sedimentary Research, **A64**, 741-751.

Matley, C.A. 1924a. Reconnaissance geological survey of Cayman Islands, British West Indies. Pan-American Geologist, **42**, 313-315.

Matley, C.A. 1924b. Report of a reconnaissance geological survey of the Cayman Islands. Supplement to the Jamaica Gazette, June 13 1924, 69-73.

Matley, C.A. 1925. Report of a reconnaissance geological survey of the Cayman Islands. Jamaica Annual General Report for 1923, 41-45.

Matley, C.A. 1926. The Geology of the Cayman Islands (British West Indies) and their relation to the Bartlett Trough. Quarterly Journal of the Geological Society of London, **82**, 352-387.

Meyers, W.J., Feng, H.L., and Zachariah, J.K. 1997. Dolomitization by mixed evaporative brines and freshwater, Upper Miocene carbonates, Nijar, Spain. Journal of Sedimentary Research, **67**, 898-912.

Mucci, A. and Morse, J.W. 1983. The incorporation of Mg^{2+} and Sr^{2+} into calcite overgrowths: influences of growth rate and solution composition. Geochimica et Cosmochimica Acta, **47**, 217-233.

Ng, K.-C. 1990. Diagenesis of the Oligocene-Miocene Bluff Formation of the Cayman Islands. Unpublished PhD Thesis, University of Alberta.

O'Neil, T.J. (1974). Chemical interactions due to mixing of meteoric and marine waters in a Pleistocene reef complex, Rio Bueno, Jamaica. Unpublished M.Sc. Thesis, Louisiana State University.

Perfit, M.R., and Heezen, B.C. 1978. The geology and evolution of the Cayman Trench. Geological Society of America Bulletin, **89**, 1155-1174.

Pickard, J., Adamson, D.A., Harwood, D.M., Miller, G.H., Quilty, P.G., and Dell, R.K. 1988. Early Pliocene marine sediments, coastline, and climate of East Antarctica. Geology, **16**, 158-161.

Pindell, J.L. and Barrett, S.F. 1990. Geological evolution of the Caribbean region; a plate tectonic perspective. *In* The Caribbean Region. *Edited by* G. Dengo and J.E. Case. *In* The Geology of North America, **H**, 405-432.

Pleydell, S.M. 1987. Aspects of diagenesis and ichnology in the Oligocene-Miocene Bluff Formation, Grand Cayman Island, British West Indies. Unpublished M.Sc. Thesis, University of Alberta.

Pleydell, S.M., Jones, B., Longstaffe, F.J., and Baadsgaard, H. 1990. Dolomitization of the Oligocene-Miocene Bluff Formation on Grand Cayman, British West Indies. Canadian Journal of Earth Sciences, **27**, 1098-1110.

Plummer, L.N. 1975. Mixing of sea water with calcium carbonate ground water. *In* Quantitative Studies in Geological Sciences. *Edited by* E.H.T. Whitten. Geological Society of America Memoir 142, 219-236.

Quinn, T.M. 1991. Meteoric diagenesis of Plio-Pleistocene limestones at Enewetak Atoll. Journal of Sedimentary Petrology, **61**, 681-703.

Rehman, J. 1992. Diagenetic alteration of the *Strombus gigas*, *Sidastrea siderea* and *Montastrea annularis* from the Pleistocene Ironshore Formation of Grand Cayman. Unpublished M.Sc. Thesis, University of Alberta.

Reid, R.P. and MacIntyre, I.G. 1998. Carbonate recrystallization in shallow marine environments: A widespread diagenetic process forming micritized grains. Journal of Sedimentary Research, **68**, 928-946.

Rose, P.R. and Lidz, B. 1977. Diagnostic foraminiferal assemblages of shallow-water modern environments: South Florida and the Bahamas. Sedimenta VI. University of Miami, 55 pp.

Saller, A.H. 1984. Petrologic and geochemical constraints on the origin of subsurface dolomite, Enewetak Atoll: An example of dolomitization by normal seawater. Geology, **12**, 217-220.

Schlager, W. 1981. The paradox of drowned reefs and carbonate platforms. Geological Society of America Bulletin, **92**, 197-211.

Scholle, P.A. 1978. Carbonate rock constituents, textures, cements, and porosities. American Association of Petroleum Geologists Memoir 27, 241 pp.

Sharma, T. and Clayton, R.N. 1965. Measurement of $^{18}O/^{16}O$ ratios of total oxygen of carbonates. Geochimica et Cosmochimica Acta, **29**, 1347-1353.

Shourie, A. 1993. Depositional architecture of the Late Pleistocene Ironshore Formation, Grand Cayman, British West Indies. Unpublished M.Sc. Thesis, University of Alberta.

Sibley, D.F. 1980. Climatic control on dolomitization, Seroe Domi Formation (Pliocene), Bonaire, N.A. *In* Concepts and Models of Dolomitization. *Edited by* D.H. Zenger, J.B. Dunham, and R.L. Ethington. Society of Economic Paleontologists and Mineralogists Special Publication 28; 247-258.

Sibley, D.F. 1982. The origin of common dolomite fabrics: clues from the Pliocene. Journal of Sedimentary Petrology, **52**, 1087-1100.

Squair, C.A. 1988. Surface Karst on Grand Cayman Island, British West Indies. Unpublished M.Sc. Thesis, University of Alberta.

Swart, P.K. and Melim, L.A. 2000. The origin of dolomites in Tertiary sediments from the margin of Great Bahama Bank. Journal of Sedimentary Research, **70**, 738-748.

Triffleman, N.J., Hallock, P., and Hine, A.C. 1992. Morphology, sediments and depositional environments of a small carbonate platform: Serranilla Bank, Nicaraguan Rise, southwest Caribbean Sea. Lournal of Sedimentary Petrology, **62**, 591-606.

Tucker, M.E. and Wright, V.P. 1990. Carbonate Sedimentology. Blackwell Scientific Publications, 482 pp.

Vahrenkamp, V.C. and Swart, P.K. 1990. New distribution coefficient for the incorporation of strontium into dolomite and its implications for the formation of ancient dolomites. Geology, **18**, 387-391.

Vahrenkamp, V.C. and Swart, P.K. 1994. Late Cenozoic dolomites of the Bahamas: metastable analogues for the generation of ancient platform dolomites. *In* Dolomites: a Volume in Honor of Dolomieu. *Edited by* B.H. Purser, M.E. Tucker, and D. Zenger. International Association of Sedimentology Special Publications 21, pp. 133-153.

Vahrenkamp, V.C., Swart, P.K., and Ruiz, J. 1991. Episodic dolomitization of Late Cenozoic carbonates in the Bahamas: evidence from strontium isotopes. Journal of Sedimentary Petrology, **61**, 1002-1014.

Vail, P.R., Mitchum, R.M., and Thompson, S. 1977. Seismic stratigraphy – Applications to hydrocarbon exploration. American Association of Petroleum Producers Memoir 26, pp. 99-116.

Vénec-Peyré, M.T. 1991. Distribution of living benthic foraminifera on the back-reef and outer slopes of a high island (Moorea, French Polynesia). Coral Reefs, **9**, 193-203.

Vezina, J.L. 1997. Stratigraphy and sedimentology of the Pleistocene Ironshore Formation at Rogers Wreck Point, Grand Cayman: a 400 ka record of sea-level highstands. Unpublished M.Sc. Thesis, University of Alberta.

Walters, L.J., Claypool, G.E., and Choquette, P.W. 1972. Reaction rates and $\delta^{18}O$ variation for the carbonate – phosphoric acid preparation method. Geochimica and Cosmochimica Acta, **36**, 129-140.

Ward, W.C. and Halley, R.B. 1985. Dolomitization in a mixing zone of near-seawater composition, Late Pleistocene, Northeastern Yucatan Peninsula. Journal of Sedimentary Petrology, **55**, 407-420.

Wardlaw, B.R., and Quinn, T.M. 1991. The record of Pliocene sea-level change at Enewetak Atoll. Quaternary Science Reviews, **10**, 247-258.

Wheeler, C. and Aharon, P. 1997. Geology And Hydrogeology Of Niue. *In* Geology and Hydrogeology of Carbonate Islands. *Edited by* H.L. Vacher and T.M. Quinn. Elsevier, Developments in Sedimentology 54, pp. 537- 564.

Wheeler, C., Aharon, P., and Ferrell, R.E. 1999. Successions of Late Cenozoic platform dolomites distinguished by texture, geochemistry, and crystal chemistry: Niue, South Pacific. Journal of Sedimentary Research, **69**, 239-255.

Whitaker, F.F., Smart, P.L., Vahrenkamp, V.C., Nicholson, H. and Wogelius, R.A. 1994. Dolomitization by near-normal seawater? Field evidence from the Bahamas. *In* Dolomites: a Volume in Honor of Dolomieu. *Edited by* B.H. Purser, M.E. Tucker, and D. Zenger. International Association of Sedimentology Special Publications 21, pp. 111-132.

Wignall, B.W. 1995. Sedimentology and diagenesis of the Cayman (Miocene) and Pedro Castle (Pliocene) Formations at Safe Haven, Grand Cayman, British West Indies. Unpublished M.Sc. Thesis, University of Alberta.

Appendix 1:
Section Locations

UTM Grid Zone Designation 17Q, Letters PM

All measurements were made with a GPS unit, and verified against a map of the island, published by the British Government's Ministry of Overseas Development (1978).

Section	UTM	Unabbreviated name of section
ASQ	620280E, 2178460N	Abandoned Scott Quarry
ASQ-2	620361E, 2178561N	Abandoned Scott Quarry
BLX	617900E, 2177810N	Billy's X
BLY	618780E, 2178490N	Billy's
GAM	618140E, 2178069N	G & M Diner
GMD*	618040E, 2177900N	G & M Diner
HPS	620300E, 2178276N	Hayman's Pond Section
RC	619270E, 2177580N	Rebecca's Cave
STS	618343E, 2178168N	Satellite Tower Section
SQA**	618370E, 2177630N	Scott Quarry Active
SQA-1	618622E, 2177750N	Scott Quarry Active
SQA-2	618437E, 2177906N	Scott Quarry Active
SQA-3	618479E, 2177786N	Scott Quarry Active
SQA-4	618371E, 2177832N	Scott Quarry Active
SWP	620270E, 2177920N	Salt Water Point
WTB	619880E, 2177740N	Walk Through Bush

* This is an inaccurate GPS measurement. GMD was located ~20 m East of GAM (Jones, pers. comm. 1999).

** This is an inaccurate GPS measurement. SQA was located ~20 m West of SQA-1 (Jones, pers. comm. 1999).

Appendix 2:
Sample Data

1. All data are from the Pedro Castle Formation on Cayman Brac.
2. Depth (m) is below the present-day surface.
3. All calcite carbon and oxygen isotopes are expressed as PDB normalized to NBS-18.
4. Selected calcite samples from the bases of sections GAM and SQA-2, due to unusually positive isotope values (relative to total data set), were re-ran. Contamination by dissolution of the most calcian dolomite was suspected. To avoid this factor, the gases on the second run were isolated after 40 minutes of reaction, instead of the standard 60 minutes. The results are presented in the "Calcite Isotopes*" column.
5. All dolomite carbon and oxygen isotopes are expressed as PDB normalized to NBS-18. Raw oxygen data was corrected for phosphoric acid fractionation (α) using a value of 1.01109. This is ~-0.88 relative to the value of α for calcite, 1.01025. Data was then corrected for non-stoichiometry by addition of 0.742, following the calculation method of Vahrenkamp and Swart (1994).
6. Ca and Sr content in dolomite was determined by Electron Microprobe Analysis (EMPA).

Appendix 2 Data															
Sample #	Section	Depth (m)	Calcite Isotopes			Calcite Isotopes*		Dolomite Isotopes			Dolomite			
			13/12C	18/16O	87Sr/86Sr	13/12C	18/16O	13/12C	18/16O	87Sr/86Sr	Ca (ppm)	Sr (ppm)	%Ca PF-XRD	%Ca EMPA
GAM-15	GAM	0	-7.78	-6.18				-1.99	-0.82					
GAM-14	GAM	-0.33	-6.93	-4.75				0.55	1.38	0.709073 +/-0.000023			57.18	
GAM-13	GAM	-0.66	-7.10	-4.69				0.50	1.13				57.07	
GAM-12	GAM	-1	-8.20	-5.79				-1.34	-0.22				56.36	
GAM-11	GAM	-1.33	-7.24	-4.94				0.45	1.41				56.75	
GAM-10	GAM	-1.66	-3.55	-3.86				0.63	0.86				58.5	
GAM-9	GAM	-2	-1.98	-1.90		-2.28	-2.41	0.88	1.32				57.58	
GAM-8	GAM	-2.33	-1.74	-0.54		-2.51	-2.45	1.07	1.58	0.709057 +/-0.000014			57.8	
GAM-7	GAM	-2.66	-4.17	-3.93				0.78	0.91				57.37	
GAM-6	GAM	-3	-3.09	-1.52		-4.16	-2.85	0.76	1.49	0.709032 +/-0.000017			58.06	
GAM5.5A	GAM	-3.16	-0.3	1.16		-0.86	-0.18	1.16	1.61				57.87	
HPS15	HPS	0	-7.99	-5.50				-0.17	0.96					
HPS14	HPS	-0.66	-6.29	-5.55				-0.20	1.23					
HPS13	HPS	-1.33	-5.18	-3.64				0.21	1.43					
HPS12	HPS	-2	-6.29	-5.06				0.22	1.49					
STS15	STS	0	-3.77	-3.40				0.92	1.43					
STS14	STS	-0.33	-4.85	-4.43				1.06	1.36					
STS13	STS	-0.66	-4.70	-3.72				0.96	1.23					
5012.2	SQA-2	0	-2.84	-2.99				-0.21	1.97		323.3	256471.2	57.7	58.06
5011	SQA-2	-0.1	-6.74	-3.48				0.17	2.02	0.709106 +/-0.000014			56.95	
5010	SQA-2	-0.66	-6.84	-5.28				-0.95	0.24		354.58	255068.8	56	57.19
5009	SQA-2	-1.33	-6.32	-4.20				-0.07	1.38		358.9	253942.2	57.16	57.07
5008	SQA-2	-2	-3.31	-1.46	0.709093 +/-0.000015	-3.68	-3.26	0.75	1.38	0.709042 +/-0.000014	368.75	251253.9	57.72	57.76
5007	SQA-2	-2.66	-7.52	-5.60				-1.81	0.35				55.85	
5006	SQA-2	-3	-1.81	0.25		-3.65	-2.66	0.63	0.94	0.709064 +/-0.000015	399.8	255362	57.7	57.41
5005	SQA-2	-3.33	-1.29	0.59	0.70970 +/-0.000011	-3.45	-2.51	0.70	1.20	0.709051 +/-0.000014	353.65	256467.3	57.2	57.57
5004	SQA-2	-3.66	-7.42	-4.84				0.52	1.25				56.72	
5003.2	SQA-2	-4	-2.74	-0.26		-4.25	-2.76	1.42	1.44	0.709046 +/-0.000015	350.47	249136	57.53	57.49
5042	SQA-4	0	-5.39	-5.00				-0.41	0.46				57.57	
5041	SQA-4	-0.16	-5.58	-5.30				-0.69	-0.06	0.709085 +/-0.000020			57.62	
5040	SQA-4	-0.49	-6.20	-5.40				-0.35	0.29				58.05	
5039	SQA-4	-0.82	-6.69	-4.74				0.21	0.93				58.06	
5038.2	SQA-4	-1.15	-6.54	-5.11				0.14	1.37	0.709073 +/-0.000015			57.3	
5037	SQA-4	-1.48	-7.32	-4.75				0.21	1.65				57.06	
5036	SQA-4	-1.81	-8.05	-5.42				-0.37	0.99	0.709090 +/-0.000017			57.39	
5035	SQA-4	-2.14	-6.63	-4.46				0.49	1.07				58.36	
5034	SQA-4	-2.47	-6.76	-4.92				0.17	1.02				57.62	
5033	SQA-4	-2.72	-3.94	-3.71				0.34	0.93				58.45	
5032.2	SQA-4	-2.88	-6.41	-4.80				0.39	1.34	0.709102 +/-0.000014			57.71	
5031	SQA-4	-3.13	-5.32	-4.57				0.48	1.37	0.709064 +/-0.000018			57.13	
5030	SQA-4	-3.46	-5.49	-5.20				-1.32	-1.00					
5029	SQA-4	-3.79	-5.18	-3.96				0.34	0.32	0.709069 +/-0.000018			57.6	
5057	ASQ-2	0	-3.56	-4.94				n/a	n/a					
5060	ASQ-2	-0.16	-3.75	-5.07				n/a	n/a					
5054	ASQ-2	-0.96	-6.27	-5.60				n/a	n/a					
5053	ASQ-2	-1.29	-5.40	-5.50				n/a	n/a					
5051	ASQ-2	-2	-8.40	-5.99				n/a	n/a					
5045.1	ASQ-2		-2.13	-2.15				n/a	n/a					
4491	SQA-1				0.709080 +/-0.000013									

Appendix 3:
Calcite – Dolomite Separation Method for Strontium Analysis

1. Splits of coarser powder and fine grit were collected from the same aliquots of each sample from which all stable isotopic and PF-XRD analyses were made. These splits were ground to a fine powder in an agate mortar and pestle.
2. To determine the dissolution rates of bi-minerallic samples, dissolution curves of calcite and dolomite were calculated for monominerallic samples (determined by XRD and thin section examination) through several timed experiments.
3. The following procedure was used:

a) A solution of 5% acetic acid and 95% millipore water was mixed.
b) 50 mg monominerallic samples were reacted for specific time intervals. 5 minute intervals were used for calcite. 5 minute intervals (x2) followed by 10, 20, 60, 180, and 175 minute intervals were used for dolomite.
c) At the end of each interval the sample was centrifuged and the acetic acid solution removed. Meticulous care was taken to ensure no powder was removed during removal of the acetic acid solution. The actual time of the interval was then recorded – time intervals were affected by the amount of time required for the centrifuge and removal of the acid. The remaining powder was then flushed and centrifuged with millipore water. The flushed powder was then dried in an oven at low temperature. After desiccation, the sample was weighed – the difference from the start of that interval indicates the amount of dissolution that took place in the amount of time.
d) Calcite samples (n =3) were reacted for a total of ~42 minutes. This was sufficient for dissolution of ~49 mg. Dolomite samples (n = 3) were reacted for a total of ~455 minutes. This was sufficient for dissolution of ~30 mg.
e) Curves were plotted and it was determined that reaction of samples with at least 25% dolomite with 5% acetic acid for 50 minutes would remove all calcite, as detectable by XRD. This was tested and found successful. When the actual samples were being prepared for strontium analysis, the actual time of reaction varied from 55 minutes to 70 minutes, adding assurance that all calcite had been removed.

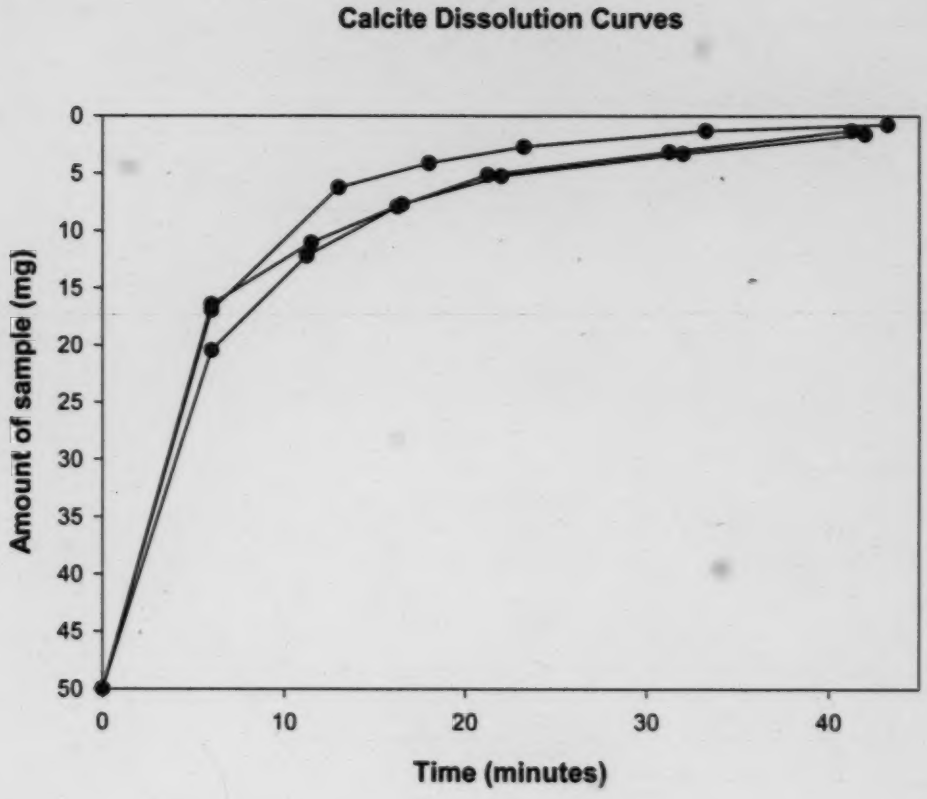
Calcite Dissolution Curves
Amount of sample (mg)
0
5
10
15
20
25
30
35
40
45
50
0
10
20
30
40
Time (minutes)

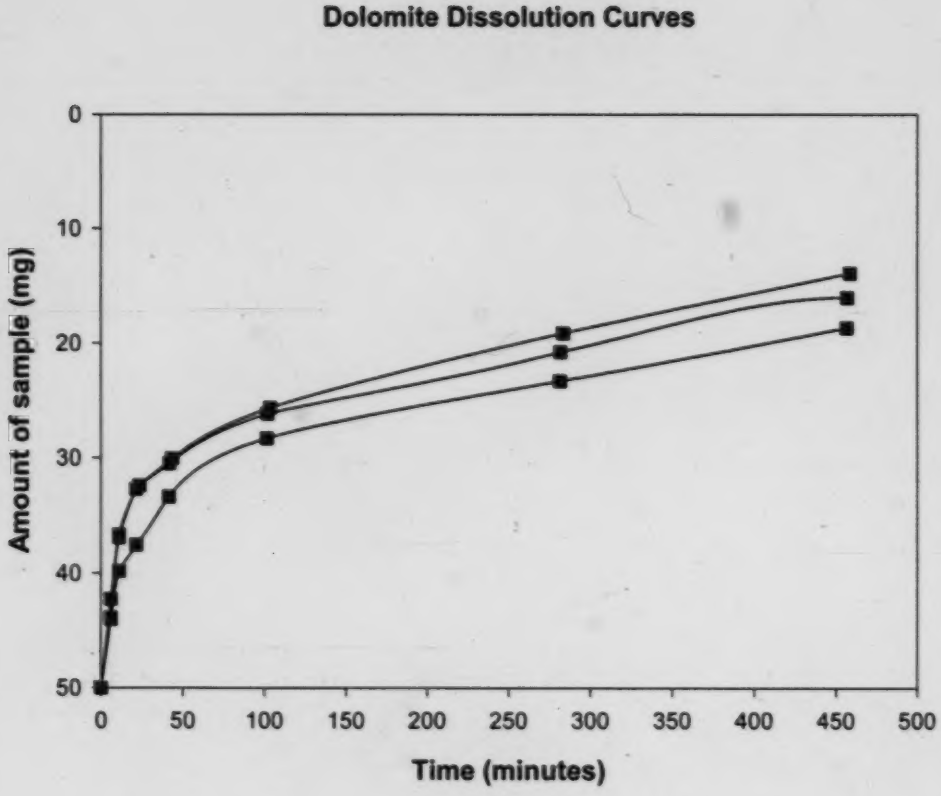
Dolomite Dissolution Curves
Amount of sample (mg)
0
10
20
30
40
50
0
50
100
150
200
250
300
350
400
450
500
Time (minutes)

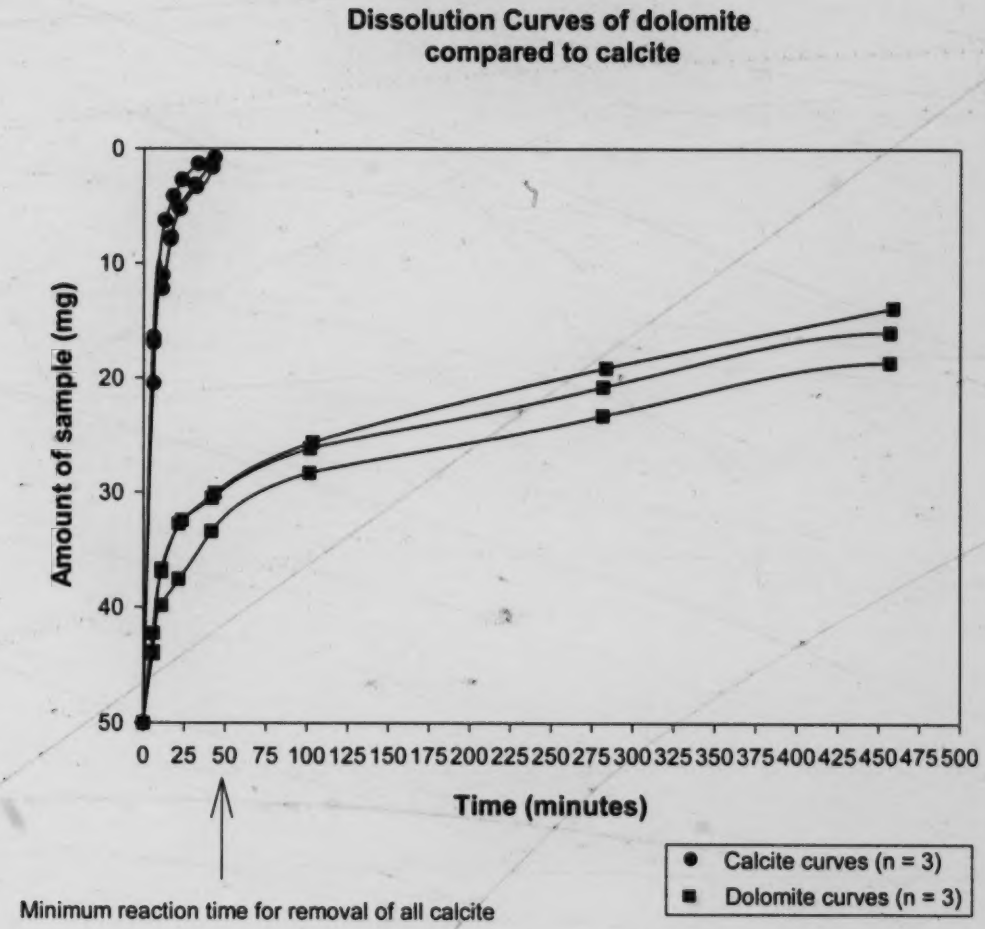
Dissolution Curves of dolomite compared to calcite
Amount of sample (mg)
0
10
20
30
40
50
0 25 50 75 100 125 150 175 200 225 250 275 300 325 350 375 400 425 450 475 500
Time (minutes)
Minimum reaction time for removal of all calcite
Calcite curves (n = 3)
Dolomite curves (n = 3)